ANALYSIS OF ATTRACTOR PATTERNS AND BEHAVIOR

FOR THE LASER WITH INJECTED SIGNAL

By

JOSHUA RAY HALL

Bachelor of Science in Physics
Oklahoma State University
Stillwater, OK
2016

Bachelor of Science in Chemistry
Oklahoma State University
Stillwater, OK
2016

Submitted to the Faculty of the
Graduate College of the
Oklahoma State University
in partial fulfillment of
the requirements for
the Degree of
DOCTOR OF PHILOSOPHY
July, 2022

ANALYSIS OF ATTRACTOR PATTERNS AND BEHAVIOR

FOR THE LASER WITH INJECTED SIGNAL

Dissertation Approved:

Dr. Donna Bandy

Dissertation Adviser

Dr. Albert Rosenberger

Dr. Joseph Haley

Dr. Barry Lavine

ACKNOWLEDGEMENTS

I would like to thank my advisor Dr. Donna Bandy for her support and friendship throughout my time here. I cannot express my appreciation enough for taking me under her wing and giving me this opportunity. I would also like to thank Erikk Burton, Dylan Chapman, and Justin Elrod for their help, camaraderie, and being a sounding board for thoughts and ideas. The experiences and knowledge you all have given me the ability to see things from different angles, and it has helped me grow as a person.

I would like to thank my father, Randy Hall, and brother, Dak Hall, for all of their kindness and support, and for getting me through hard times in my life. I would not be here without you. I am eternally grateful for everything you have done for me.

I would also like to thank Nina Paulin for her support and encouragement through the writing process.

Life is a beautiful storm.

Name: Joshua Hall

Date of Degree: JULY 2022

Title of Study: ANALYSIS OF ATTRACTOR PATTERNS AND BEHAVIOR FOR THE LASER WITH INJECTED SIGNAL

Major Field: PHYSICS

Abstract: In this dissertation an understanding of the properties and characteristics of coexisting attractors is discussed. Lyapunov exponent (LE) patterns are shown to be predictors of the dynamics of the laser with injected signal (LIS). These patterns are believed to be universal and can be applied to any nonlinear system with a simple control parameter. Patterns such as steady states, limit cycles, bifurcations, torus behavior, and chaos are known to exist. The patterns are found using the full LE spectrum to also predict (i) attractor domains that are surrounded by converging and diverging LEs; (ii) bifurcation sequences with the appearance of asymmetric bubbles; and (iii) imminent bifurcation with the appearance of a symmetric-like bubble before or after a system parameter is changed. These predictors are shown to exist in an optomechanical system as well.

Further, the system is evaluated using incremental perturbations of the state parameters in the LIS model. The perturbation study shows the potential for dynamical changes in the system and different attractor selection. By plotting the percent occurrences that transition to a coexisting attractor against the different values of the perturbations, the system shows distinct pattern variations and distinct differences between positive and negative perturbations. The structures are compared to the basins of attraction to analyze their effects on predicting which attractor the system lands.

TABLE OF CONTENTS

Chapter Page

LIST OF TABLES

Table Page

LIST OF FIGURES

Figure Page

Figure Page

Figure Page

CHAPTER I

INTRODUCTION

Nonlinear systems exist in many different fields and disciplines. The methods of analysis and procedures herein can be applied to most systems that experience nonlinear effects. This study focuses on nonlinear optics using the model: laser with injected signal (LIS), a complex system that has universal application. The calculations involve evaluating a set of nonlinear differential equations that must be solved numerically. Nonlinear systems, in general, have been studied for decades in order to understand the many mysteries that continue to challenge scientists.

One study of nonlinear optics dates back to the 1960s where linear and nonlinear optics are compared in laser theory [1-3]. These studies showed that while the linear theory explained laser behavior for a small population inversion, there exists a critical threshold where the system can only be described accurately by a nonlinear approach. These early studies and many others laid the groundwork to evaluate different nonlinear systems. One such system is optical bistability (OB), where the name characterizes both the phenomenon and the system.

1.1. Optical Bistability

Optical bistability describes a region where two stable states of the system exist simultaneously for the same control parameter. Early studies that examined OB were focused on passive systems. In 1976 Gibbs, et al. [4] studied optical bistability using a sodium vapor cell with a strong focus on nonlinear dispersion effects. These early experiments showed that bistability using

a Fabry-Perot interferometer involved a large hysteresis effect in the system. This not only showed the possibility for two different outputs for the same input, but also that nonlinear dispersion could dominate smaller nonlinear absorption effects. Later, Bonifacio and Lugiato [5, 6] found bistability in resonance fluorescence and bistability in a fully quantum mechanical systems. The bistability was predicted by a first-order phase transition in the fluorescence. Other studies in the 1980s by Gibbs, et al. [7] were able to see optical turbulence and periodic oscillations in both ring-cavities and delay-line hybrid devices. These experiments showed that other interesting nonlinear features besides bistability were present in experimental systems. In 1982 Arecchi et al. [8] demonstrated good agreement between theory and experimental systems by showing "subharmonic bifurcations, generalized multistability, and chaotic behavior" experimentally for the first time in a Q-switched CO_2 laser system. Later, intensive studies and comparisons were made by Orozco, Rosenberger, and Kimble [9 – 12] that compares the theoretical model and experimental system in order to investigate optical bistability. These investigations focused on systems with two energy levels and the occurrence of bistability in an absorptive system that was homogeneously broadened. The results showed that the experimental data did indeed match what was expected from the model, which included characteristic dynamics and quantum phenomena. Further, investigations of OB by Orozco et al. [13] continued to compare experimental and theoretical studies that led to further understanding of OB and showed that a gaussian wave matched the model while a plane wave did not. These studies and others in OB leed to the investigations of the laser with injected signal (LIS), which is the active counterpart to OB.

1.2. The Laser with Injected Signal

The laser with injected signal is just as well studied and dynamically interesting as OB [14]. The LIS models further develop the understanding of nonlinear optics. The instabilities of OB and LIS are self-induced within the system. In one study by Lugiato et al. [15] interesting nonlinear phenomena were observed for a model of LIS that exhibited complicated self-pulsing regimes,

including limit cycles, torus behavior, period-double episodes, and chaos. Later various types of chaos and methods that transition to chaos were studied [16, 17]. Thirty years ago studies in LIS investigated and characterized nonlinear phenomena with an emphasis on coexisting attractors [18]. Recently, attractor selection [19] and unique universal Lyapunov exponent (LE) patterns are reported in Ref. [20]. Lyapunov exponents are calculated using the technique described in Benettin et al. [21]. They are used to predict dynamic behaviors in theoretical systems, such as chaos, steady states, limit cycles, and torus behaviors [22]. This dissertation explores new patterns and predictors of dynamic behavior in LIS that are different from previous studies. This study identifies predictable behaviors using LEs that have remained unexplained since the first LE characterizations of this system in 1985. Detailed explanations into the processes and methodology used to study and understand these new patterns and to gain better understanding of nonlinear effects are developed.

CHAPTER II

LASER WITH INJECTED SIGNAL, SYSTEM AND ANALYSIS

2.1. Laser with Injected Signal Model

The laser with injected signal is a semiclassical model that is developed from the Maxwell-Bloch equations. In this study the laser is based on a homogeneously broadened two-level atom. The cavity frequency is usually tuned to the atomic frequency, $\omega_a=\omega_c$, and produces a stable carrier frequency, ω_c, when no eternal signal is applied to the system. A continuous wave (cw) laser is injected into the cavity with a frequency of $\omega_0\neq\omega_a$, where the driving field and the laser oscillator can compete with one another. The difference in these frequencies, $|\omega_a-\omega_0|$, can cause beats to appear when at lower input-signals. Here the laser acts as a local oscillator. For larger external field amplitudes, the laser stably locks to the injected field and produces a constant output amplitude, known as injection locking. The laser with injected signal in this study is a single-mode non-resonant unidirectional ring laser. See Fig. 1.

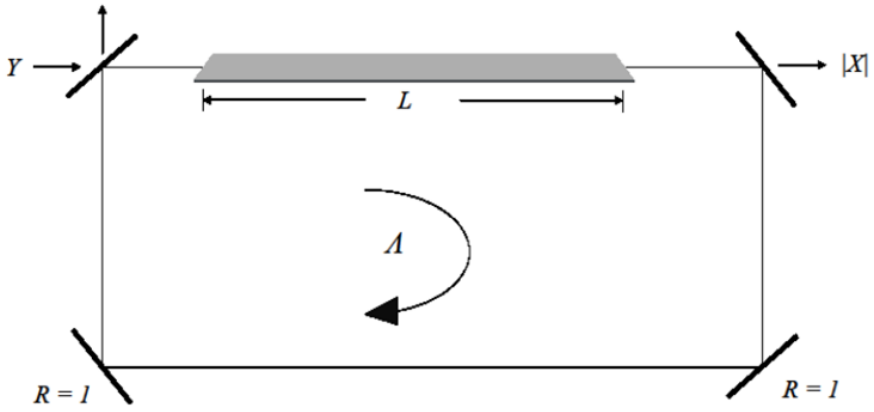

Figure 1: Non-resonant unidirectional ring diagram. Y is the input field amplitude and $|X|$ the modulus of the output field amplitude. There are four mirrors. The top left and top right mirrors are partially reflective mirrors with small transmissivity. The bottom two mirrors are 100% reflective, $R = 1$. The length of the lasing medium is L, and Λ is the round-trip path length of the cavity.

The equations of motion consist of two complex variables and one real variable. X is the complex field amplitude and P is the complex polarization. D is the real population difference. Y is the control parameter. It is proportional to the incident field amplitude and is real and positive for definiteness.

$$\frac{\partial X}{\partial \tau} = -\tilde{\kappa}\left[\left(1 - i\frac{\Phi}{\tilde{\kappa}}\right)X - Y + 2CP\right] \quad , \tag{1}$$

$$\frac{\partial P}{\partial \tau} = -\left(1 + i\tilde{\Delta}\right)P + XD \quad , \tag{2}$$

$$\frac{\partial D}{\partial \tau} = -\tilde{\gamma}\left[\tfrac{1}{2}\left(XP^{*} + X^{*}P\right) + D + 1\right] \quad , \tag{3}$$

where the system parameters are: C is the small-signal atomic gain, $\tilde{\Delta} = (\omega_a - \omega_0)/\gamma_\perp$ is the scaled atomic detuning from the injected signal carrier, $\tilde{\kappa} = \kappa/\gamma_\perp$ is the scaled cavity relaxation rate, $\tilde{\gamma} = \gamma_\parallel/\gamma_\perp$ is the scaled population decay rate, and $\Phi = (\omega_0 - \omega_c)/\gamma_\perp$ is the scaled cavity mistuning. The relaxation rate of the population inversion is $\gamma_\parallel$ and $\gamma_\perp$ is the polarization relaxation rate. The time τ is measured in units of the polarization relaxation time $\gamma_\perp^{-1}$. In order to model a realistic laser system, the following parameter values were chosen: $C = 3$, $\tilde{\Delta} = 0.5$, $\tilde{\kappa} = 0.1$, $\tilde{\gamma} = 0.01$, and $\Phi/\tilde{\kappa} = -0.5$. The chosen parameter values are between the Class B [23] and Class C [24] laser types. See Appendix I for class characterizations.

Between the regions of injection locking and the laser acting as a local oscillator, the system experiences complex, interesting nonlinear phenomena. This system of equations is studied by examining five real equations. That is, in order to make the evaluation process quick, the complex equations are split into two real equations. The output field amplitude $X=A+iB$, the polarization $P=R+iS$, and the real population difference D remains the same. The equation are as follows:

$$\dot{A} = -\widetilde{\kappa}\left[A + \left(B\ \frac{\phi}{\widetilde{\kappa}}\right) - Y + (2\ C\ R)\right], \quad (4)$$

$$\dot{B} = -\widetilde{\kappa}\left[B - \left(A\ \frac{\phi}{\widetilde{\kappa}}\right) + (2\ C\ S)\right], \quad (5)$$

$$\dot{R} = -\left[R - \left(\widetilde{\Delta}\ S\right)\right] + (A\ D), \quad (6)$$

$$\dot{S} = -\left[\left(\widetilde{\Delta}\ R\right) + S\right] + (B\ D), \quad (7)$$

$$\dot{D} = -\widetilde{\gamma}\left[(A\ R) + (B\ S) + D + 1\right] \quad (8)$$

The five equations are solved numerically using Mathematica's NDSolve function. The system can be explored in a variety of ways: Temporally, in phase-space, using Fourier analyses, by sweeps, by volumes, and by studying their Lyapunov exponents. The collected information is used to create a map of the system's dynamics and complex phenomena. Each attractor is numbered in the order in which it was found.

Attractors are a set of points, or system states, that the system is drawn to when allowed to evolve in time [25]. They are invariant and cannot be split into smaller attractors or subgroups. Each attractor has its own shape temporally and in phase space. It has unique features such as frequency spectra, periodicity, domain of existence in terms of the range of the control parameter, and basins of attraction [26]. The phase space of an attractor can be as simple as a circle with a single period, called a 1P. It is typically more complicated having a series of subharmonics, and/or corkscrews as seen in this study. However, to confirm that the attractor has a higher periodicity other than a 1P, whether that is a 2P, 3P, etc., requires confirmation of a Fourier analysis. See Appendix II for a more in depth explanation.

Another type of dynamic feature that appears in the system is a *window in chaos*. Windows are regions surrounded by chaos, but they do not coexist with chaos. Chaos is characterized as a broadband spectrum with no overriding frequencies in the Fourier analysis. In phase space chaos simply fills in the space and temporally never repeats itself. In Fig. 2, each attractor is vertically positioned by its relative frequency. The horizontal ranges of the attractors are the identified

domains of the attractors as a function of the input field amplitude, *Y*. The callouts for the smaller attractors are in blue. Highlighted in red are two windows in chaos. The windows only exist for a brief region of the input amplitude, and in these regions, chaos cannot coexist with the windows. This is unlike an attractor where they can coexist with chaos. The windows for these parameters have a high periodicity and inverse bifurcations. Only two windows are found in this system so far.

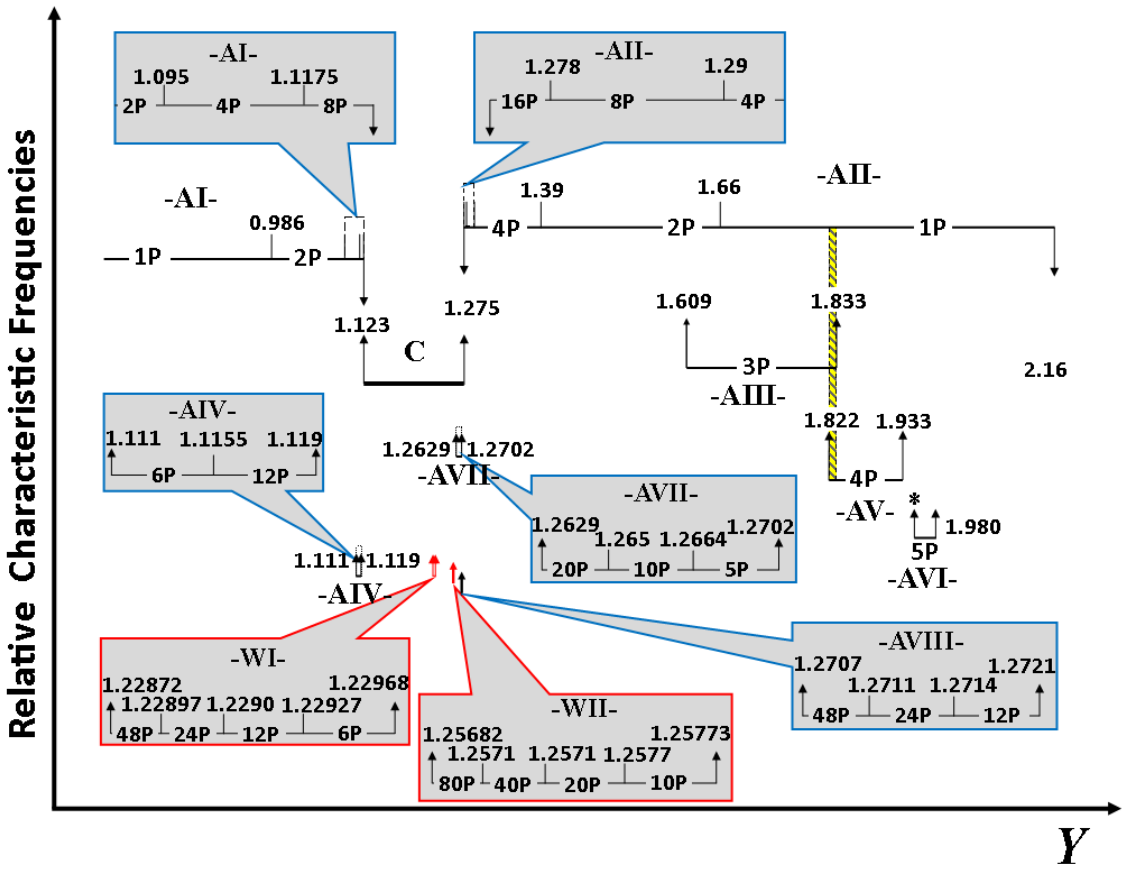

Figure 2: Attractor map of the laser with injected signal for the identified parameters. The map shows the relative position of each attractor and window using their fundamental frequencies as a function of the input field amplitude, *Y*. Two windows are found in the chaos, shown in red. Attractor callouts are in blue. The * denotes *Y=1.948* at the beginning of the domain of AVI.

2.1.1. Steady State

The steady state is a point in phase space where the system is invariant in time. To determine the steady state, the time dependent derivatives of the model equations are taken to be zero and reduced to the equation below:

$$Y = |X| \sqrt{\left\{1 - \frac{2\,C}{1+\tilde{\Delta}^2+|X|^2}\right\}^2 + \frac{2\,C\,\tilde{\Delta}}{1+\tilde{\Delta}^2+|X|^2} - \left(\frac{\Phi}{\tilde{\kappa}}\right)^2}. \tag{9}$$

The resulting equation is plotted in Fig. 3 with the input field amplitude, *Y*, on the horizontal axis and the output field amplitude, |*X*|, on the vertical axis.

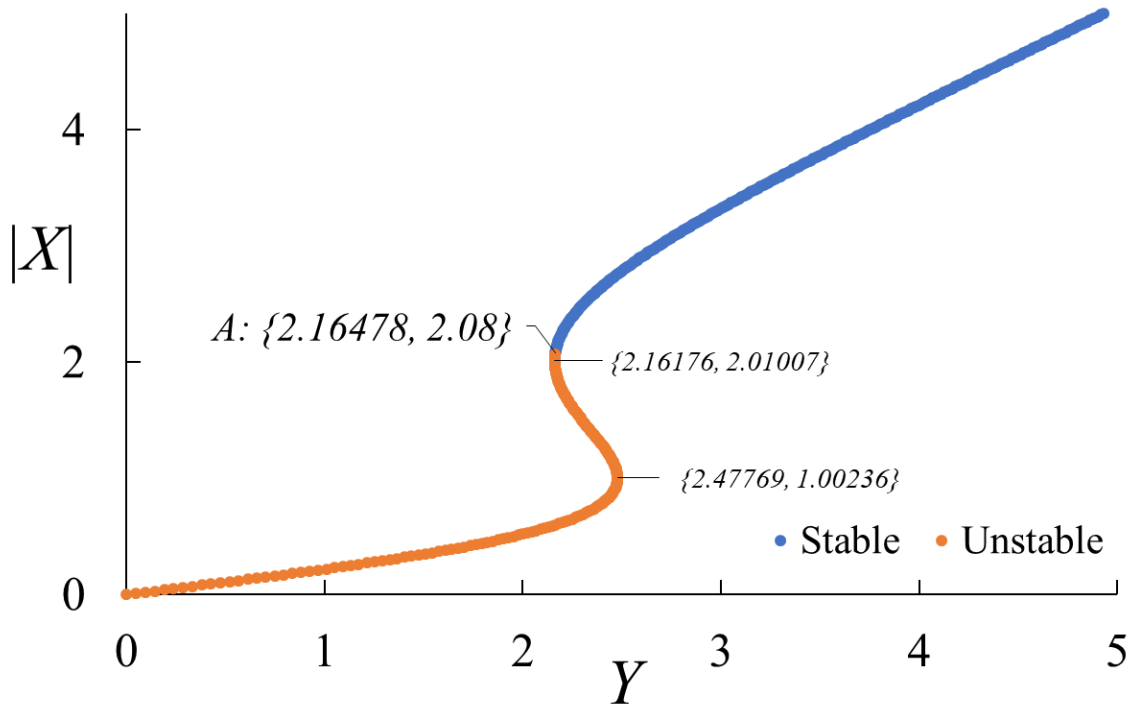

Figure 3: Shows the steady-state curve for the laser with injected signal. The input amplitude, *Y*, is on the horizontal and the output amplitude, |*X*|, is on the vertical axis. The two turning points are identified by their coordinates. *A* marks injection locking. The lower branch of the curve is unstable, *0<Y<2.16478* and *0<|X|<2.08*. The blue region above point A denotes the stable region, and the orange region below point *A* is unstable.

2.1.2. Stability Analysis

To do the stability analysis it is easiest to start with the set of five real equations, Eqs. (4)-(8), and linearize each around a steady state. The Hurwitz criterion is used to determine the stability or instability of the system. See Appendix III. For this set of parameters, the entire lower branch and some of the upper branch are unstable. This is color coded in Fig. 3. The blue stable region is where injection locking occurs and no interesting features are observed. Nonlinear phenomenon are observed in the orange unstable region.

2.2. Dynamics

Evaluation of the dynamics in LIS requires specialized programs in order to understand the dynamics and collect the appropriate data on the state variables. Since there are five interconnected nonlinear equations, and they are only solved numerically, then most programs are built in Mathematica and analyzed using the function NDSolve. As the system is allowed to evolve in time it can be drawn to an attractor. Different values of the input amplitude can affect the final state of the system depending on the existence of attractor types and coexisting attractors. Once stably on the attractor it is possible to collect data about the specific attractor. While following the attractor the system is allowed to evolve in time and the attractor can be followed adiabatically for its domain of existence in *Y*. "The idea behind an adiabatic scan is similar to a thermodynamic adiabatic expansion" [20]. Once the system is stable on an attractor, small steps of the control parameter are taken such that the system remains on the attractor until the end of its domain. Several potential dynamics can occur, possible states include attractors, chaos, torus behavior, and steady states.

2.2.1. Sweeps

A sweep of the system is another tool that can be applied to find regions where different instabilities might exist. This is calculated by putting a time dependent ramp on the input amplitude, $Y=Y_0+r\,\tau$, Y_0 is the original input, r is the rate of change, this makes the system non-autonomous. The system is linearly evolved through a series of input field amplitudes and it does not have time to equilibrate on a single event. Thus, the system is essentially being dragged in time causing a lag effect in the dynamic events. The linear ramp therefore does demonstrate changes to the system; however, it only gives an approximate location of the feature and/or event. Further, the direction, whether increasing or decreasing the ramped Y, can also affect the output of the sweep depending on which attractors the system encounters. The domains of those attractors and the rate that the system changes with respect to time are critical to what is observed. A unique benefit to this tool is that the discrepancies can show the potential for coexisting attractors. To observe this, the ramp is completed twice, both forward and backward. One starts at an input amplitude of $Y_0=0$ with a positive rate of $2*10^{-4}*(t)$ in the forward sweep, the second starts in the region of injection locking at $Y_0\approx2.5$ with an equivalent but negative rate for the backward sweep. Figures 4 show the forward and backward sweeps for the chosen LIS system. The difference in the dynamics that occur between $1.0<Y<1.6$ indicates the possibility of coexisting attractors in this region. The instabilities around $Y\approx2.0$ in the backward ramp are caused by initiating the system in the stable region of injection locking and moving the system quickly into the unstable region. The system reacts with a jolt or a large set of erratic oscillations that require some time to normalize.

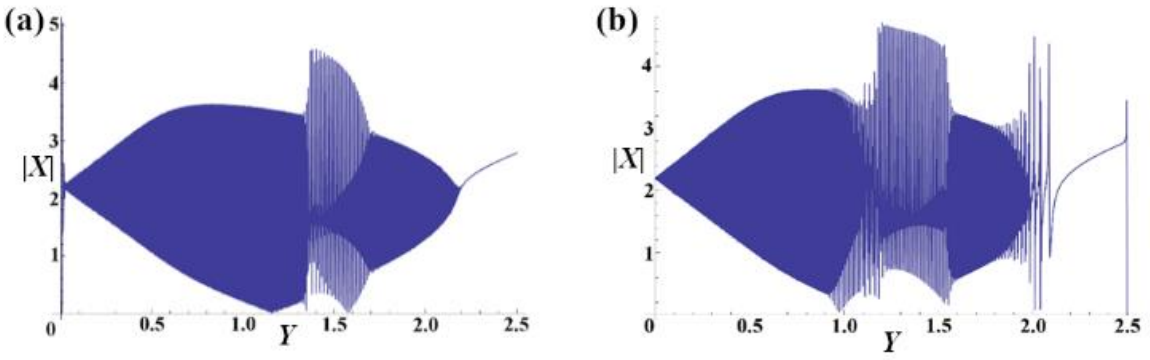

Figures 4: (a) A forward sweep for $\Delta Y=(2.0*10^{-4})*\tau$ that shows instabilities from $0<Y<1.35$, followed by a region of chaos, and then another period of instability, $1.67<Y<2.2$. (b) The backward sweep for $\Delta Y=2.5—(2.0*10^{-4})*\tau$, its regions of instability are $1.6<Y<2.1$, chaos $1.6<Y<1.15$, followed by periodic instabilities until $Y=0.0$.

2.2.2. Volume Calculation

The volume is calculated using the Mathematica function of RegionMeasure and ConvexHullMesh. To do this, a set of points is placed into the ConvexHullMesh function which generates a mesh for the area within the points that corresponds to the volume of the attractor for that value of Y and outputs data in a usable form for RegionMeasure. RegionMeasure takes the generated mesh and calculates the volume from the irregularly shaped phase space of the attractor. Figures 5 display the volumes for AII, AIII, AV, and AVI, respectively. While AIII, AV, and AVI keep the same periodicity throughout their domain of existence, AII experiences an inverse bifurcation sequence which is visible at $Y=1.39$ and $Y=1.66$, where the system transitions from a 4P to a 2P and a 2P to a 1P, respectively. AIII, AV, and AVI do not experience bifurcations and keep their periodicity, 3P, 4P, and 5P, respectively. The volumes of these attractors increase and then decrease as the input amplitude changes over the domain of the attractor. That is, the volume of the attractor is lowest as the domain of the attractor begins and ends.

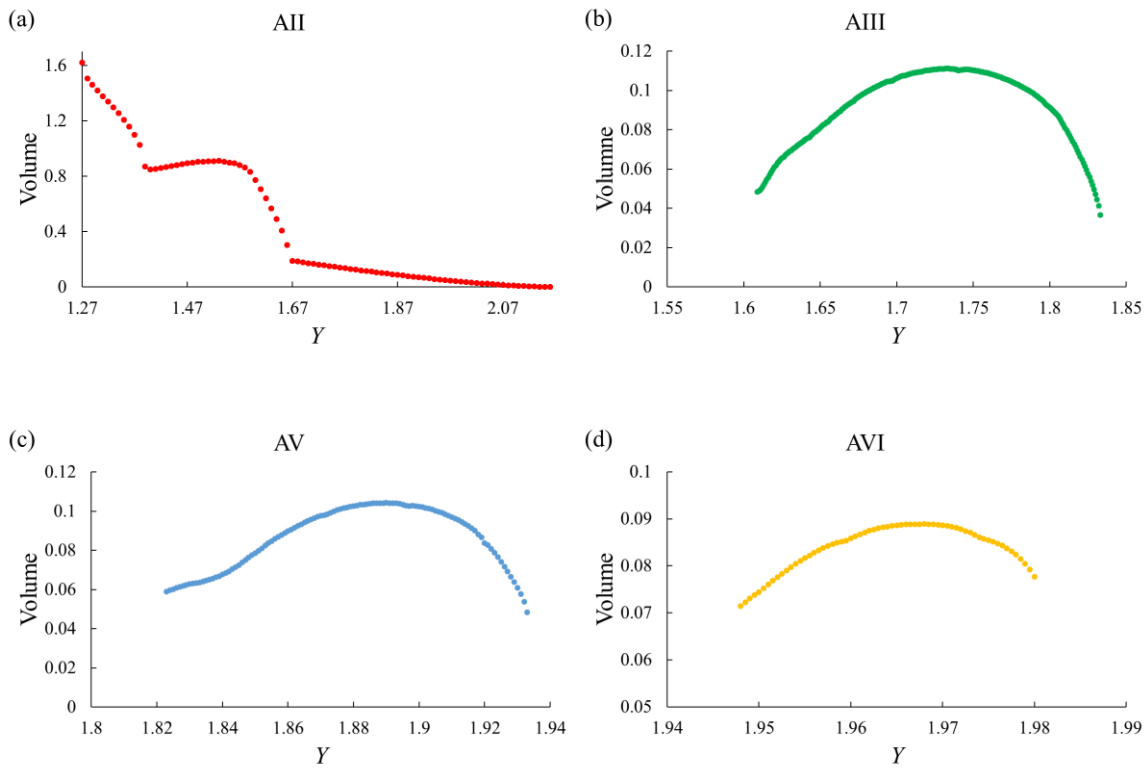

Figures 5: The volumes are color coded (a) AII in red, (b) AIII in green, (c) AV in blue, and (d) AVI in yellow.

2.3. Lyapunov Exponents

Lyapunov exponents are a way of analyzing close trajectories of a system for infinitesimal changes by indicating if the system is stable, oscillating, or chaotic. They are also used to identify torus behavior and other system dynamics depending on the pattern that the LE values take, as demonstrated in Table 1. In this system there are five LEs, LE1 is the largest Lyapunov exponent. It shows whether the system is stable LE1<0, unstable LE1≅0, or chaotic LE1>0. The other four LEs (LE2, LE3, LE4, and LE5) are in order from largest to smallest, and are typically negative numbers. They can demonstrate unique patterns that impart more information about the system dynamics. Table 1 shows the dynamics and their associated LE characteristics, followed by the pattern type [20, 22].

Table 1. Patterns of Lyapunov Exponents

Dynamics as a function of *Y*	LE characteristics LE4 < 0, LE5 < 0	LE pattern
Steady state	LE1 < 0, LE2 < 0, LE3 < 0	
Limit cycle;	LE1 = 0, LE2 < 0, LE3 < 0	
2D torus	LE1 = LE2 = 0, LE3 < 0; LE1 = LE2 = LE3 = 0; LE1 = LE2 = LE3 = 0; LE1 = LE2 = 0, LE3 < 0	Converging LE1 and LE2 = LE3 to LE1 = LE2 = LE3 = 0
Chaos	LE1 > 0, LE2 = 0, LE3 < 0	One or more LE > 0
Period-doubling episode at each apex	Begin: Linear formation LE1 = 0, LE3 = LE2 < 0; asymmetric bubble LE1 = 0, LE3 < LE2 ≤ 0; apex LE1 = LE2 = 0, LE3 < 0; ending is reverse of beginning	Asymmetric bubble repeats with an interval of equal LEs between bubbles
Imminent path to period-doubling	LE1 = 0, LE3 < LE2 < 0	Symmetric-like bubble
Beginning of coexisting attractor Ending of coexisting attractor	Maximum at LE1 = LE2 = 0, LE3 < 0; LE3 < LE2 ≤ 0 converge to LE2 = LE3 Reverse of beginning LE3 < LE2 ≤ 0 diverge to maximum at LE1 = LE2 = 0, LE3 < 0	Attractor birth: LE1 = LE2 at max; LE2, LE3 converge to LE2 = LE3 < 0e Attractor death: Reverse process of attractor birth

These patterns range from simple to complex, and are unique predictors of system characteristics and dynamics. Figures 6 show the three largest LEs and plots of these LE values are a function of *Y* for the attractors AII, AIII, and AV. The asymmetric bubble is a predictor of a bifurcation occurring in the system. This is shown in Fig. 6(a) where the peak of the asymmetric bubble occurs at the value of the input amplitude where the bifurcation occurs. The LE pattern that illustrates the bifurcation, as shown in Table 1, is where LE1=LE2=0 and LE3<0. An example of this can be seen in AII in Fig. 6(a) at *Y=1.2905, 1.395,* and *1.6656*. Symmetric-like bubbles have LE1=0, LE2 thru LE5<0, and do not show bifurcations, or any significant change to the attractor. As seen in AIII of Fig. 6(b). It is determined that they predict an imminent bifurcation. When one of the system parameters is changed the symmetric-like bubble changes to an asymmetric bubble. This was

initially discovered to be the case when the value of the gain was changed and a bifurcation occurred. This was a suggestion by Erikk Burton after initial investigations of the region only showed small changes to the dynamics and no major cause for the pattern. A more extensive investigation was carried out after this discovery that shows changes to the system parameter not only can cause the system to bifurcate, but additional increases in the input can cause further bifurcations to occur. Lowering the gain on the other hand caused the symmetric-like bubble to vanish to two equal LEs. The last pattern in Table 1 is an open, one sided, bubble that denotes the origin and demise of an attractor, which can be seen in both Figure 6(b) and (c). Similar to the asymmetric bubble when LE1=LE2=0 the attractor has reached a point where the attractor no longer exists after/before that point. It is not seen in Fig. 6(a) because of injection locking.

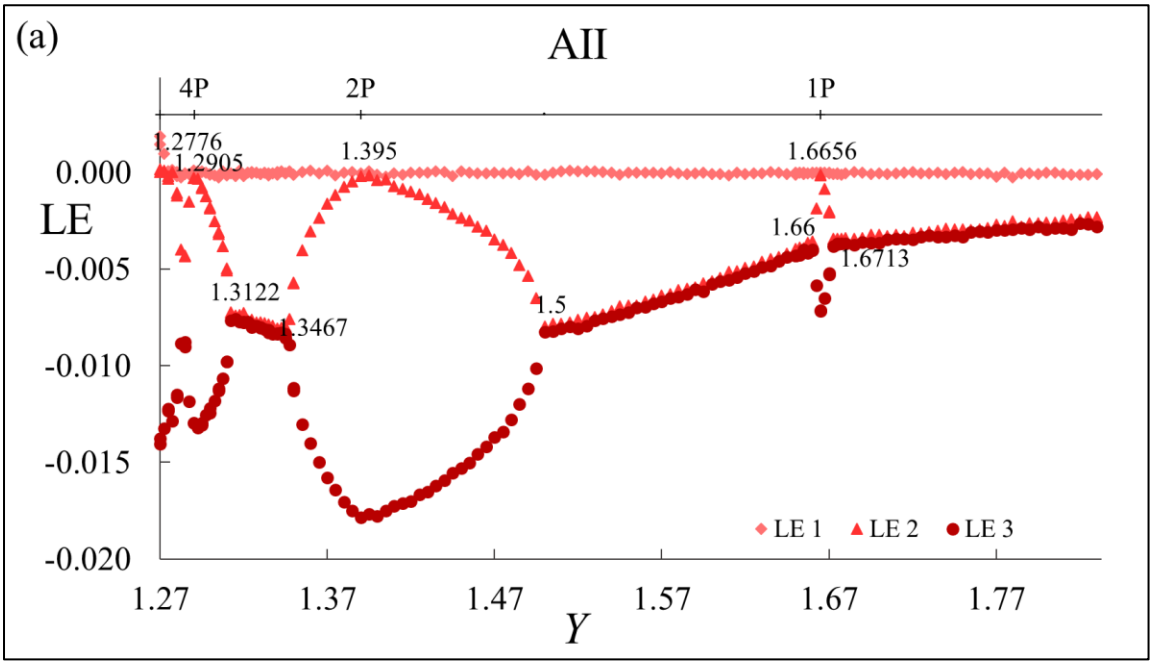

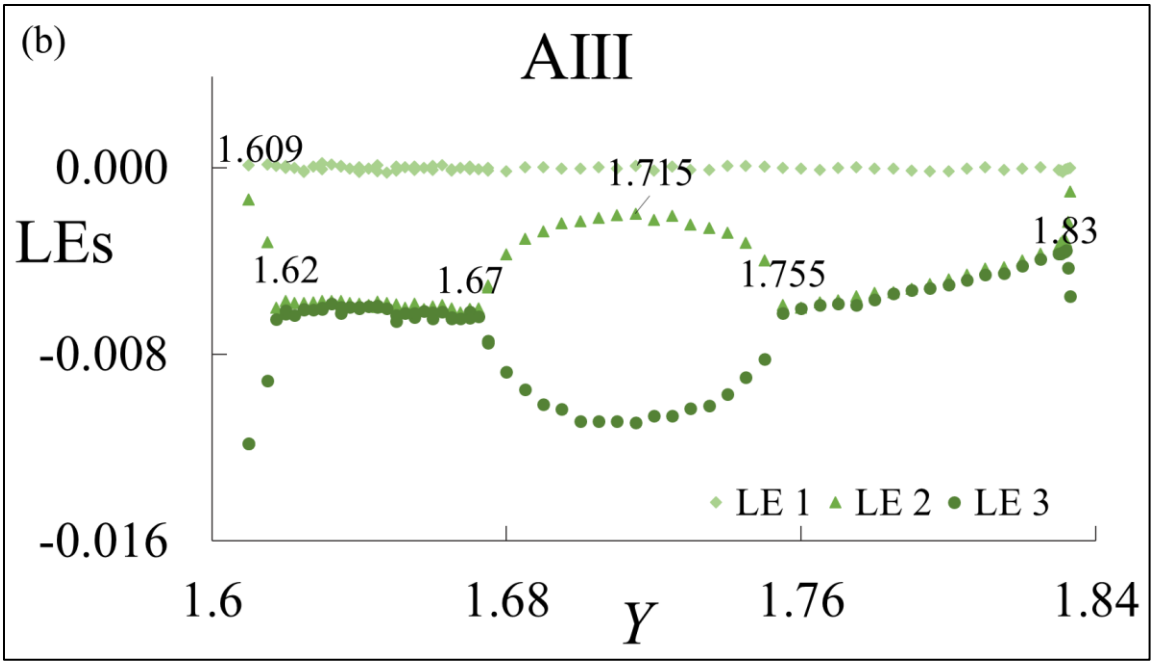

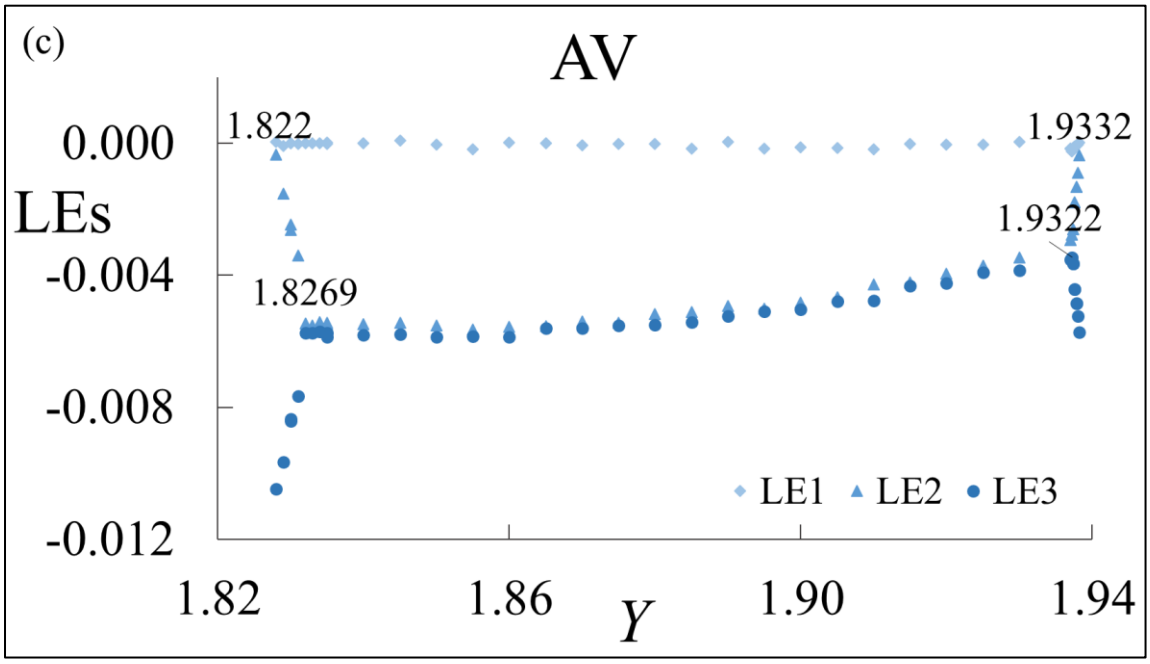

Figures 6: The three largest LEs, showing the domain of existence for (a) AII, (b) AIII, and (c) AV. (a) On the scale shown AII displays asymmetric bubbles throughout its inverse bifurcation sequence, points of bifurcations are marked, as well as the peaks of the asymmetric bubbles. (b) AIII shows first the converging and diverging patterns for the beginning and ending of an attractor's domain, and second, a symmetric-like

bubble structure with the peak of the bubble at *Y=1.715*. (c) AV only shows the beginning and ending LE attractor domain.

A set of Lyapunov exponents has unique patterns that characterizes each attractor and gives a comprehensive, but not complete, understanding of the system. Figures 7 show the LEs for the LIS system plotted against the input amplitude, *Y*. The number of LEs that can be obtained for a system is based on the number of system coordinates. For LIS, five LEs can be obtained. For this system the trace of the Jacobian, *-2.21*, can characterize the system also. Figure 7(a) shows the first three LEs as a function of *Y* and some interesting structures: a symmetric-like bubble as in AIII, asymmetrical bubbles as in both AI and AII. Note, these patterns are seen also in AIV, AVII, and AVIII, the scale of the graph makes them difficult to see. These types of structures were reported by Gu et al. [22] for a different set of parameters, but were not understood and generally dismissed as unimportant at the time. Figure 7(b) shows the lowest two LEs as a function of *Y*. Each attractor has a unique LE spectrum associated with the attractor and when a non-adiabatic scan of the system is done using the LEs, the system can fall off to another attractor. This results in a clear discontinuity and identifies a region of coexistence.

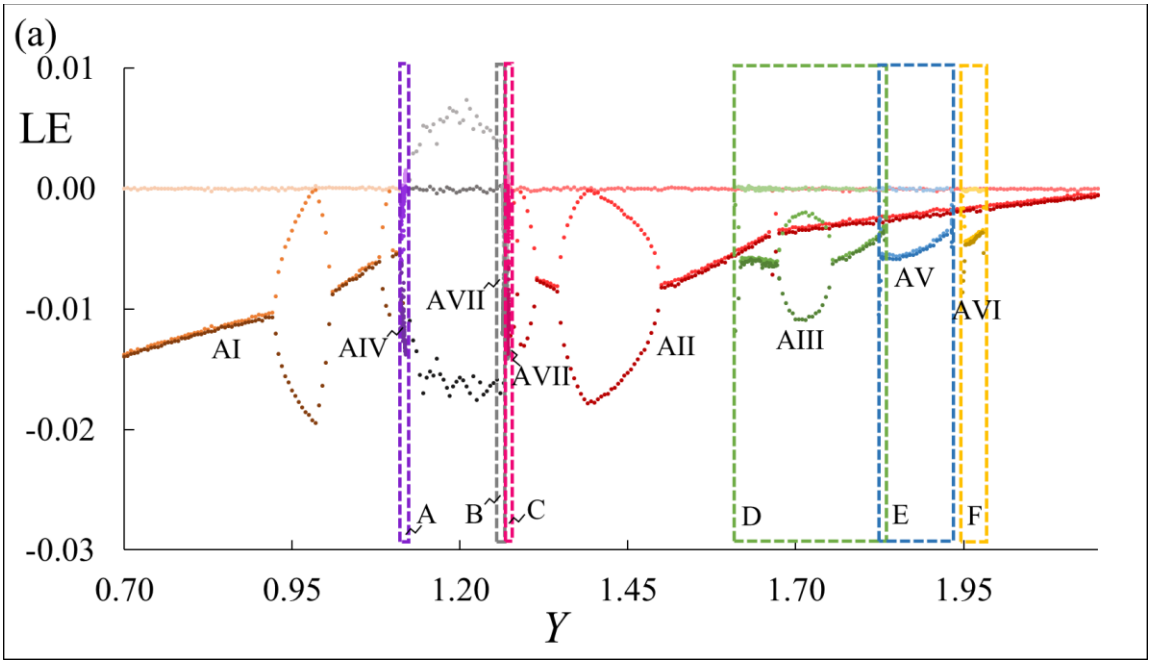

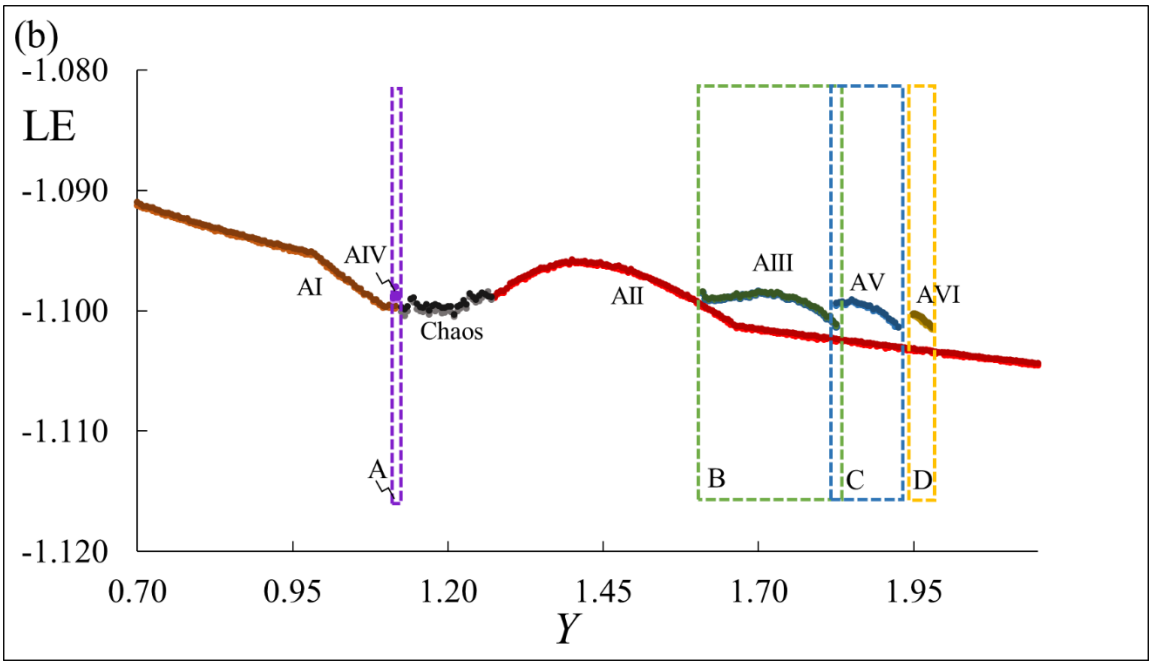

Figures 7: The Lyapunov exponent spectra for the global domain of the system before injection locking. The domain of each attractor is plotted in a unique color, AI is orange, AII is red, AIII is green, AIV is purple, AV is blue, AVI is yellow, AVII is gray, and AVIII is pink. (a) Displays the first three Lyapunov exponents as a function of *Y* for each individual attractor. Each of the smaller coexisting attractors has a dashed boundary around its domain of existence. (b) The bottom two smallest Lyapunov exponents for each attractor.

2.4. Attractor Identifier

Barring labor intensive manual identification of attractors, it becomes apparent that a faster computational method is needed to identify known attractors, in order to have a reliable way of identifying unique attractors for their full range of existence. One idea was to allow the system to evolve for enough time to stabilize on an attractor and then save the coordinates of that attractor for one period of the motion. This is archived for the computer to check against the known data of each attractor of the system. While this method is effective, there were some drawbacks. The first being that each individual attractor must be saved at every value of the input amplitude. This leads to the second problem, the attractor changes adiabatically when the input amplitude is changed. Since there is no fixed value for the entire domain of the attractor, the data has to be collected for

every *Y* value for the attractor's domain of existence. Also, several periods of motion need to be taken in order to make an accurate comparison to the known attractors. Collecting the archived data of known attractors takes a lot of time and is not 100% accurate. To identify an unknown attractor the system has to be allowed to evolve for a significant amount of time for every perturbation taken; otherwise the program runs the risk of misidentifying an attractor. So a better method for quickly and effectively having the computer identify attractors became important.

During an investigation of the temporal graphs, interesting result appeared. Since each attractor has a unique frequency and amplitude, as well as a different number of peaks (though it can have the same number of peaks as another attractor), a comparison between the local maximums can be used as a quick identifier of an individual attractor in a range of input signals where two or more attractors coexist with little risk of misidentification. By taking the difference between the maxima for one period of motion at a single value of the input amplitude, *Y*, the peak difference is obtained. This process is repeated for a range of *Y* values in order to collect enough data to form a curve for the full domain of the attractor. This difference is then plotted against the *Y* values and an equation is fit to the curve. Figures 8 show the calculated peak difference and fitted curve for AII, AIII, and AV. Attractors with multiple peaks were tested using primarily the 3P of AIII, and the 4P of AV. For consistency and ease of programing the largest peak difference was used since it also possessed the biggest difference in values and the most distinct numbers.

(a)

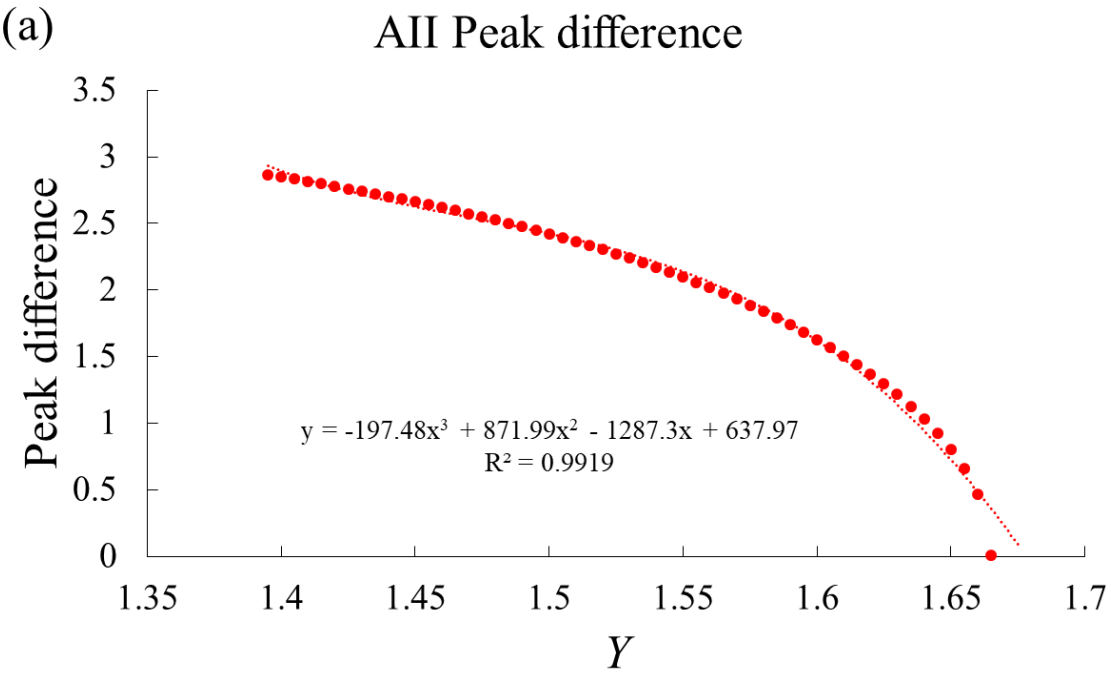
AII Peak difference
Peak difference
3.5
3
2.5
2
1.5
1
0.5
0
1.35
1.4
1.45
1.5
1.55
1.6
1.65
1.7
Y
y = -197.48x³ + 871.99x² - 1287.3x + 637.97
R² = 0.9919

(b)

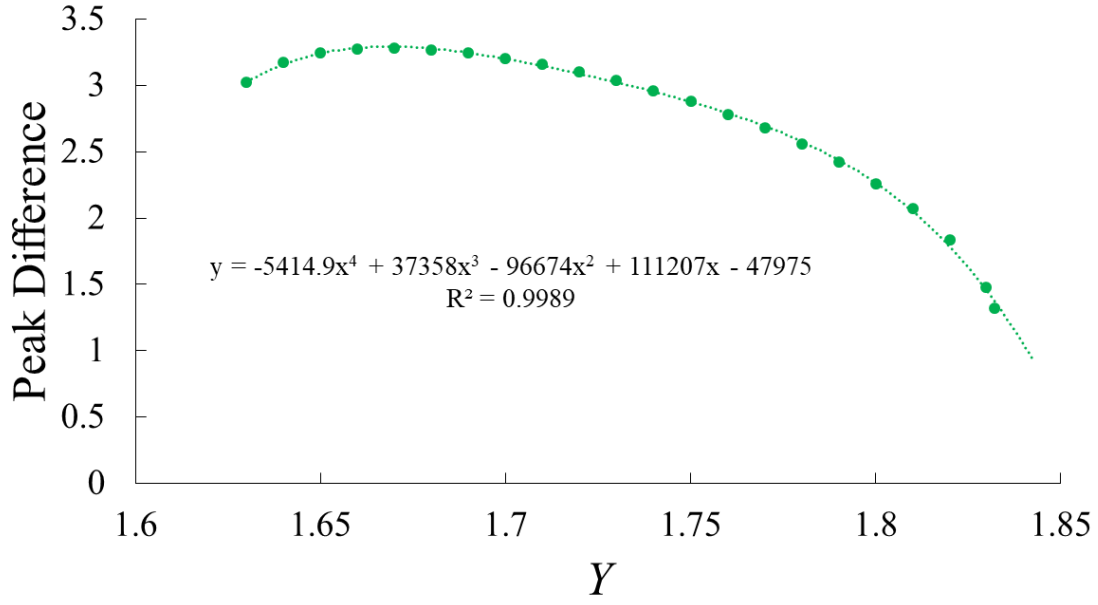
AIII Peak Difference
Peak Difference
3.5
3
2.5
2
1.5
1
0.5
0
1.6
1.65
1.7
1.75
1.8
1.85
Y
y = -5414.9x⁴ + 37358x³ - 96674x² + 111207x - 47975
R² = 0.9989

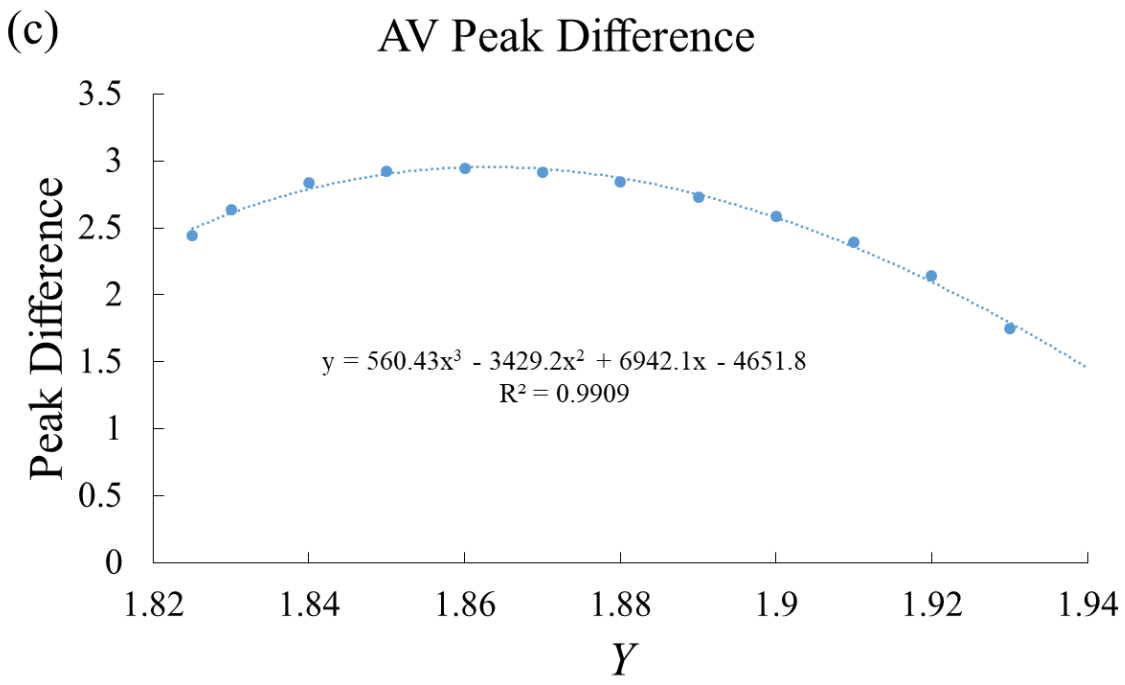

Figures 8: Peak difference for attractor identification. (a) AII for the region where it is a 2P, and a third order polynomial fit to the data with an accuracy of $R^2=0.9919$. (b) AIII for its entire domain of existence, with a fourth order polynomial fit of $R^2=0.9989$. (c) AV for its domain of existence, with a fourth order polynomial fit of $R^2=0.9909$.

Another benefit of these distinct unique values is that the amount of points that are needed to evaluate and compare the attractor to a reference is greatly reduced. In this way only a small number of points for an attractor need to be evaluated and calculated in order to obtain a higher order polynomial that uniquely fits an attractor. This equation for the fitted curve can now be used for comparison instead of having lists of saved values. A buffer of 2%-5% is allowed for any variations between the equation and the data. The process is not only quick but less memory intensive, since it now only relies on the higher order polynomial. The only real draw back to this process is that it requires a minimum of a 2P attractor. If the attractor is a 1P, then the peak difference obtained is zero. Since there are not two maxima, so when AII transitions to a 1P at $Y\approx1.66$ the peak difference goes to zero, as seen in Fig. 8(a). Other methods have to be used in

the identification of these types of attractors. For example, the amplitude of the peak or the difference between the minimum and maximum can be used.

2.5. Perturbations

The study of perturbations was initially designed to test if the proximity to coexisting attractors effected the systems preference to one of the attractors. By moving the initial starting point a fixed amount away from the base attractor it was possible to then observe if the system returned to that attractor or if it transitioned to a coexisting attractor. The total number of times that the system landed on a specific attractor is recorded and the percentage chance of going to that attractor is calculated.

In order to do a perturbation calculation on the system, it must first be stably on a base attractor. This is the attractor that the system moves off by a fixed amount for one of the state variables. Once the base attractor is selected, 40 equally spaced points around one period of motion of the attractor are taken and used as the set of initial values for future perturbations. Figures 9 are 2-D projections of coexisting attractors AII, AIII, and AV showing the 40 points evenly spaced in time for a single period of the attractors at $Y=1.83$. Each one of those 40 points are perturbed for the full range of the perturbations, $-0.3 \leq \delta v \leq 0.3$, with a step size of $\Delta \delta v = 0.005$. Where δv is a vector representing the displacement from one of the 40 points on the attractor.

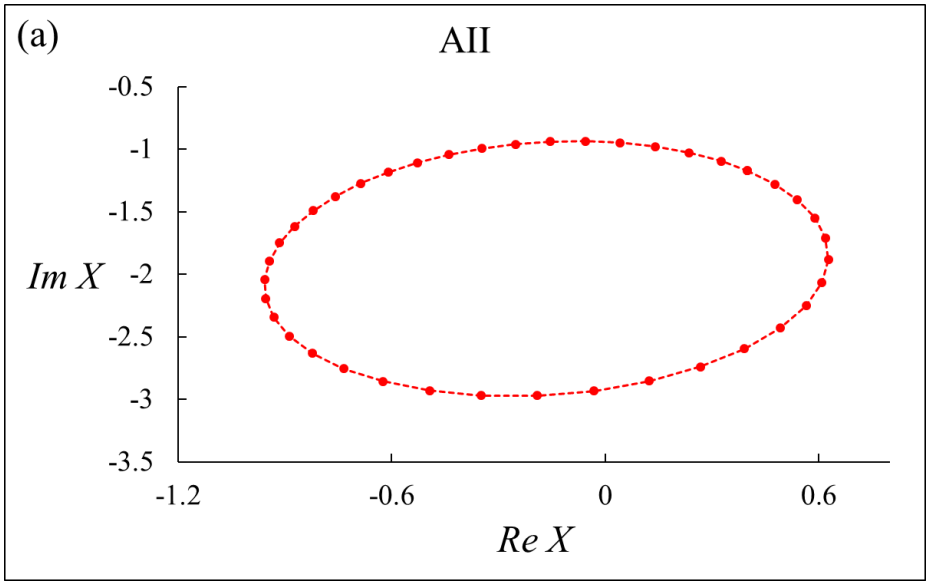
(a)
AII
-0.5
-1
-1.5
Im X
-2
-2.5
-3
-3.5
-1.2
-0.6
0
0.6
Re X

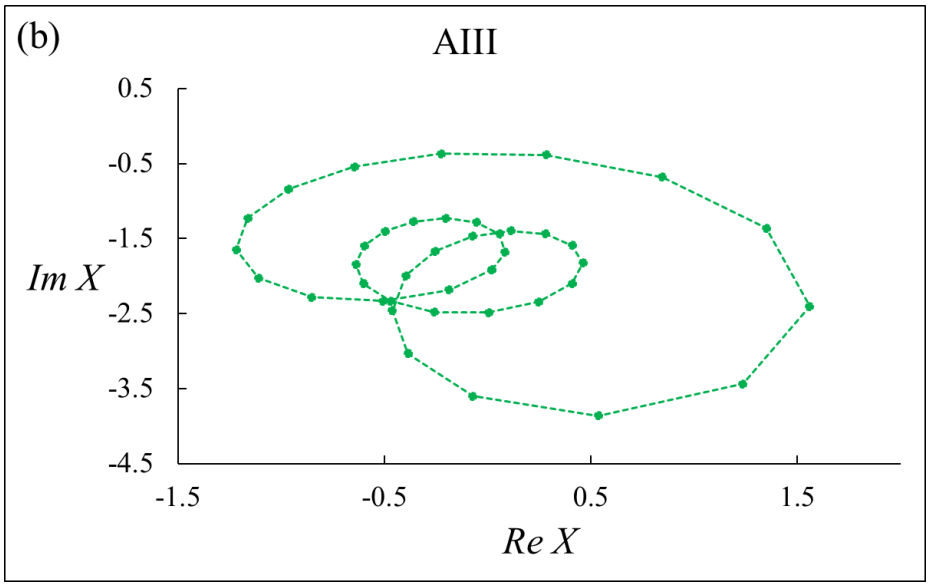
(b)
AIII
0.5
-0.5
-1.5
Im X
-2.5
-3.5
-4.5
-1.5
-0.5
0.5
1.5
Re X

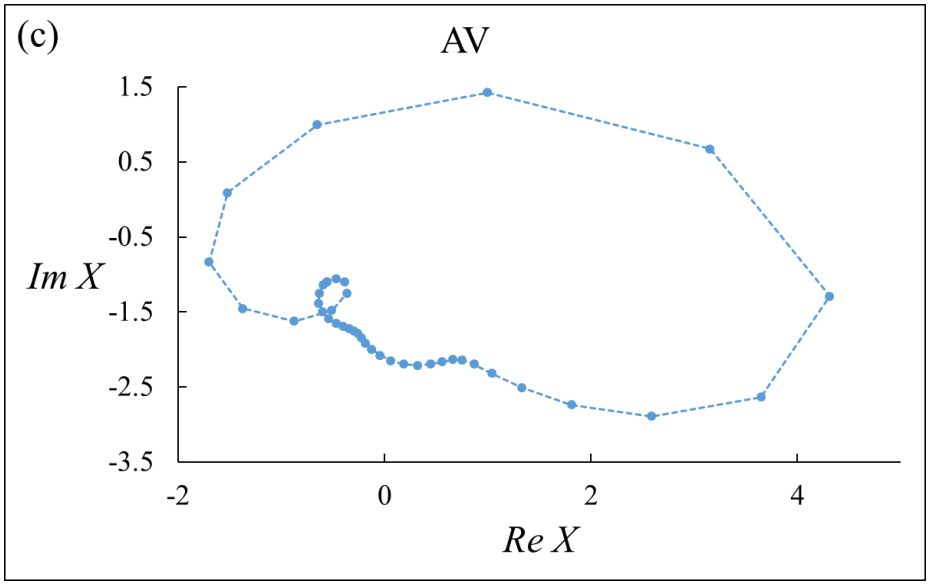

Figures 9: One period of motion for (a) AII in red, (b) AIII in green, and (c) AV in blue at *Y=1.83*. Each figure has 40 points that are evenly spaced in time depending on the period of the motion for each attractor. AII has a period of *~52τ*, AII has a period of *~156τ*, and AV has a period of *~208τ*.

As each point is moved away by the perturbation the new coordinate point is saved. This point becomes the initial condition for the system to evolve in time until it lands stably on an attractor. After enough time has elapsed the system either returns to the starting attractor or transitions to a coexisting attractor. The final attractor and the original perturbed coordinate is recorded. This is done for the full range of perturbations, $-0.3 \leq \delta v \leq 0.3$, for all *40* points around the attractor. The input field amplitude is then increased and the next *Y* value is evaluated using the same process. The full coexisting range of the two attractors is completed in this fashion. Then the whole procedure is repeated using a different base (starting) attractor, whether that is AII, AIII, or AV for this study. The number of times that the system lands on an attractor is plotted against each perturbation. The results for each base attractor are shown in Appendix IV. Figure 10 shows the perturbation to base attractor AII at *Y=1.68*, where only AII and AIII coexist. For small perturbations the system returns to AII, but once the system crosses a certain threshold it begins transitioning to AIII. The value of the threshold varies for each base attractor. Attractor AII requires

the largest perturbation to start transitioning to a coexisting attractor. A distinct difference can be seen in the positive and negative perturbations. The total chance of returning to AII is *71.20%*, while the chance of transitioning to AIII is *28.80%* of this *Y* value.

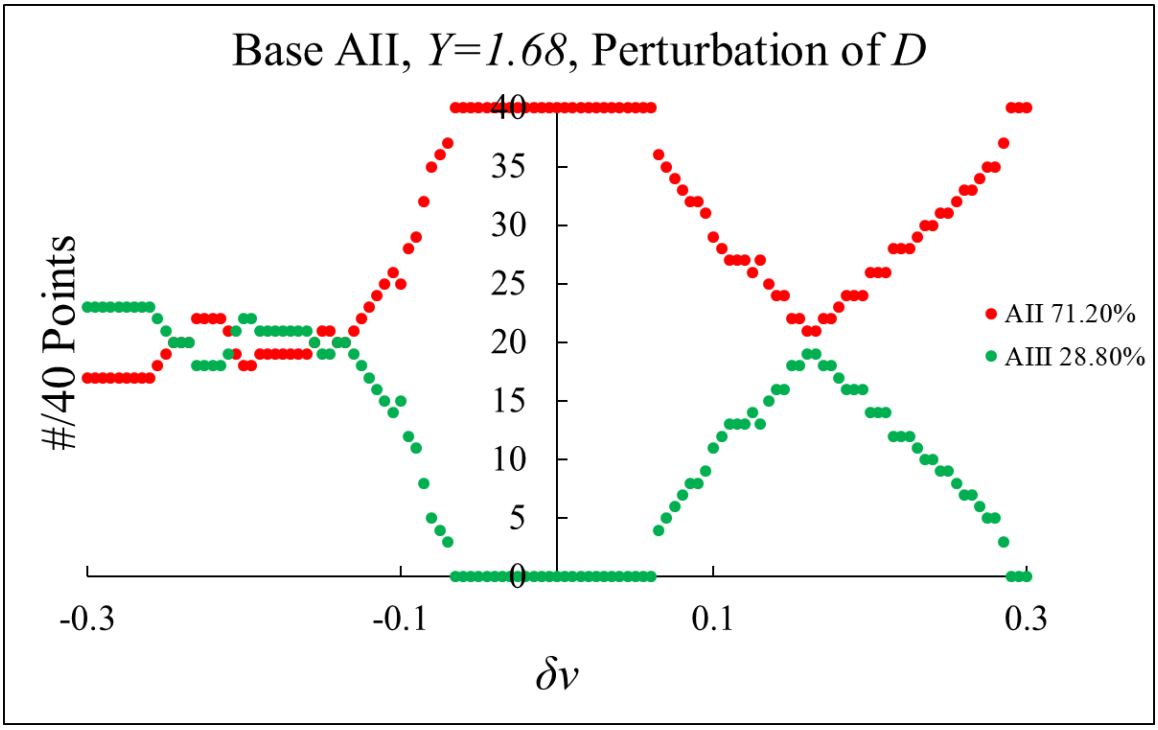

Figure 10: Perturbation for *Y=1.68* for the base attractor AII. The system returns to AII *71.20%* of the time, and transitions to AIII *28.80%* of the time.

2.6. Basins of Attraction

The basins of attraction are a time intensive way of visualizing which attractor the system ends on for a specific set of initial conditions once the system is allowed to evolve in time. To actually form the basin a large number of initial conditions must be used. An easy way of making the basin of attraction comprehensible is to use a 2-D plane that is a viewable slice of the 5-dimensional LIS system. The structure of the 5-D basin is determined by the five real nonlinear equations. So when looking at the slice of the basin, depending on how many coexisting attractors exist for that input value, different patterns can form. In Fig. 11 the basin for *Y=1.88* is shown for the state variables of *-0.5<D<0.5* verses *-1.5<Re X<2.5*. The other state variables are fixed and

each point on the graph is used as a set of initial conditions. Once the system is allowed to evolve in time all of the state variables can change. Only the initial conditions used to generate the plane and the final attractor the system lands on are recorded. For Fig. 11, the system only has two coexisting attractors for this value of the input field amplitude, AII in red and AV in blue. If the system were to start on any initial condition in this plane, then the attractor that the system stabilizes on is known. However, changes to any state variable that causes the system to move away from this region results in uncertainty as to the final state of the system. When the system has more than two coexisting attractors the complexity of the basin increases. For this LIS system the maximum number of known coexisting attractors is three.

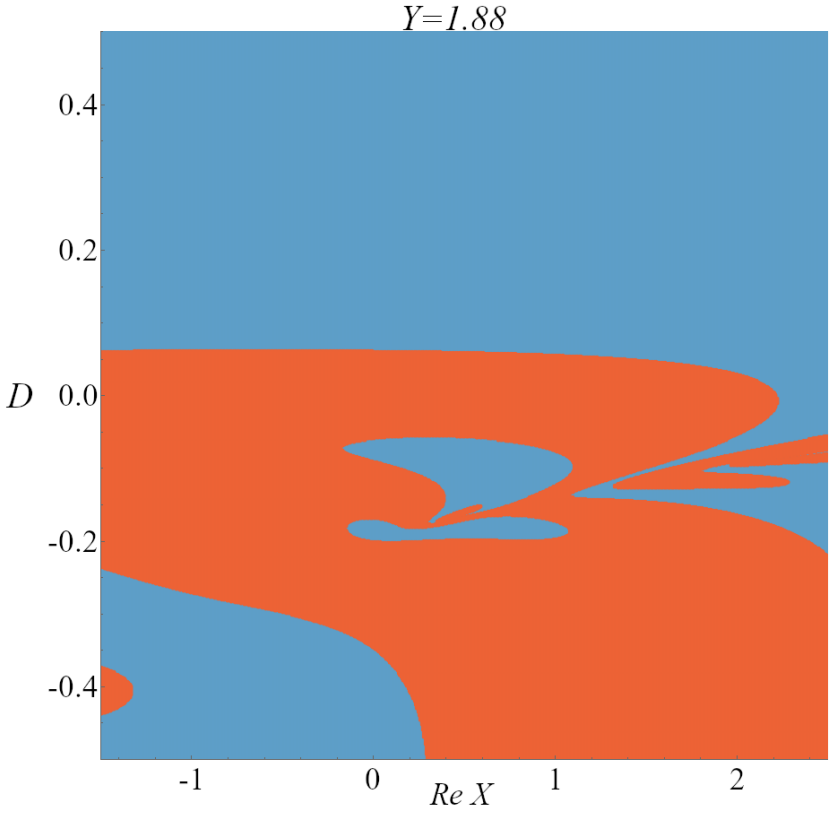

Figure 11: Basin of attraction for *Y=1.88*. The plot is a 2-D slice of a 5-D basin. The population difference, *D*, is plotted against the real component of the output field amplitude, *Re X*, for the ranges of *-0.5<D<0.5* and *-1.5<Re X<2.5*. The other variable are held constant for their use as initial conditions and are allowed to change as time evolves. *Im X=-2.2937*, *Re P=0.3035*, and *Im P=0.2611*.

Figure 12 shows the system with three coexisting attractors at *Y=1.823*. The basin at this value of *Y* is more complicated than the system with only two coexisting attractors. Other systems, whether that is for different parameters of LIS or an entirely different set of modeled equations, can have more coexisting attractors for the same value of the control parameter.

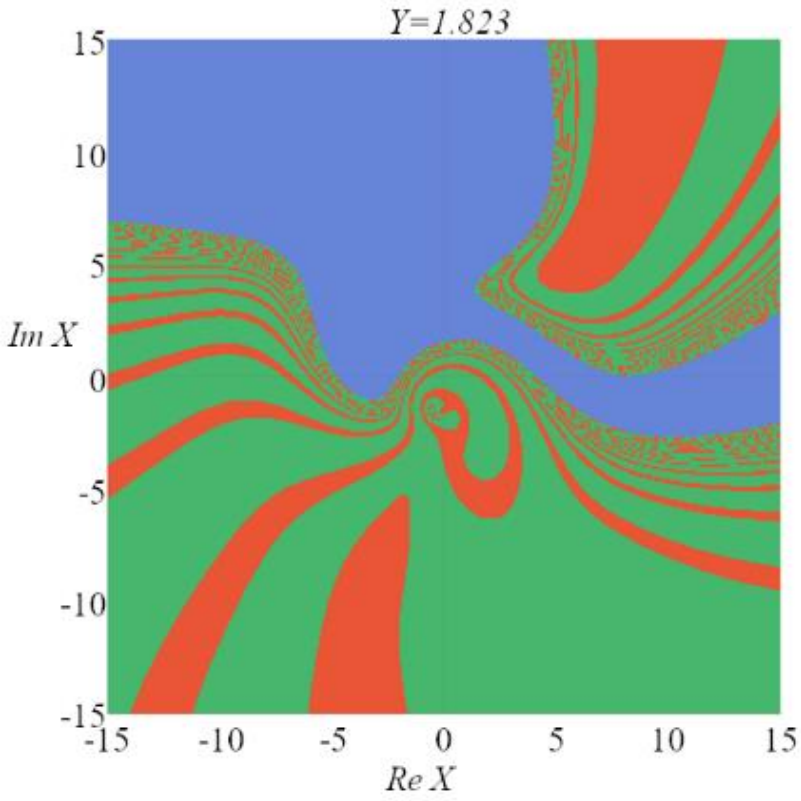

Figure 12: At *Y = 1.823* the basins of attraction for three coexisting attractors are illustrated as a two-dimensional slice in phase space. The system is evaluated as *Re X* and *Im X* are changed from *-15 to 15*, *D*, *Re P*, and *Im P* are held at zero. The colored regions correspond to the different coexisting attractors, AII is red, AIII is green, and AV is blue.

CHAPTER III

DATA AND ANALYSIS

The results for the Lyapunov exponent studies, the perturbation studies, and the corresponding analysis of the basins of attraction are discussed in this chapter. Further explanation of the LE patterns and predictions are expounded upon in the case of the symmetric-like bubble where a system parameter is changed. The results of the perturbations and the attractor schemes that are formed for each value of the input field amplitude are developed. A comparison is then made to the basins of attraction for these regions.

3.1. Lyapunov Exponents

Recently, LE patterns were found as predictors of system characteristics associated with the attractor's dynamics [27]. When a value of the system parameters is changed the LE spectrum demonstrates changes to the attractor's pattern. Figures 13 show these features for AIII as the value of the system's gain, *C*, is changed. The LIS system in this study has a gain at *C=3.0*, when the symmetric-like bubble was first found; the dynamics around the peak of the bubble were evaluated and no appreciable dynamic change was observed. So what did the symmetric-like bubble mean? The implication was that some potential change to the system might occur when a parameter is changed [28]. When the value of the gain was increased to *C=3.1* the system was found in fact to experience a bifurcation. Figure 13(c) shows the system at the new value of the gain; the system developed a bifurcation, 3P to 6P, at *Y=1.7233* and an inverse-bifurcation, 6P to 3P, at *Y=1.7709*. When the gain is decreased, Fig. 13(a), the system loses the symmetric-like bubble and instead has

a curved section of the LE spectrum where LE2=LE3<0.

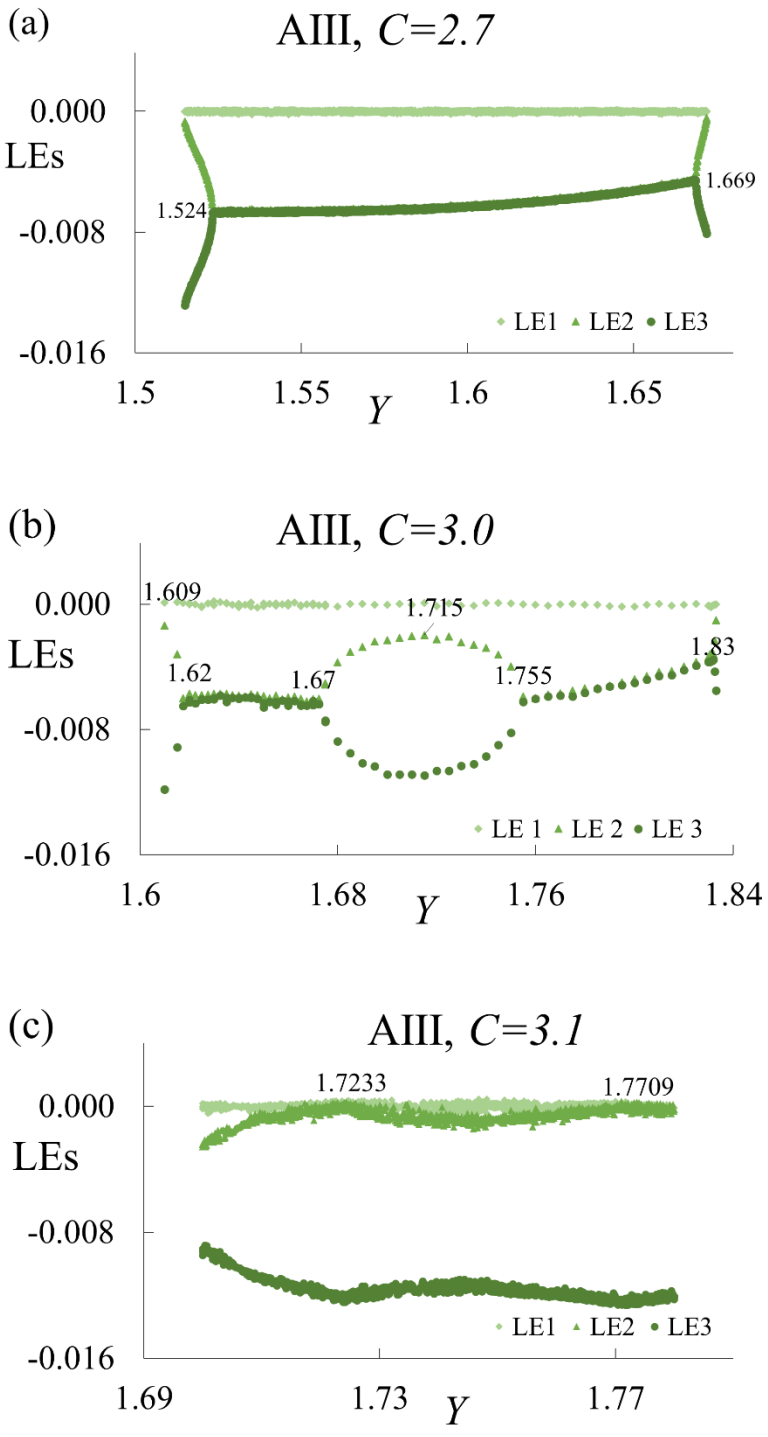

Figures 13: Variations in the gain for AIII. (a) Shows AIII when the gain is decreased to *C=2.7* causing the symmetric-like bubble to vanish. (b) At *C=3.0* the system has its symmetric-like bubble. Finally, (c) at *C=3.1* the symmetric-like bubble changes to a bifurcation and inverse-bifurcation sequence.

This pattern is observed in not only AIII but AV and AVI as well. As shown in Figs. 14 for AV and AVI, when the value of the gain is increased, the system develops from two equal LEs and forms a symmetric-like bubble. As the value of the gain is increased further, bifurcations start to appear in the system. In Fig. 14(g), another symmetric-like bubble forms when the gain is increased to *C=3.3*, and then further bifurcations are observed when the gain is increased to *C=3.35*, Fig. 14(h). Two interesting notes: (i) The system develops not only a bifurcation, but an inverse-bifurcation as the gain is increased. (ii) The changes to the gain cause the domain of the attractors to change as well.

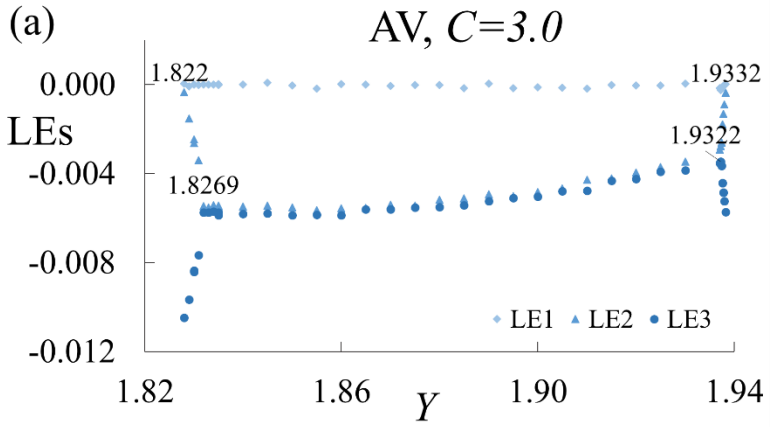

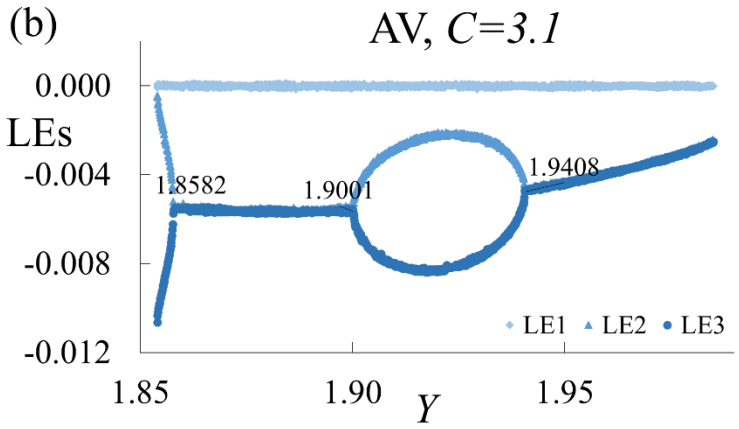

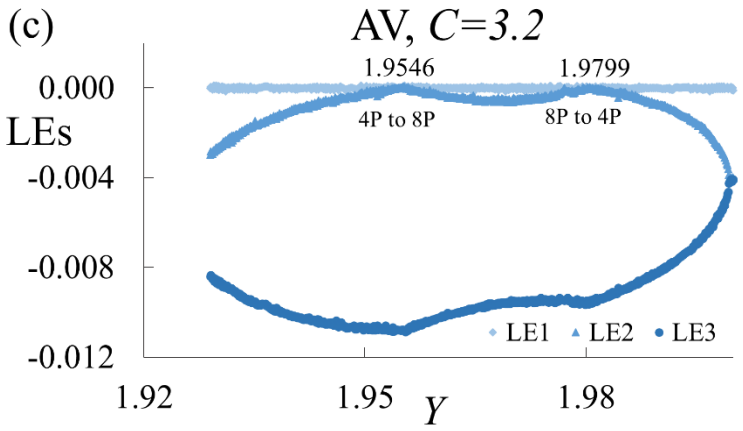
(c)
AV, C=3.2
1.9546
1.9799
4P to 8P
8P to 4P
0.000
LEs
-0.004
-0.008
-0.012
LE1
LE2
LE3
1.92
1.95
Y
1.98

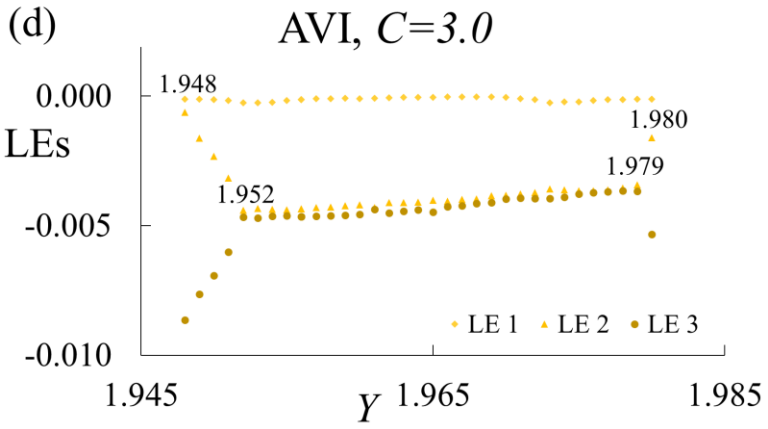
(d)
AVI, C=3.0
1.948
1.980
1.979
1.952
0.000
LEs
-0.005
-0.010
LE 1
LE 2
LE 3
1.945
Y
1.965
1.985

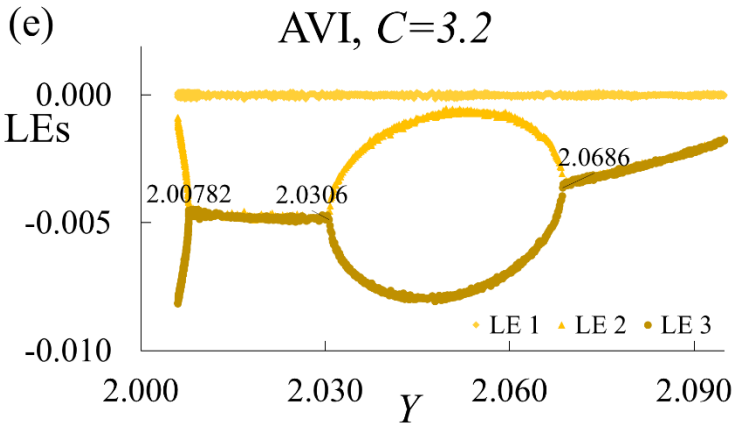
(e)
AVI, C=3.2
0.000
LEs
2.0686
2.00782
2.0306
-0.005
-0.010
LE 1
LE 2
LE 3
2.000
2.030
Y
2.060
2.090

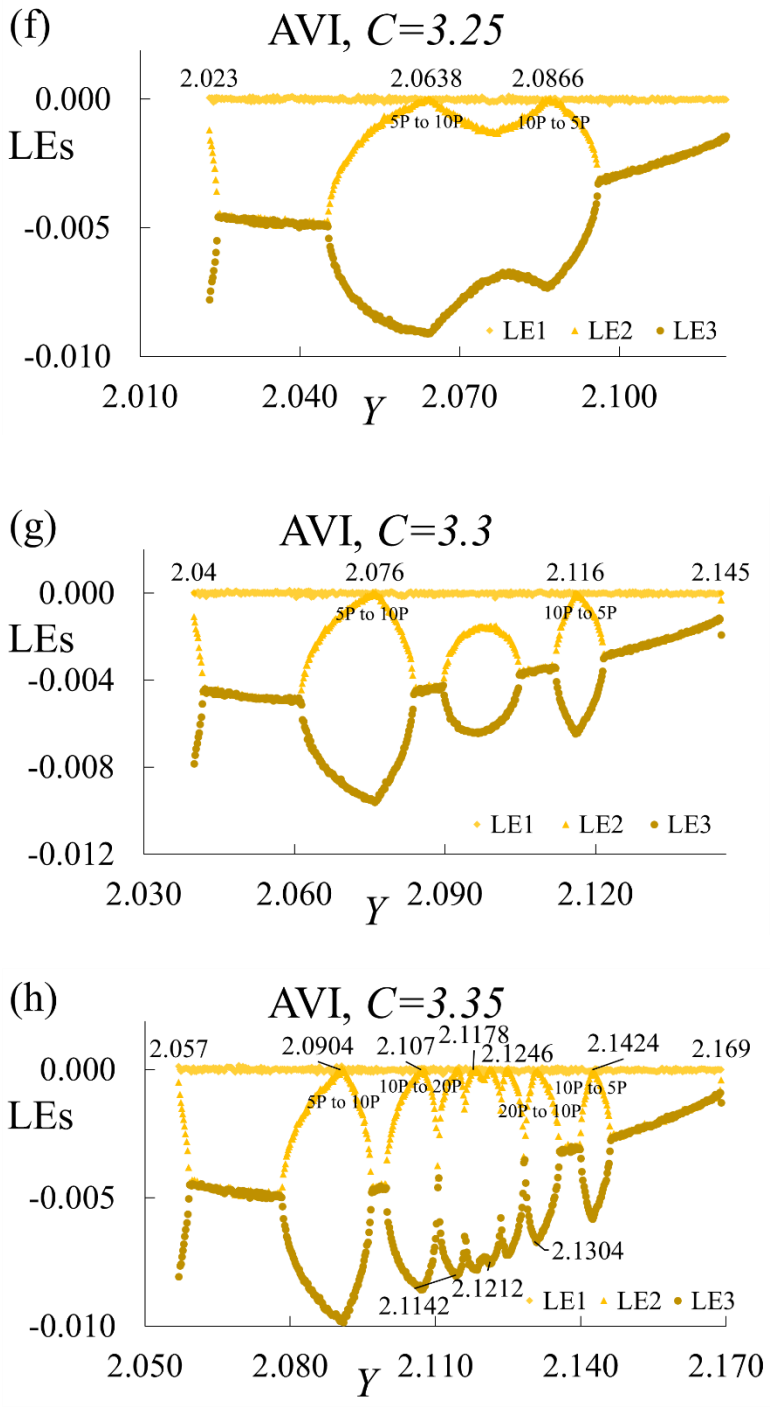

Figures 14: AV is shown with increasing gain in the system, (a) *C=3.0*, (b) *C=3.1*, and (c) *C=3.2*. The attractor transitions from two equal exponents, LE2=LE3, to a symmetric-like bubble followed by a bifurcation when the gain is increased further. AVI goes through the same series as the gain is increased from (d) *C=3.0* to (e) *C=3.2*, (f) *C=3.25*, (g) *C=3.3*, and (h) *C=3.35*. Another symmetric-like bubble forms in the

middle between the two bifurcation at (g) *C=3.3* which bifurcates further as the gain is increased to (h) *C=3.35*.

3.2. Perturbations and Basins of Attraction

The first set of perturbations that is evaluated for the system involves perturbing all of the state variables of the system. However, changing the output field amplitude $|X|$ is not experimentally viable. Further studies of the other parameters lead to the discovery that the polarization, *Re P* and *Im P*, caused an insignificant effect on the system when perturbed. This can be seen by comparing Figs 15. The system returns to AII for every perturbation of all 40 points around the attractor. When the system is perturbed for the state variable *D* however, the system transitions from the base attractor to one of the coexisting attractors a significant percentage of the time: The likelihood of the system returning to AII is *41.43%*, to AIII is *49.03%*, and to AV is *9.44%*. The perturbations were only evaluated for *D* due to the chance of transitioning attractors. The full domains of AIII, $1.61<Y<1.83$, and AV, $1.82<Y<1.93$, are evaluated using the perturbations. The domain of AII is so extensive that only the regions of coexistence are analyzed. It should also be noted that the order of magnitude of the population difference, *D*, is the same as the range of the perturbations.

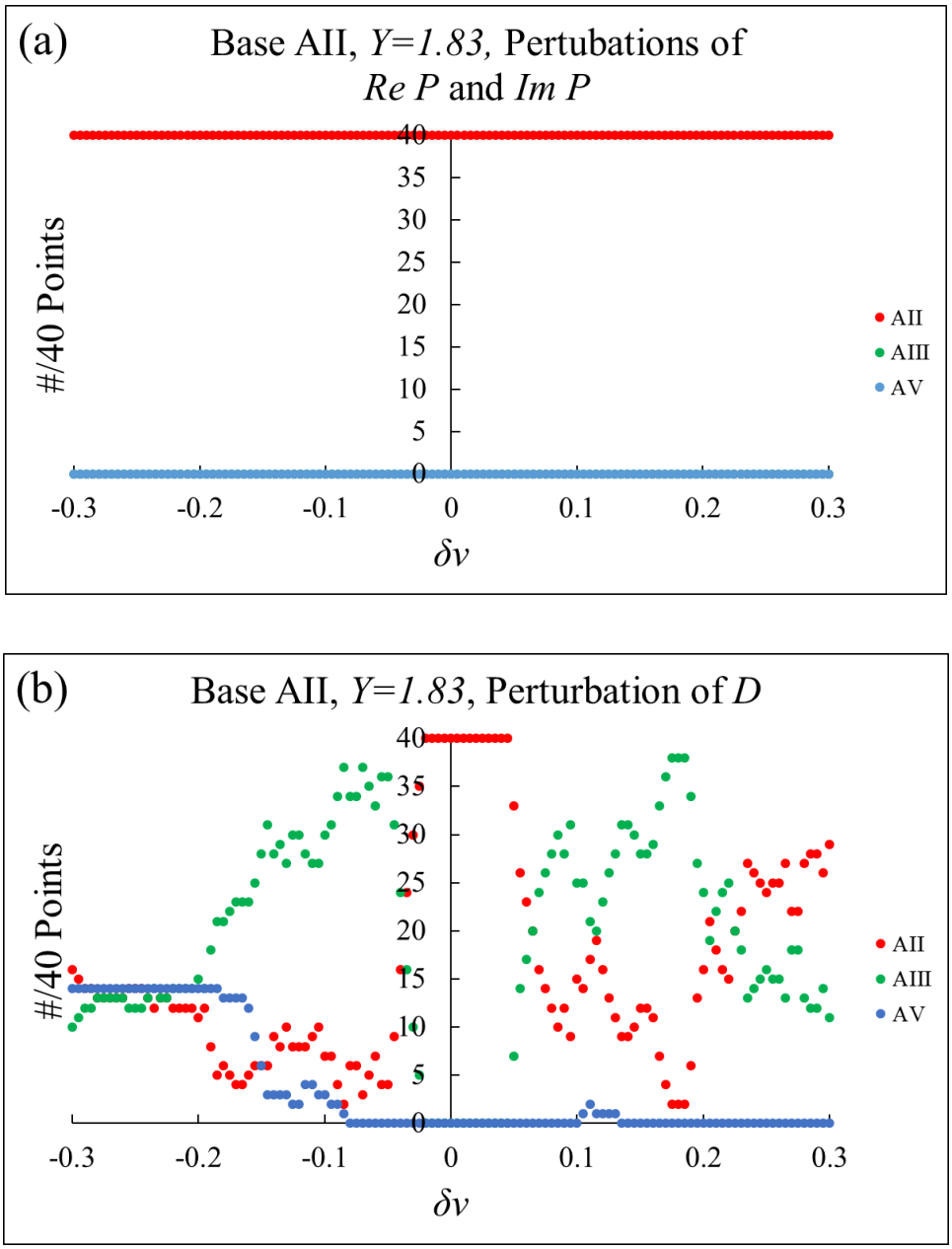

Figures 15: Perturbations from base AII where (a) *Re P* and *Im P* are perturbed, and (b) *D* is perturbed. The range of the perturbation is from $-0.3<\delta v<0.3$ in step of $\Delta\delta v = 0.005$. For the perturbations to the polarization, (a) the system never transitioned away from AII. When the perturbations are applied to the population difference, (b) the system returns to AII *41.43%* of the time and transitions to AIII *49.03%* of the time, and to AV *9.44%* of the time.

A significant difference is shown between positive and negative values of the perturbations. When the percentages are plotted against the input amplitude, Figs. 16 exhibit interesting features for several different base attractors in the coexisting region. For example, base attractors AII and AIII both show several changes to the slope of the data at the same values of *Y=1.695*, *1.75*, and *1.77* in both Figs. 16(a) and (b). Similarly, Figs. 16(a) and (c) both have changes in slope at the corresponding value of *Y=1.89*. It is certain the system experiences a change in either the dynamics, or some other property, that results in the slope change at these points of interest. Appendix IV shows the plots for all three of the discussed base attractors for each value of *Y* for the attractor's domain of existence.

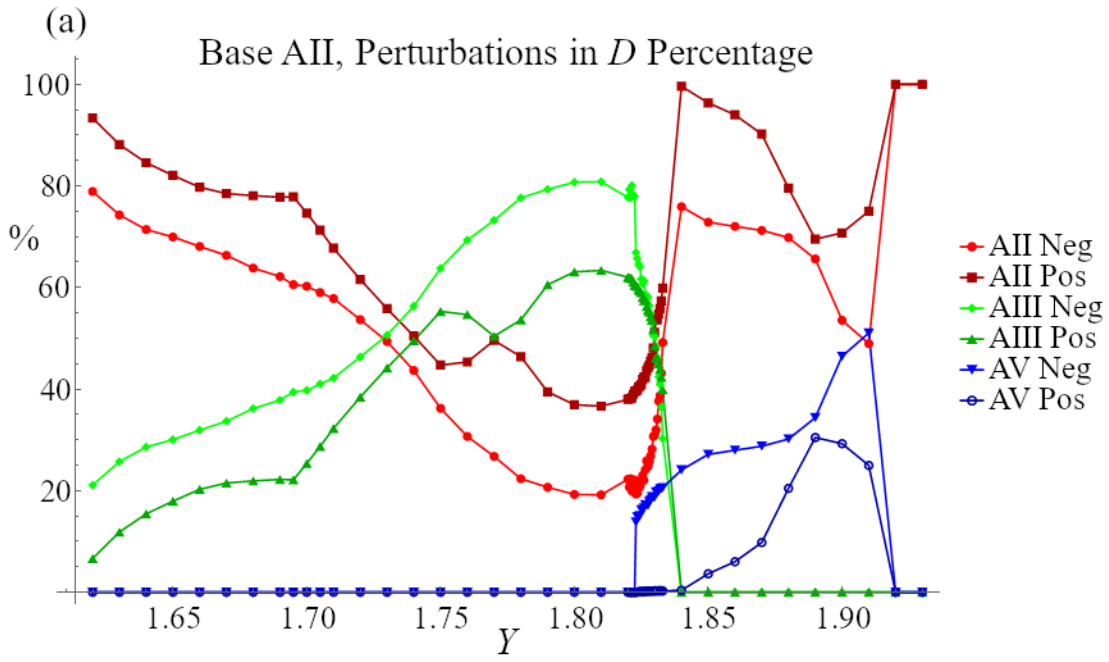

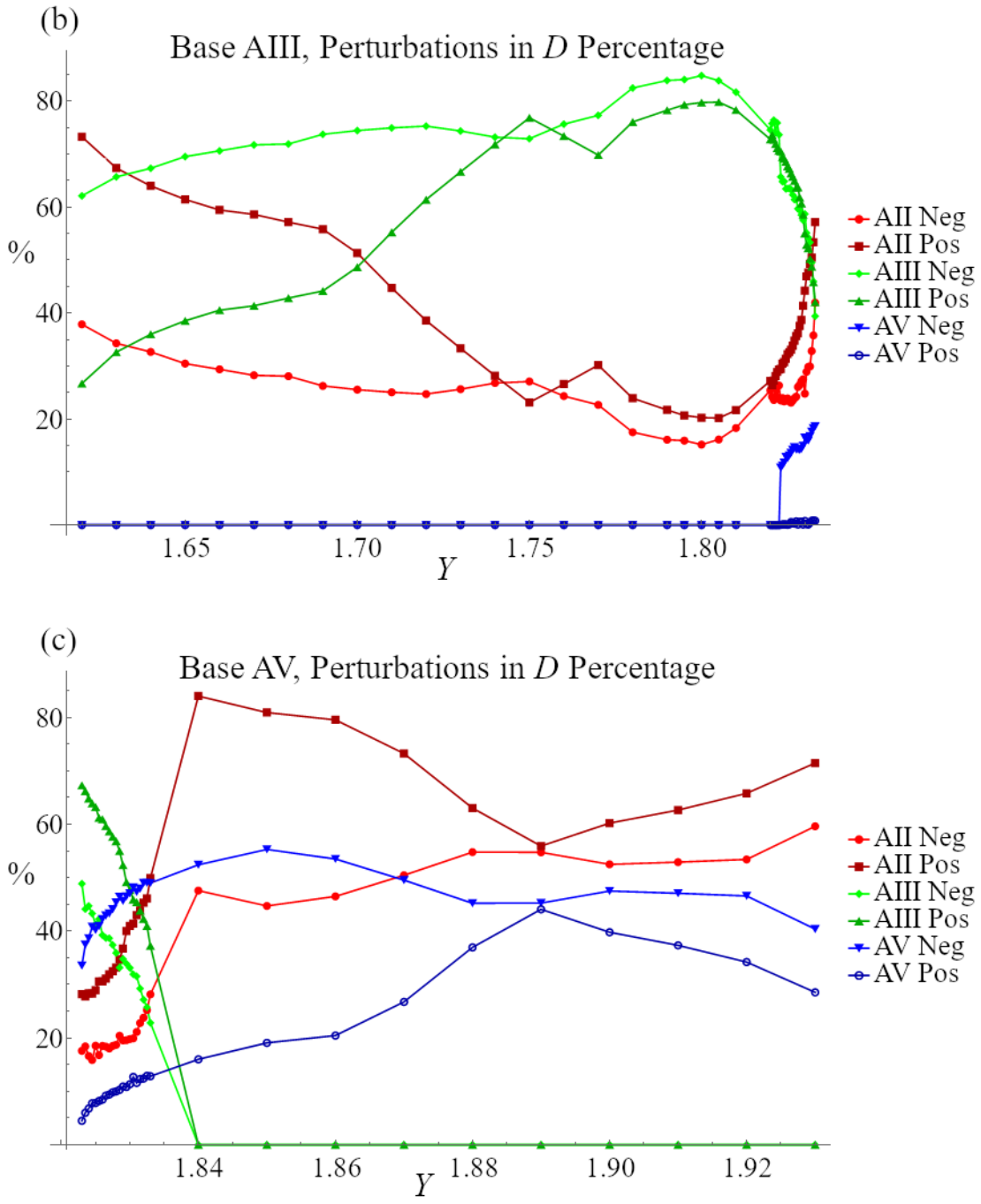

Figures 16: Percentage chance of transferring to an attractor with a positive or negative perturbation from base (a) AII, (b) AIII, and (c) AV.

The evaluation of the attractor dynamics where the slope of the data changes dramatically yields no significant change to the system. Figures 17 compares the temporal graphs, phase space plots, and Fourier analysis of AV at *Y=1.88*, *1.89*, and *1.90*. Comparing Figs. 17(a-c), no significant

change occurs between the temporal graphs. All three *Y* values have the same period of motion and similar amplitudes. For the phase space plots, minor changes to the size of the attractor's phase-space loops are visible. However, the increase in the control parameter could account for the changes to the loop size. The Fourier analysis for all three *Y* values show the height of the harmonics and subharmonics changing as *Y* is increased. Though the power of these peaks change again after this range of values as well. No significant change occurs in the system that correlates to the slope changes observed in Figs. 16. The volumes for each attractor show small dips do occur around the points of interest, as shown in Figs. 5. However, dips also occur that do not correlate to a change in the slope of the perturbation percentages. Finally an analysis of the system is explored by looking for changes in the basin of attraction.

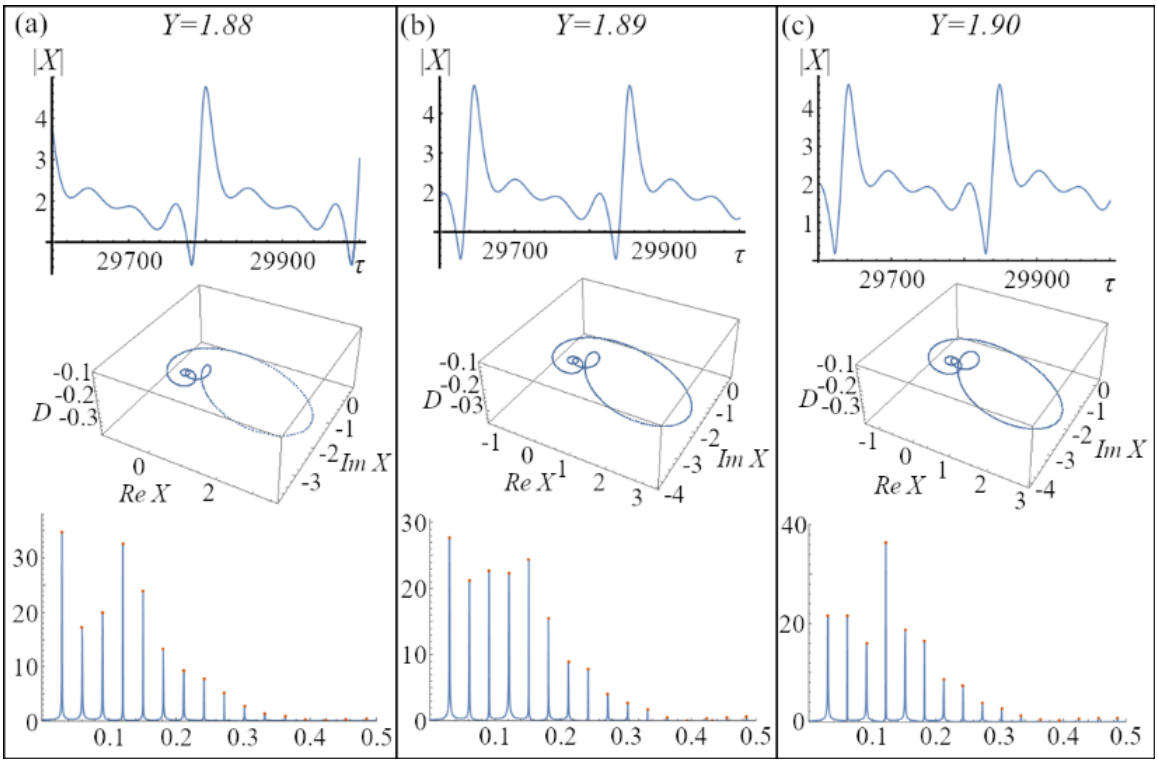

Figures 17: The temporal, phase space, and Fourier plots for AV at (a) *Y=1.88*, (b) *Y=1.89*, and (c) *Y=1.90*.

The basins of attraction show changes around these slope changes. Figures 18 show two perspectives: 2-D slices of the basin of attraction in phase space and the basin as a 2-D plot. The

basins shown in Figs. 18 are for the regions where only AII and AV coexist. This corresponds to the value of the input field amplitude around the point of interest *Y=1.89*. A clear difference can be observed between Figs. 18(a) and (b) when transitioning from *Y=1.88* to *Y=1.89*. In the upper region of the basin of attractor for Fig. 18(a) the system transitions to AV primarily for positive values of *D*. In Fig. 18(b) the positive domain of the population difference now primarily transitions for AII. Comparing Figs. 18(b) and (c) on the other hand shows less observable difference between the two basins. The shapes of the attractors in all three dimensions do not change significantly as previously observed.

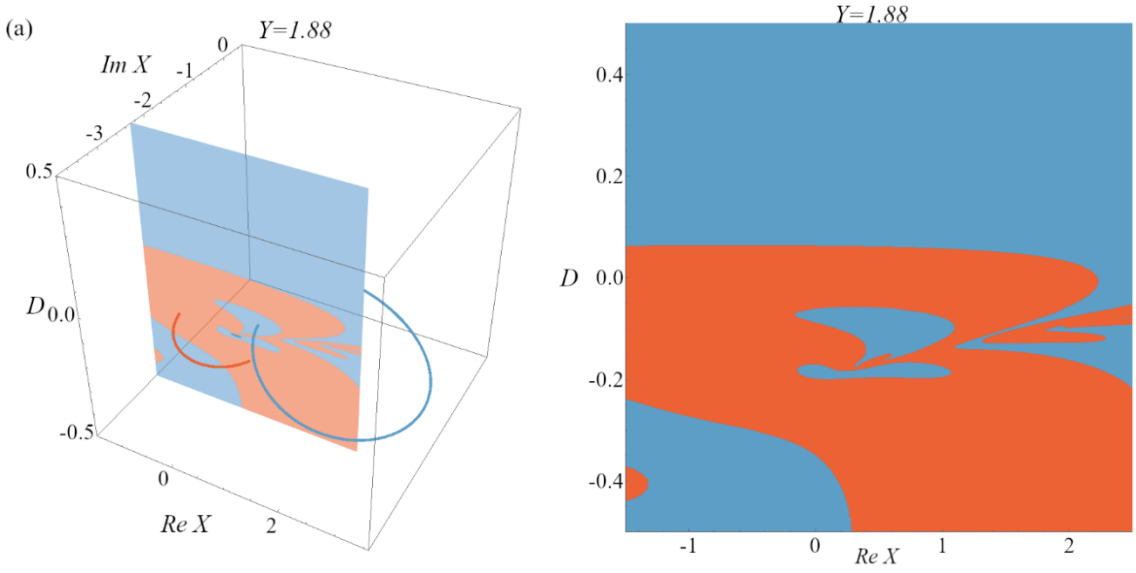

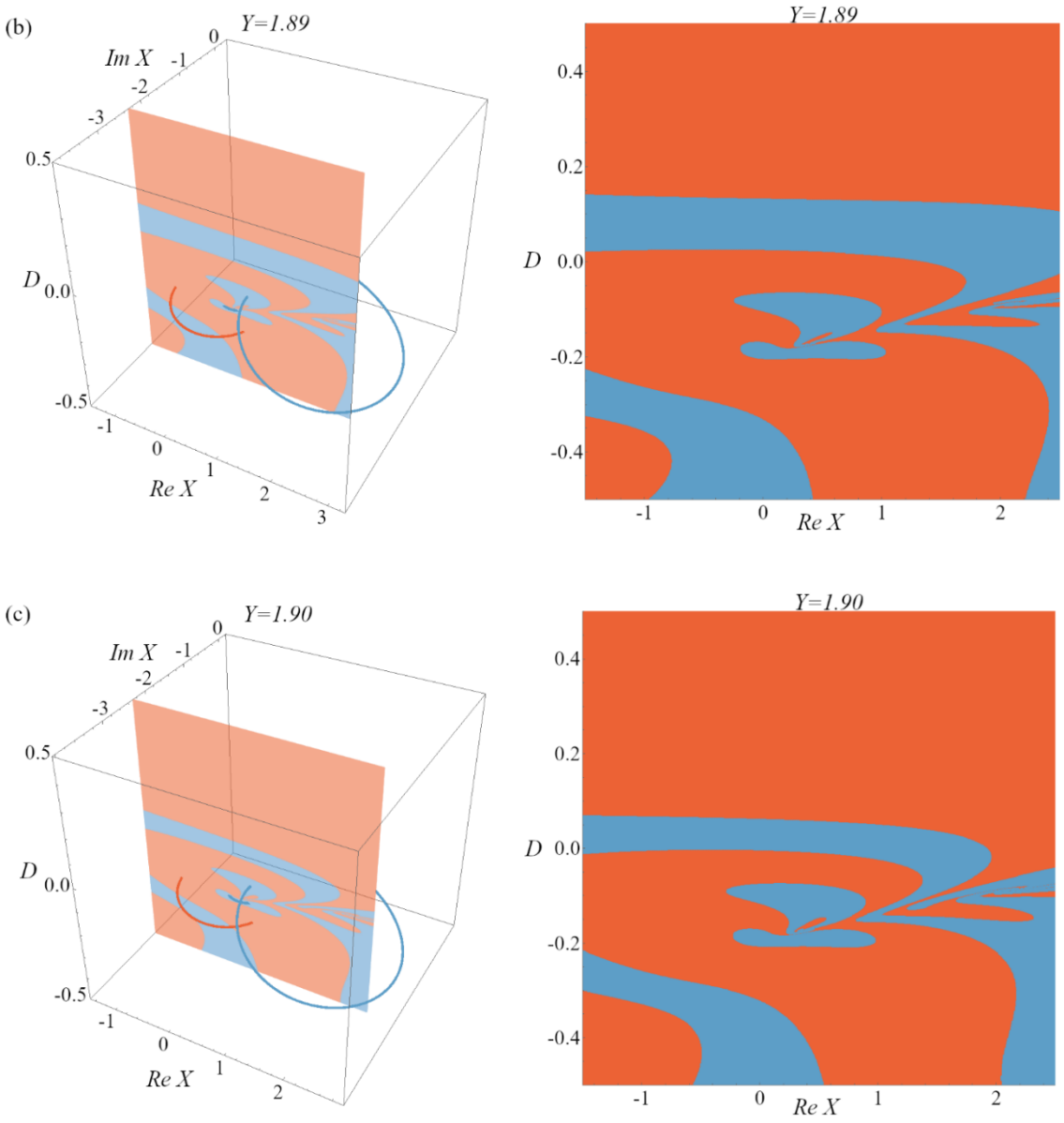

Figures 18: The basin of attraction of AII and AV at (a) *Y=1.88*, (b) *Y=1.89*, and (c) *Y=1.90*, also show the location of the slice is in the third dimension.

Another part of the perturbations that is predicted by the basins of attraction is seen when one point of the 40 points on the attractor is taken and perturbed with respect to the population difference, *D*. Since the basin is a 2-D plane with respect to the population difference *D vs Re X*, then the perturbation being applied to the system causes the point to move linearly up, or down, the plane depending on the perturbation sign. This line is shown in Fig. 19 for *Y=1.80*. Starting on base AII

located at the magenta dot, the black line denotes the path the initial conditions follow when perturbed in *D*. At this *Y* value only AII and AIII coexist. When the plot in Fig. 19 is compared to Fig. 20 in the region of positive or negative perturbation values, the magenta dot represents one value of the initial conditions that when perturbed causes the coordinates to cross from one attractor's domain in the basin to the other attractor's domain.

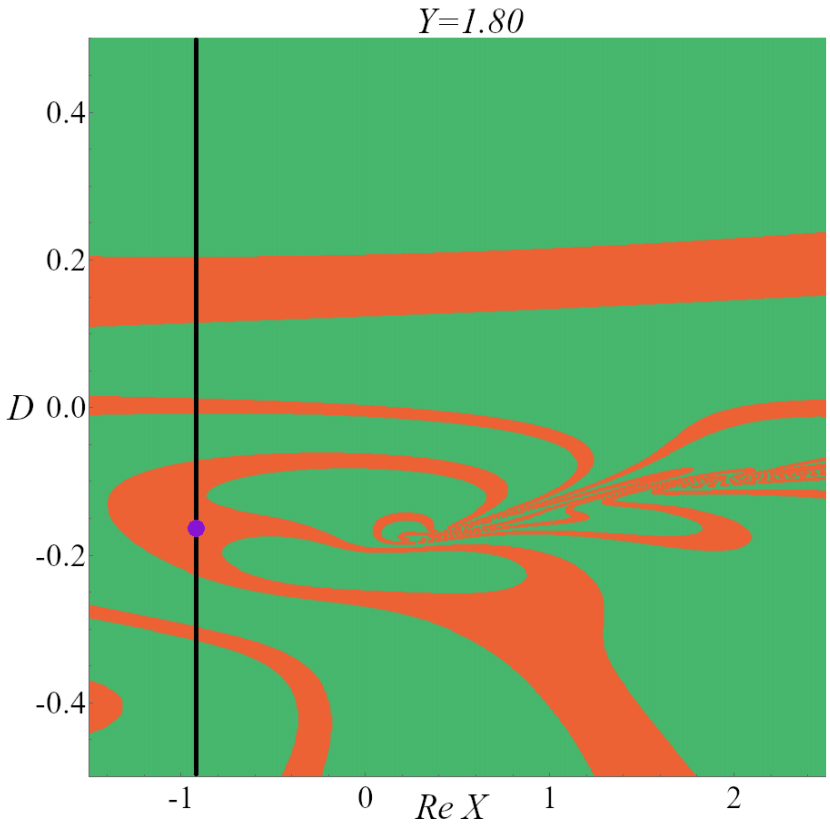

Figure 19: Basin of attraction for *Y=1.80*. The magenta point marks the location of AII when crossing through the plane. The black line shows where the coordinate point moves to if a perturbation in *D* were applied.

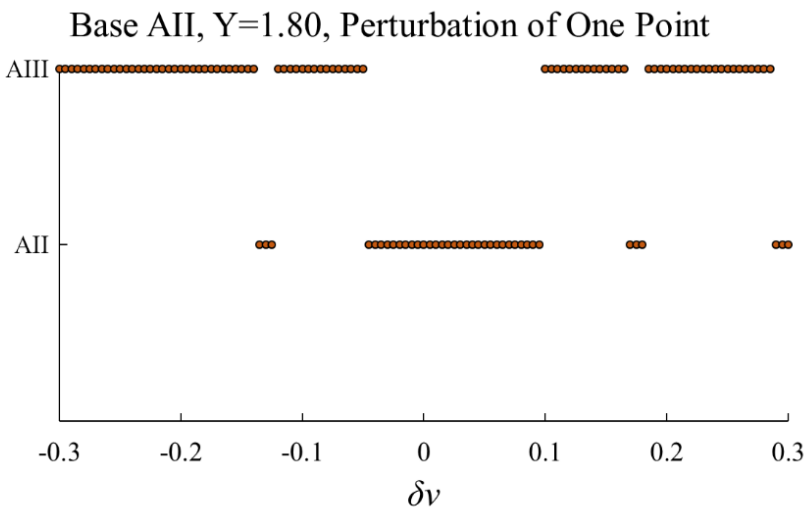

Figure 20: Changes in attractors occur for perturbations applied to a single point on base AII at *Y=1.80*. The attractor changes coincide with the basin of attraction shown in Fig. 19.

CHAPTER IV

CONCLUSIONS

This study of the laser with injected signal shows that attractor characteristics can be predicted using various methods of analysis. Using Lyapunov exponents it is possible to discover, identify, and predict dynamic behaviors of not only the LIS system actively being studied, but variations of other nonlinear systems as well. Symmetric-like bubbles and asymmetric bubbles configured by the LEs indicate immanent bifurcations and active bifurcations, respectively. The symmetric-like bubbles are the most interesting. Their initial mystery existence can now be explained by changing a system parameter, whereby the symmetric-like bubble becomes asymmetric; ergo the symmetric-like bubbles are forecasters of immanent bifurcation dynamics. Further universal LE boundary conditions were found to predict the origin and demise of the active regions of all given attractors—domains of existence. Note, these three LE configurations are also identified in a nonlinear optomechanical system that is more complex than LIS. Therefore, it is suggested that these defined LE patterns are universal predictors.

The investigation into perturbing the LIS system away from a base attractor to see whether the system transitions or not to the coexisting attractor results in an unexpected unique feature of the LIS system. There is a significant difference in attractor dispensation between the positive and negative perturbation values imposed on the population difference. When the occurrence percentages of the two attractors are plotted against the input amplitude, the system exhibits significantly different attractor percent schemes associated with negative perturbations versus that

of positive perturbations in the coexisting region. Investigations show interesting changes in the dynamics.

Another comparison is made between the perturbation results and the basins of attraction. This comparison shows that the system follows the basin of attraction for any set of initial conditions and lands on the attractor that the basin predicts. However, the way that the basin is calculated is by starting on sets of initial conditions and evolving them in time until the system lands on an attractor. This circular logic does not explain why the system has a sudden change to the basin between two closely valued control parameters, and it is not understood at this time. One other speculation is that the density of points around the attractor could change causing the shifts in the basin, though the periods of motion stay the same.

REFERENCES

[1] H. Haken, A nonlinear theory of laser noise and coherence. I, Z. Physik. 181 (1964) 96–124. https://doi.org/10.1007/BF01383921.

[2] H. Haken, A nonlinear theory of laser noise and coherence. II, Z. Physik. 182 (1965) 346–359. https://doi.org/10.1007/BF01383115.

[3] H. Haken, Theory of intensity and phase fluctuations of a homogeneously broadened laser, Z. Physik. 190 (1966) 327–356. https://doi.org/10.1007/BF01333598.

[4] H.M. Gibbs, S.L. McCall, T.N.C. Venkatesan, Differential Gain and Bistability Using a Sodium-Filled Fabry-Perot Interferometer, Phys. Rev. Lett. 36 (1976) 1135–1138. https://doi.org/10.1103/PhysRevLett.36.1135.

[5] R. Bonifacio, L.A. Lugiato, Cooperative effects and bistability for resonance fluorescence, Optics Communications. 19 (1976) 172–176. https://doi.org/10.1016/0030-4018(76)90335-7.

[6] R. Bonifacio, L.A. Lugiato, Mean field model for absorptive and dispersive bistability with inhomogeneous broadening, Lett. Nuovo Cimento. 21 (1978) 517–521. https://doi.org/10.1007/BF02763163.

[7] H.M. Gibbs, F.A. Hopf, D.L. Kaplan, R.L. Shoemaker, Observation of Chaos in Optical Bistability, Phys. Rev. Lett. 46 (1981) 474–477. https://doi.org/10.1103/PhysRevLett.46.474.

[8] F.T. Arecchi, R. Meucci, G. Puccioni, J. Tredicce, Experimental Evidence of Subharmonic Bifurcations, Multistability, and Turbulence in a Q -Switched Gas Laser, Phys. Rev. Lett. 49 (1982) 1217–1220. https://doi.org/10.1103/PhysRevLett.49.1217.

[9] A.T. Rosenberger, L.A. Orozco, H.J. Kimble, Observation of absorptive bistability with two-level atoms in a ring cavity, Phys. Rev. A. 28 (1983) 2569–2572. https://doi.org/10.1103/PhysRevA.28.2569.

[10] A.T. Rosenberger, L.A. Orozco, H.J. Kimble, P.D. Drummond, Absorptive optical bistability in two-state atoms, Phys. Rev. A. 43 (1991) 6284–6302. https://doi.org/10.1103/PhysRevA.43.6284.

[11] L.A. Orozco, A.T. Rosenberger, H.J. Kimble, Intrinsic Dynamical Instability in Optical Bistability with Two-Level Atoms, Phys. Rev. Lett. 53 (1984) 2547–2550. https://doi.org/10.1103/PhysRevLett.53.2547.

[12] L.A. Orozco, A.T. Rosenberger, H.J. Kimble, Optical bistability in the mixed absorptive-dispersive regime with two-state atoms, Phys. Rev. A. 36 (1987) 3248–3252. https://doi.org/10.1103/PhysRevA.36.3248.

[13] L.A. Orozco, H.J. Kimble, A.T. Rosenberger, L.A. Lugiato, M.L. Asquini, M. Brambilla, L.M. Narducci, Single-mode instability in optical bistability, Phys. Rev. A. 39 (1989) 1235–1252. https://doi.org/10.1103/PhysRevA.39.1235.

[14] H. Haken, Light: Laser Dynamics (North-Holland Physics, New York, 1985), Vol. 2.

[15] L.A. Lugiato, L.M. Narducci, D.K. Bandy, C.A. Pennise, Breathing, spiking and chaos in a laser with injected signal, Optics Communications. 46 (1983) 64–68. https://doi.org/10.1016/0030-4018(83)90032-9.

[16] J. Guckenheimer, P. Holmes, Nonlinear Oscillations, Dynamical Systems, and Bifurcations of Vector Fields, Springer Science & Business Media, 1983.

[17] F.T. Arecchi, G.L. Lippi, G.P. Puccioni, J.R. Tredicce, Deterministic chaos in laser with injected signal, Optics Communications. 51 (1984) 308–314. https://doi.org/10.1016/0030-4018(84)90016-6.

[18] D.J. Jones, D.K. Bandy, Attractors and chaos in the laser with injected signal, J. Opt. Soc. Am. B. 7 (1990) 2119. https://doi.org/10.1364/JOSAB.7.002119.

[19] E.K.T. Burton, J.R. Hall, D.M. Chapman, D.K. Bandy, Shifts in control parameter dynamically access individual attractors in a multistable system, Nonlinear Dyn. 105 (2021) 1877–1883. https://doi.org/10.1007/s11071-021-06667-x.

[20] D.K. Bandy, E.K.T. Burton, J.R. Hall, D.M. Chapman, J.T. Elrod, Predicting attractor characteristics using Lyapunov exponents in a laser with injected signal, Chaos. 31 (2021) 013120. https://doi.org/10.1063/5.0018586.

[21] G. Benettin, L. Galgani, J.-M. Strelcyn, Kolmogorov entropy and numerical experiments, Phys. Rev. A. 14 (1976) 2338–2345. https://doi.org/10.1103/PhysRevA.14.2338; G. Benettin, L. Galgani, A. Giorgilli, J.-M. Strelcyn, Lyapunov Characteristic Exponents for smooth dynamical systems and for hamiltonian systems; a method for computing all of them. Part 1: Theory, Meccanica. 15 (1980) 9–20. https://doi.org/10.1007/BF02128236

[22] Y. Gu, D.K. Bandy, J.-M. Yuan, L.M. Narducci, Bifurcation routes in a laser with injected signal, Phys. Rev. A. 31 (1985) 354–360. https://doi.org/10.1103/PhysRevA.31.354.

[23] Weiss, C.O. Instabilities And Chaotic Emission Of Far-Infrared NH3-Lasers.;

Abraham, N.B., Chrostowski, J., Eds.; Quebec City, Canada, October 14 1986; Vol. 0667, p. 26.

[24] Abraham, N.B.; Narducci, L.M. Laser Physics & Laser Instabilities; World Scientific Publishing Company: Singapore, 1988; ISBN 978-9971-5-0063-4.

[25] Weisstein, E.W. Attractor Available online: https://mathworld.wolfram.com/Attractor.html (accessed on 21 September 2021).

[26] Sprott, J.C.; Wang, X.; Chen, G. Coexistence of Point, Periodic and Strange Attractors. Int. J. Bifurcation Chaos 2013, 23, 1350093, doi:10.1142/S0218127413500934.

[27] J.R. Hall, E.K.T. Burton, D.M. Chapman, D.K. Bandy, Experimentally Viable Techniques for Accessing Coexisting Attractors Correlated with Lyapunov Exponents, Applied Sciences. 11 (2021) 9905. https://doi.org/10.3390/app11219905.

[28] C. Bonatto, J.C. Garreau, J.A.C. Gallas, Self-Similarities in the Frequency-Amplitude Space of a Loss-Modulated CO 2 Laser, Phys. Rev. Lett. 95 (2005) 143905. https://doi.org/10.1103/PhysRevLett.95.143905.

[29] Dimitrov, D.K.; Peña, J.M. Almost Strict Total Positivity and a Class of Hurwitz Polynomials. Journal of Approximation Theory 2005, 132, 212–223, doi:10.1016/j.jat.2004.10.010.

APPENDICES

Appendix 1. Class B and Class C Laser

The classification of lasers is defined by its relationship between the cavity linewidth and the material linewidths [23]. For a plane-wave ring laser: the Class B laser has the polarization relaxation rate much greater than the cavity relaxation rate which is greater than the relaxation rate of the population inversion, $\gamma_{\perp} >> \kappa >> \gamma_{\parallel}$, and "these lasers are often sensitive to harmonic perturbations$\sim\sqrt{(2\kappa\gamma_{\parallel}}$ (A-1)), where A is the threshold parameter. Laser frequencies are very close to cavity resonance frequencies" [23]. The Class C laser has all three rates approximately equal, $\kappa \sim\gamma_{\perp} \sim\gamma_{\parallel}$, and "Unstable oscillations from a single mode steady state are possible for $\kappa > \gamma_{\perp} + \gamma_{\parallel}$. Laser frequencies may be strongly pulled from cavity resonances towards the atomic frequency if $\kappa >> \gamma_{\perp}$." [23]

Appendix 2. Common Dynamic Analysis

Appendix 2.1. Temporal

Temporal plots are made by plotting the combined state variables, $|X| = \sqrt{A^2 + B^2}$, against time for a specific value of the input amplitude, *Y*. Numerical solutions must be obtained to generate the plots, and when on an attractor show that attractor's periodicity. This can be used to make a quick visual check to see if the system has landed on a certain attractor assuming that the attractors for the system are already known. Temporal graphs look at the time evolution of a single system variable. These two-dimensional plots typically are used to determine, roughly, the period and frequency of an attractor for a fixed value of *Y*. For a precise value of the frequency, or period, a Fourier analysis must be done. However, the temporal graphs also show the amplitude of the state variable observed, and the minimums and maximums for the oscillation within one period. In order to do this the set of five equations are solved numerically as the system evolves in time and then one of the state variables is plotted against time. The temporal plots of AII, AIII, and AV are shown in Figs. A1. The attractors have different periodicities associated with each. AIII has a period that is three times that of AII, because it has a subharmonic of 1/3 of its fundamental frequency it is considered a 3P. AV is a 4P due to its 1/4 subharmonic frequency. The period of the cycle is dictated by the subharmonics that the attractor has, this is shown further in the Fourier spectra. All three attractors coexist at the same value of the input amplitude, $Y = 1.83$, as shown in Fig. A4. These plots display the timing and amplitude of the attractor in terms of the output amplitude and can be used to identify the attractors.

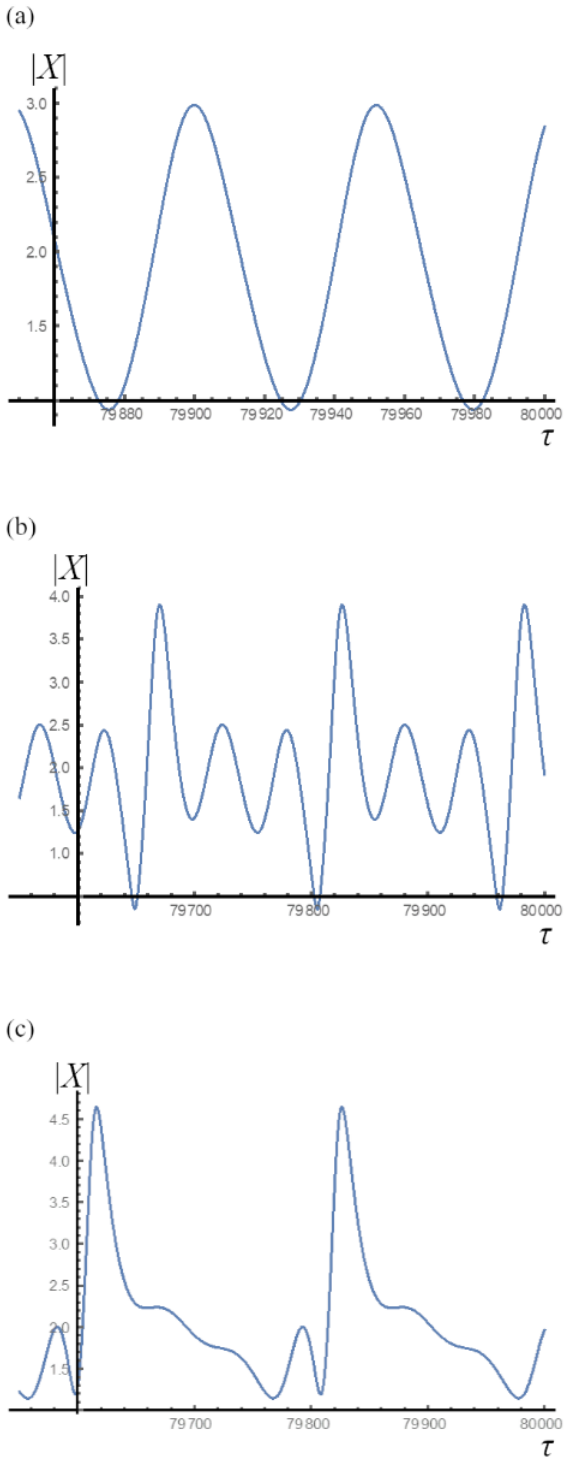

Figures A1: Temporal plots of the output field amplitude, $|X|$, vs time τ at $Y = 1.83$. (a) AII is a 1P limit cycle. (b) AIII is a 3P limit cycle (c) AV is a 4P.

Appendix 2.2. Fourier

A Fourier analysis is performed on the temporal graph, in order to obtain the frequencies of the attractor. These frequency plots have fundamental frequencies along with harmonics and subharmonics. These types of plots can clearly confirm the periodicity of an attractor based on the fundamental frequency and what fraction the smallest subharmonic it is of that frequency. A Fourier analyses is shown in Fig. A2. The graphs show the dominant frequency and harmonics or subharmonics of the attractor. The power spectra for AII, AIII, and AV are plotted at $Y=1.83$ in Figs. A2 (a-c), respectively. For this LIS system, each attractor has a shared commensurate frequency of ≈ 0.12. Some coexisting attractors have different multiples of harmonics and/or subharmonics. Due to these differences in their frequency spectra, the periods can be multiples of each other, in the case of commensurate frequencies.

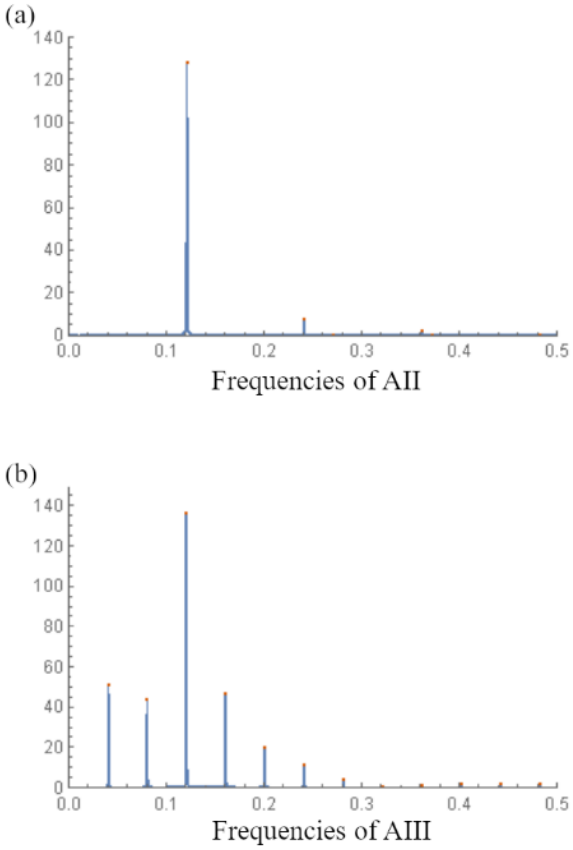

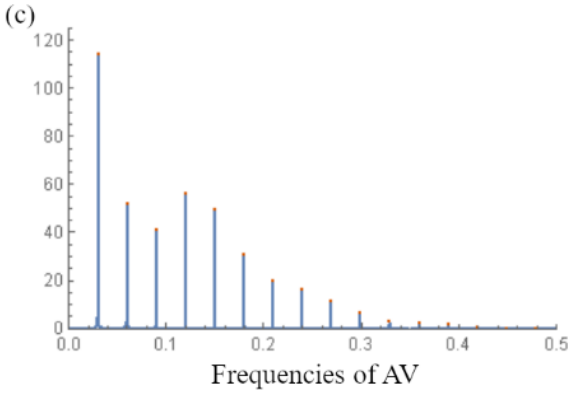

Figures A2: Fourier spectra for (a) AII, (b) AIII, and (c) AV. AIII and AV both have subharmonics as fractions of the shared frequency ≈*0.12*.

Appendix 2.3. Phase Space

As written above after the system is solved numerically three of the five system variable are plotted in order to view a 3-dimensional representation of the attractor. Depending on the attractor's frequencies and harmonics/sub-harmonics the attractor can appear as a variety of 3-dimensional shapes that loop back onto itself. The simplest is an elliptical shape, but they can be as complicated as an n-dimension torus. A phase-space graph is a three-dimensional plot of three of the five state variables as the system evolves in time. The attractors are typically plotted using the *Re X*, *Im X*, and *D*. For this discussion $Y = 1.83$ continues to be the control parameter. Figure A3 shows the phase space for AII, AIII, and AV, with each receiving its own phase space plot. All three coordinates are plotted as a function of time, forming the limit cycles shown. Figure 2 shows the full domain of coexistence is from $1.822<Y<1.833$.

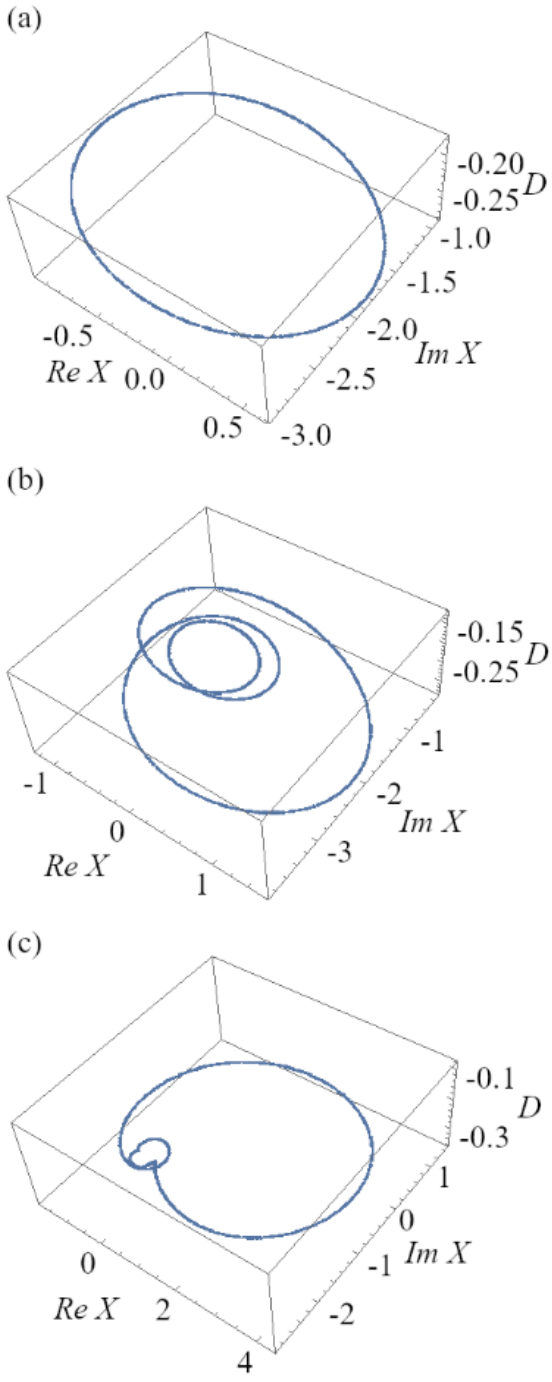

Figures A3: Phase space plots of Re *X*, Im *X*, and *D* for three coexisting attractors at *Y = 1.83*. (a) The 1P limit cycle for AII. (b) The 3P limit cycle for AIII. (c) The 4P limit cycle for AV.

Since all three attractors coexist for a domain of *Y*, Figure A4 shows AII, AIII, and AV at *Y=1.83*. The Xs mark the region where the density is lowest for the number of points plotted in phase space.

The dots mark where the points are densest. The density corresponds to how far the system travels in a single unit of time. Where longer distance cause lower densities, and short distance higher densities.

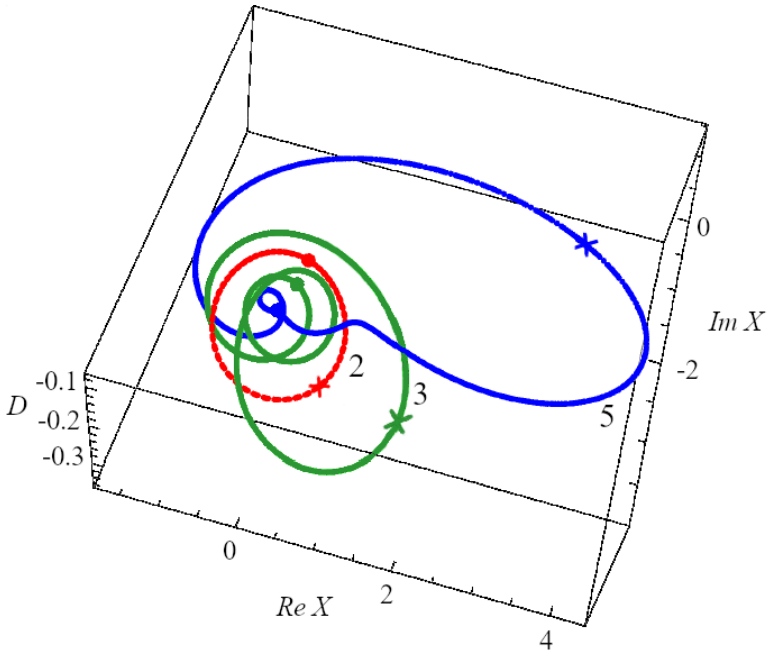

Figure A4: Phase space plot of three coexisting attractors at *Y=1.83*: AII, AIII, and AV in red, green, and blue, respectively. The dots show the location on the attractor where the density of points is greatest, while the Xs show the location where the density of points is least.

Appendix 3. Hurwitz Criterion

In this section the coefficients from the fifth order polynomial in λ, equation (10), are given. They are in terms of the system parameters and the modulus of the output field amplitude. For example, A=Ass + δA, where Ass is the steady state and δA is an extremely small step away from that steady state such that δA2 is considered zero. When the partial derivative with respect to each of the state variables small perturbation is taken for the current equations, since the steady states are constant they go to zero. The only terms remaining are with respect to the state variable after the partial derivative is applied. The solution of $c_i*e^{\lambda t}$ is used, where i=0, 1, 2, 3, 4, or 5. This gives a 5x5 matrix, where each diagonal has a λ-term. The determinant is taken to get a fifth order polynomial in terms of λ. The coefficients are used in the stability analysis. It should be noted that the K's are actual $\tilde{\kappa}$ and that other tildes are dropped due to programming limitations. The coefficients *must be positive to be considered stable, as well as the Hurwitz determinants*. The Hurwitz determinants [29] form the following matrix, equation (11), and are determined by the number of coefficients that are in the polynomial, each determinant, h_n, is the determinant of an n × n matrix, where n = 1, 2, 3, ….

$$c_0 \lambda^5 + c_1 \lambda^4 + c_2 \lambda^3 + c_3 \lambda^2 + c_4 \lambda^1 + c_5 \tag{10}$$

$$c0 = 1;$$

$$c1 = 2 + \gamma + 2K;$$

$$c2 = 1 + 2\gamma + \text{Abs}[x]^2\gamma + \Delta^2 + 4K + 2\gamma K + K^2 + \phi^2 - \frac{4cK}{1+\Delta^2+\text{Abs}[x]^2} - \frac{4c\Delta^2 K}{1+\Delta^2+\text{Abs}[x]^2};$$

$$c3 = \gamma + \text{Abs}[x]^2\gamma + \gamma\Delta^2 + 2K + 4\gamma K + 2\,\text{Abs}[x]^2\gamma K + 2\Delta^2 K + 2K^2 + \gamma K^2 + 2\phi^2 + \gamma\phi^2 - \frac{4cK}{1+\Delta^2+\text{Abs}[x]^2} - \frac{4c\gamma K}{1+\Delta^2+\text{Abs}[x]^2} - \frac{2c\,\text{Abs}[x]^2\gamma K}{1+\Delta^2+\text{Abs}[x]^2} - \frac{4c\Delta^2 K}{1+\Delta^2+\text{Abs}[x]^2} - \frac{4c\gamma\Delta^2 K}{1+\Delta^2+\text{Abs}[x]^2} - \frac{4cK^2}{1+\Delta^2+\text{Abs}[x]^2} - \frac{4c\Delta^2 K^2}{1+\Delta^2+\text{Abs}[x]^2};$$

$$c4 = 2\gamma K + 2\,\text{Abs}[x]^2\gamma K + 2\gamma\Delta^2 K + K^2 + 2\gamma K^2 + \text{Abs}[x]^2\gamma K^2 + \Delta^2 K^2 + \phi^2 + 2\gamma\phi^2 + \text{Abs}[x]^2\gamma\phi^2 + \Delta^2\phi^2 + \frac{4c^2K^2}{(1+\Delta^2+\text{Abs}[x]^2)^2} + \frac{8c^2\Delta^2K^2}{(1+\Delta^2+\text{Abs}[x]^2)^2} + \frac{4c^2\Delta^4K^2}{(1+\Delta^2+\text{Abs}[x]^2)^2} - \frac{4c\gamma K}{1+\Delta^2+\text{Abs}[x]^2} - \frac{4c\gamma\Delta^2K}{1+\Delta^2+\text{Abs}[x]^2} - \frac{4cK^2}{1+\Delta^2+\text{Abs}[x]^2} - \frac{4c\gamma K^2}{1+\Delta^2+\text{Abs}[x]^2} + \frac{2c\,\text{Abs}[x]^2\gamma K^2}{1+\Delta^2+\text{Abs}[x]^2} - \frac{4c\Delta^2K^2}{1+\Delta^2+\text{Abs}[x]^2} - \frac{4c\gamma\Delta^2K^2}{1+\Delta^2+\text{Abs}[x]^2} - \frac{4c\Delta K\phi}{1+\Delta^2+\text{Abs}[x]^2} - \frac{2c\,\text{Abs}[x]^2\gamma\Delta K\phi}{1+\Delta^2+\text{Abs}[x]^2} - \frac{4c\Delta^3K\phi}{1+\Delta^2+\text{Abs}[x]^2};$$

$$c5 = \gamma K^2 + \text{Abs}[x]^2\gamma K^2 + \gamma\Delta^2K^2 + \gamma\phi^2 + \text{Abs}[x]^2\gamma\phi^2 + \gamma\Delta^2\phi^2 + \frac{4c^2\gamma K^2}{(1+\Delta^2+\text{Abs}[x]^2)^2} - \frac{4c^2\,\text{Abs}[x]^2\gamma K^2}{(1+\Delta^2+\text{Abs}[x]^2)^2} + \frac{8c^2\gamma\Delta^2K^2}{(1+\Delta^2+\text{Abs}[x]^2)^2} - \frac{4c^2\,\text{Abs}[x]^2\gamma\Delta^2K^2}{(1+\Delta^2+\text{Abs}[x]^2)^2} + \frac{4c^2\gamma\Delta^4K^2}{(1+\Delta^2+\text{Abs}[x]^2)^2} - \frac{4c\gamma K^2}{1+\Delta^2+\text{Abs}[x]^2} - \frac{4c\gamma\Delta^2K^2}{1+\Delta^2+\text{Abs}[x]^2} - \frac{4c\gamma\Delta K\phi}{1+\Delta^2+\text{Abs}[x]^2} - \frac{4c\gamma\Delta^3K\phi}{1+\Delta^2+\text{Abs}[x]^2};$$

$$H = \begin{pmatrix} c_1 & c_3 & c_5 & 0 & 0 \\ c_0 & c_2 & c_4 & 0 & 0 \\ 0 & c_1 & c_3 & c_5 & 0 \\ 0 & c_0 & c_2 & c_4 & 0 \\ 0 & 0 & c_1 & c_3 & c_5 \end{pmatrix} \tag{11}$$

The Hurwitz determinants must also be positive for the system to be stable. If even one coefficient or determinant is negative the system is determined to be unstable at that point. The system is evaluated for each value of the input parameter. The Hurwitz determinants, the principal minors of the matrix generated from the 5th order polynomial, and the coefficients must both be positive for

the system to be considered stable. A single negative coefficient or determinant means that the system is unstable. The results from this analysis are used to find any instabilities in the system and the location of those regions of instability. If the system exhibits a stable behavior, then has a fixed output with no oscillations for a specific input value, a steady state. The explicit determinants are written below.

$$h_1 = c_1 \tag{12}$$

$$h_2 = c_1 c_2 - c_0 c_3 \tag{13}$$

$$h_3 = c_1 (c_2 c_3 - c_1 c_4) - c_0 (c_3^2 - c_1 c_5) \tag{14}$$

$$h_4 = c_1 [-c_5(c_2^2 - c_0 c_4) + c_4(c_2 c_3 - c_1 c_4)] - c_0 [-c_5 (c_2 c_3 - c_0 c_5) + c_4 (c_3^2 - c_1 c_5)] \tag{15}$$

$$h_5 = c_5 h_4 \tag{16}$$

Appendix 4. Perturbations

Perturbations for individual values of the input amplitude for AII, AIII, and AV. These plots were combined to make the plots in Figs. 16. Each plot looks at 40 points around the attractor for one period of the motion. Each of those points are perturbed off of each of those points for a total range of $-0.3<\delta v<0.3$ by steps of $\Delta\delta v = 0.005$. The figures are in order of increasing input field amplitude. Starting with AII in Appendix IV.1, AII in Appendix 4.2, and AV in Appendix 4.3.

Appendix 4.1. AII Perturbations

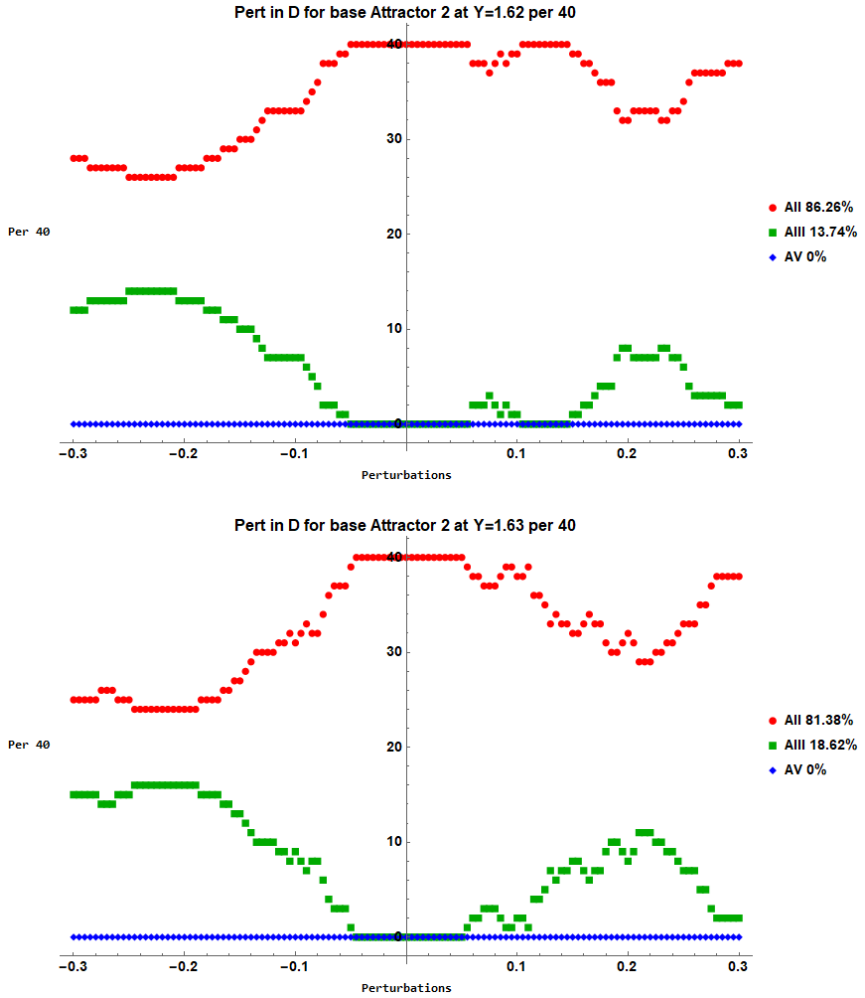

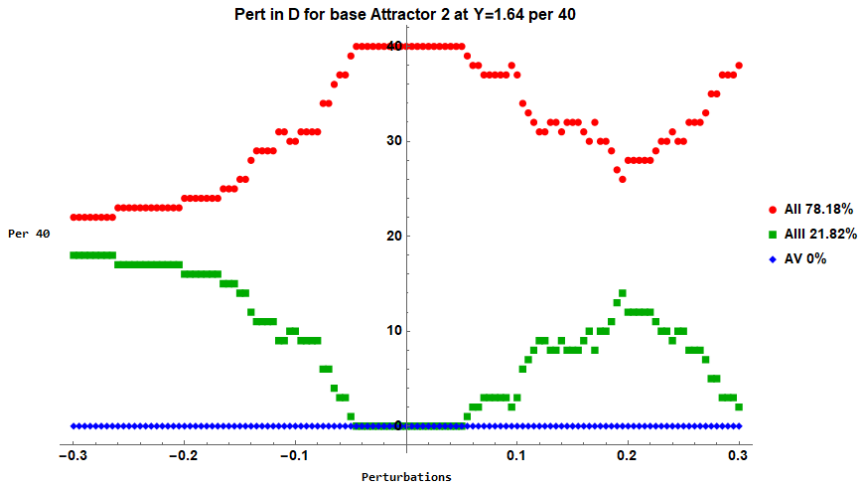
Pert in D for base Attractor 2 at Y=1.64 per 40
Per 40
Perturbations
All 78.18%
AIII 21.82%
AV 0%

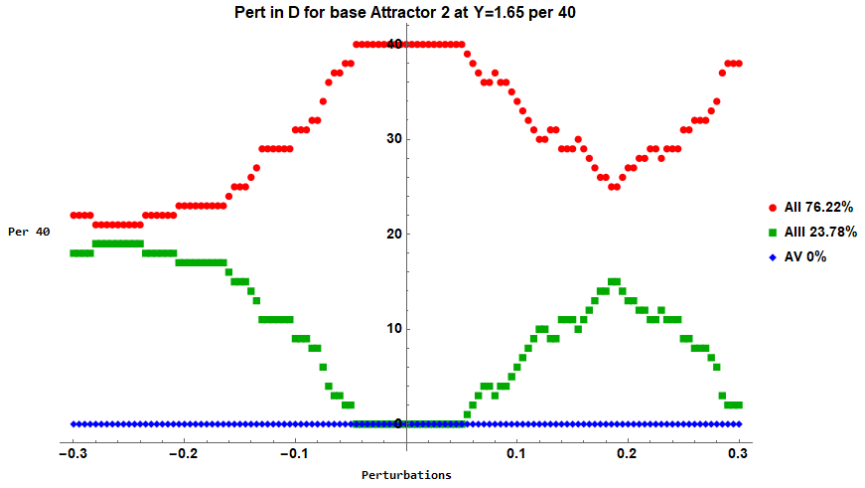
Pert in D for base Attractor 2 at Y=1.65 per 40
Per 40
Perturbations
All 76.22%
AIII 23.78%
AV 0%

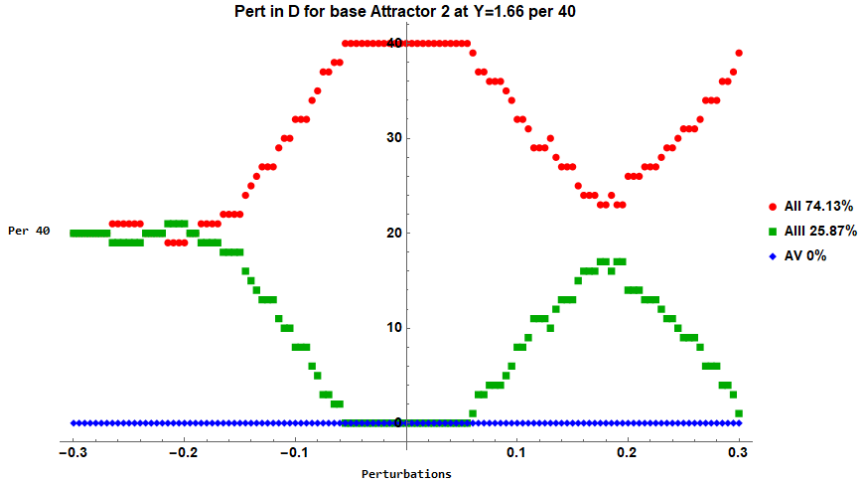
Pert in D for base Attractor 2 at Y=1.66 per 40
Per 40
Perturbations
All 74.13%
AIII 25.87%
AV 0%

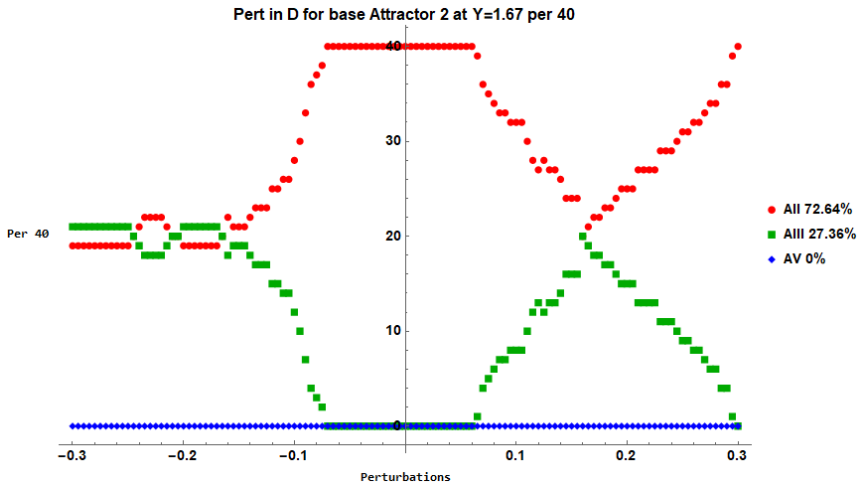
Pert in D for base Attractor 2 at Y=1.67 per 40
Per 40
Perturbations
All 72.64%
AIII 27.36%
AV 0%

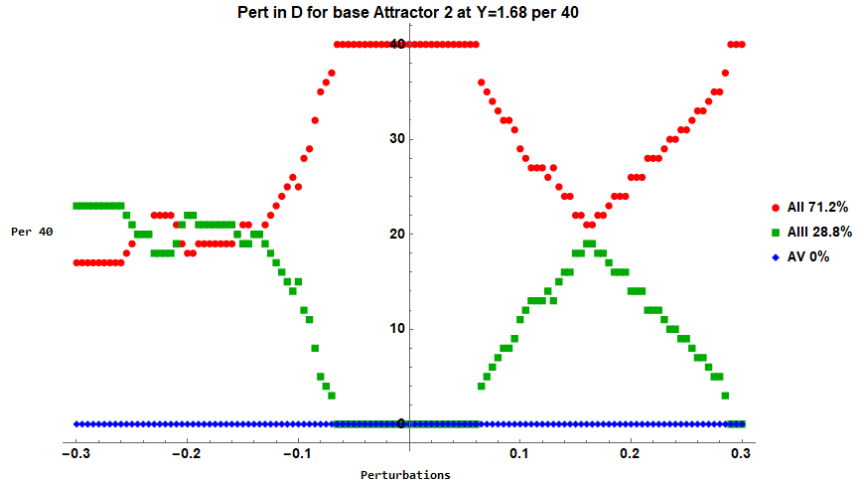
Pert in D for base Attractor 2 at Y=1.68 per 40
Per 40
Perturbations
All 71.2%
AIII 28.8%
AV 0%

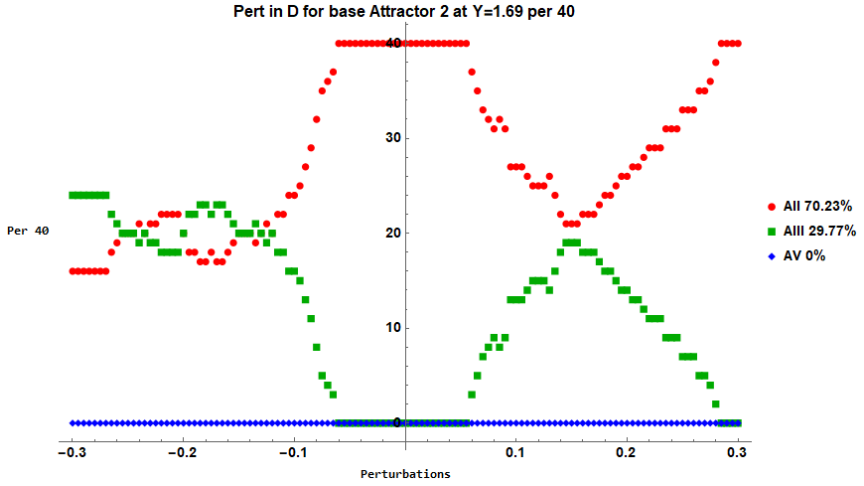
Pert in D for base Attractor 2 at Y=1.69 per 40
Per 40
Perturbations
All 70.23%
AIII 29.77%
AV 0%

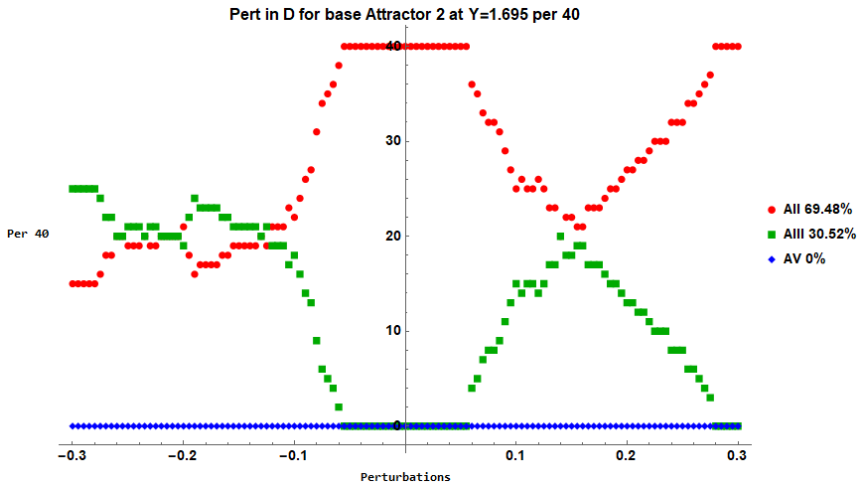
Pert in D for base Attractor 2 at Y=1.695 per 40
Per 40
Perturbations
All 69.48%
AIII 30.52%
AV 0%

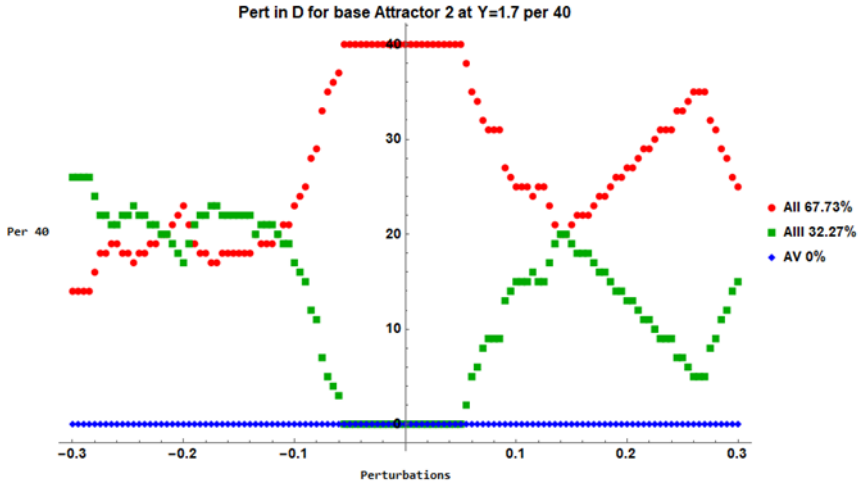
Pert in D for base Attractor 2 at Y=1.7 per 40
Per 40
Perturbations
All 67.73%
AIII 32.27%
AV 0%

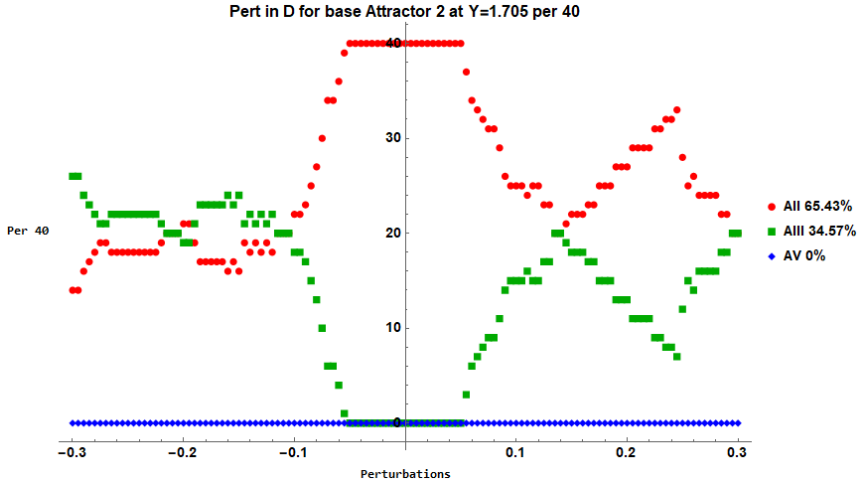
Pert in D for base Attractor 2 at Y=1.705 per 40
Per 40
Perturbations
All 65.43%
AIII 34.57%
AV 0%

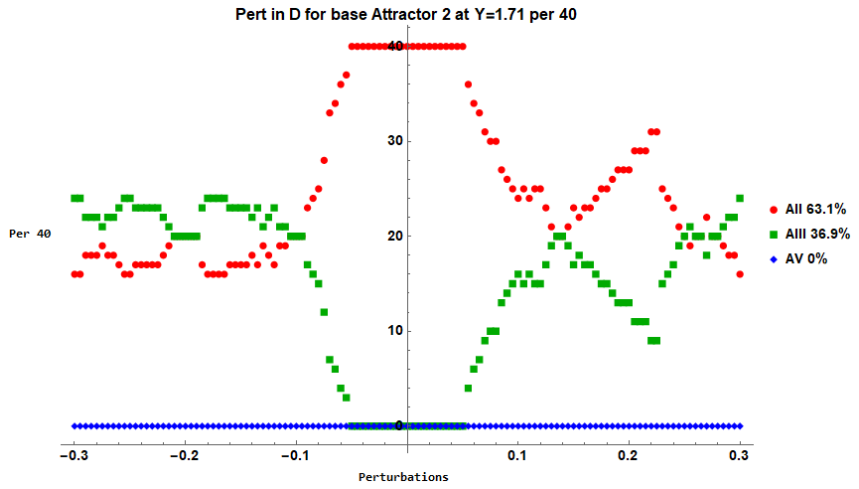
Pert in D for base Attractor 2 at Y=1.71 per 40
Per 40
Perturbations
AII 63.1%
AIII 36.9%
AV 0%

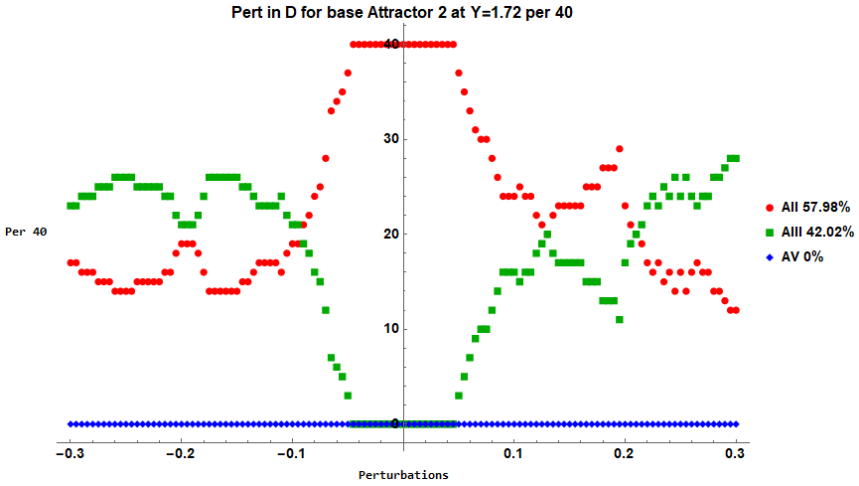
Pert in D for base Attractor 2 at Y=1.72 per 40
Per 40
Perturbations
AII 57.98%
AIII 42.02%
AV 0%

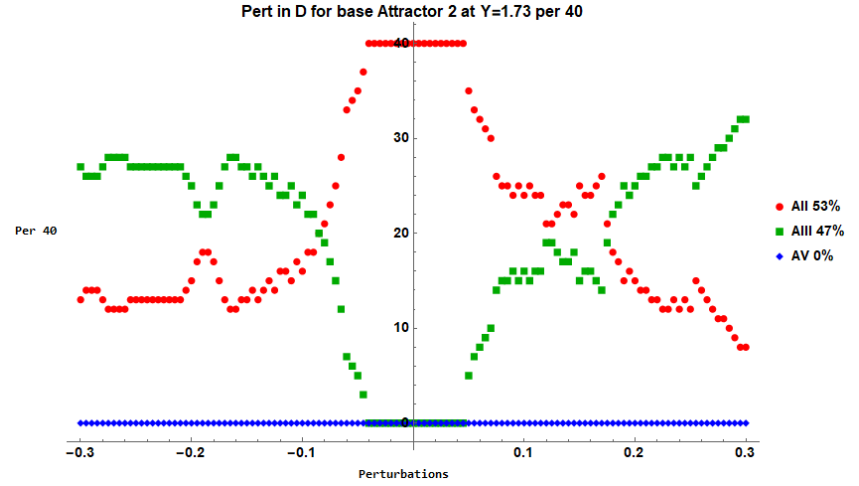
Pert in D for base Attractor 2 at Y=1.73 per 40
Per 40
Perturbations
AII 53%
AIII 47%
AV 0%

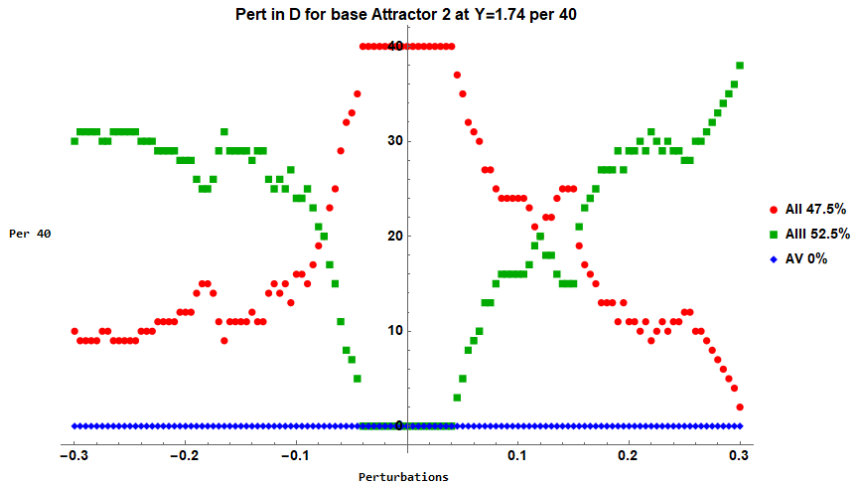
Pert in D for base Attractor 2 at Y=1.74 per 40
Per 40
Perturbations
All 47.5%
AIII 52.5%
AV 0%

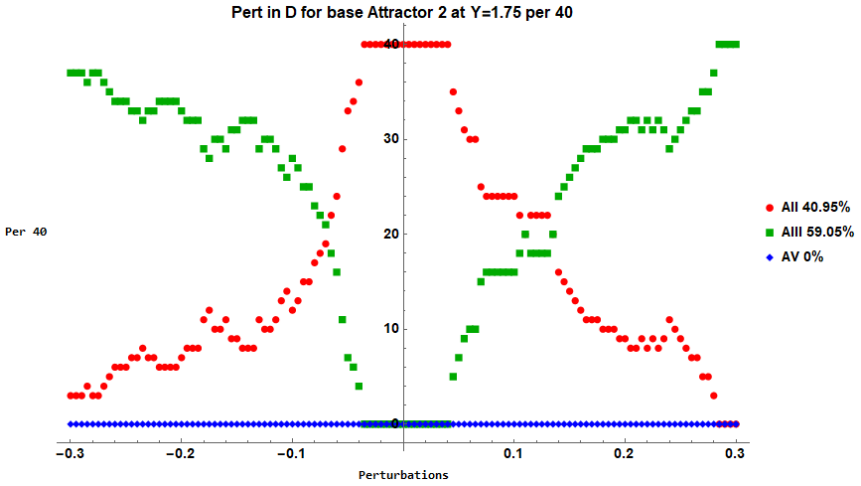
Pert in D for base Attractor 2 at Y=1.75 per 40
Per 40
Perturbations
All 40.95%
AIII 59.05%
AV 0%

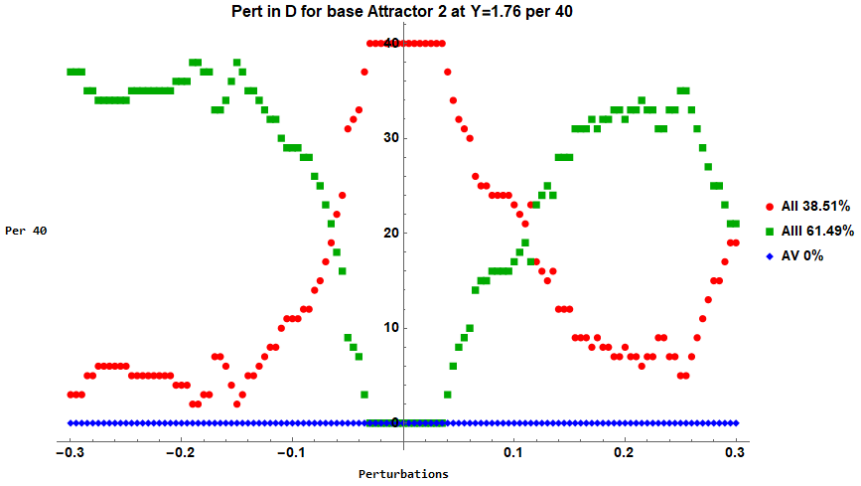
Pert in D for base Attractor 2 at Y=1.76 per 40
Per 40
Perturbations
All 38.51%
AIII 61.49%
AV 0%

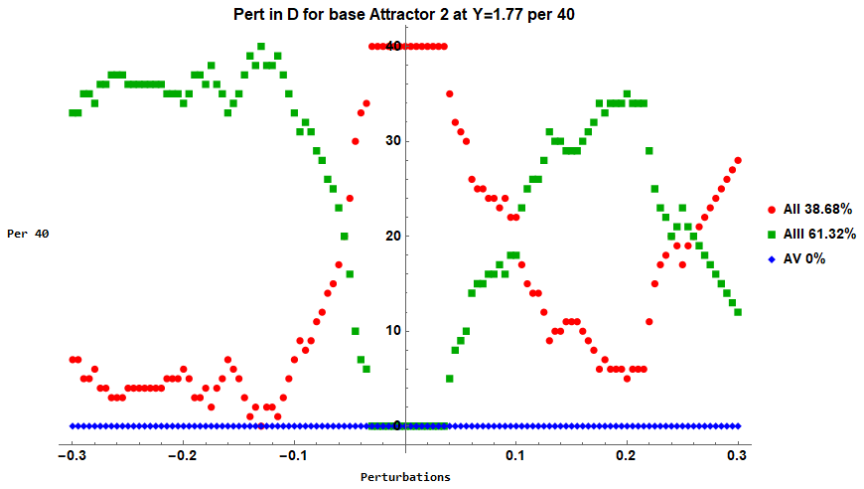
Pert in D for base Attractor 2 at Y=1.77 per 40
Per 40
Perturbations
All 38.68%
AIII 61.32%
AV 0%

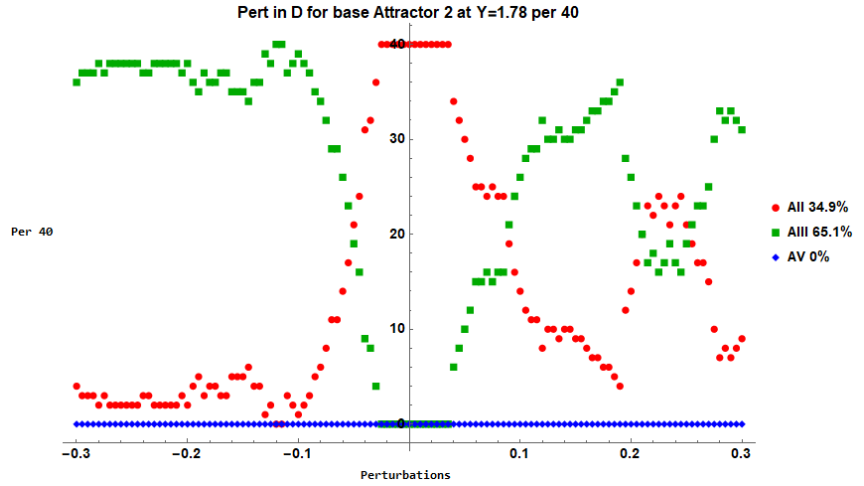
Pert in D for base Attractor 2 at Y=1.78 per 40
Per 40
Perturbations
All 34.9%
AIII 65.1%
AV 0%

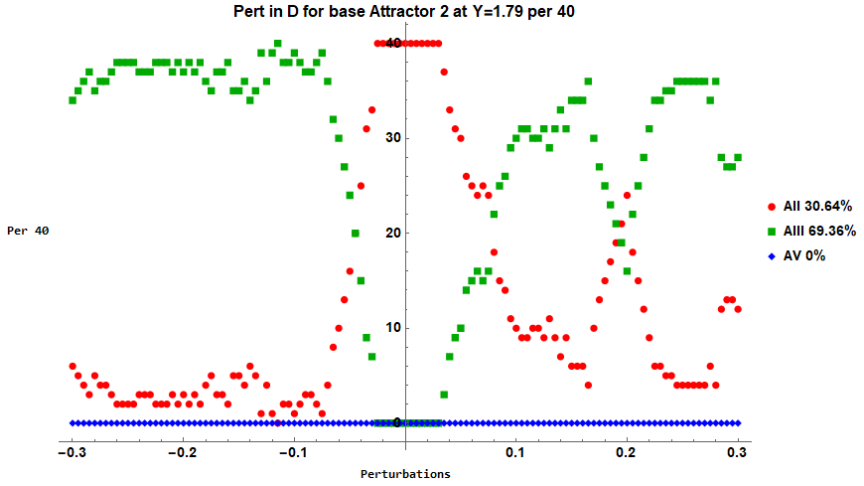
Pert in D for base Attractor 2 at Y=1.79 per 40
Per 40
Perturbations
All 30.64%
AIII 69.36%
AV 0%

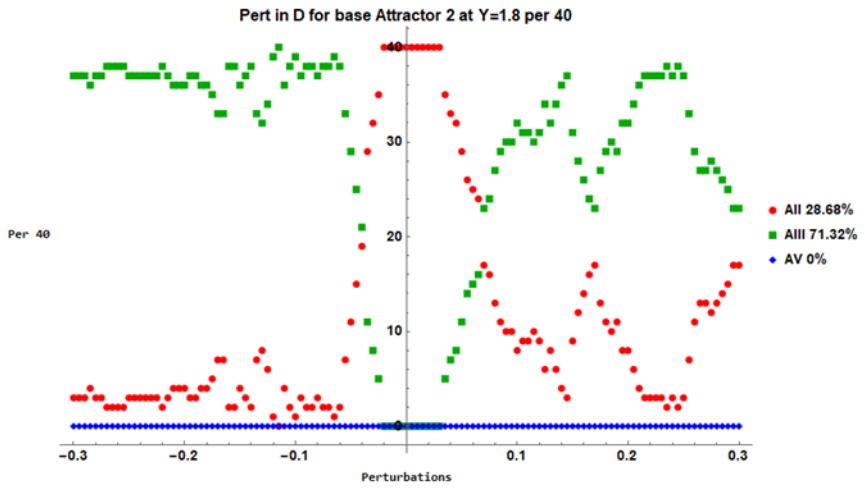
Pert in D for base Attractor 2 at Y=1.8 per 40
Per 40
Perturbations
All 28.68%
AIII 71.32%
AV 0%

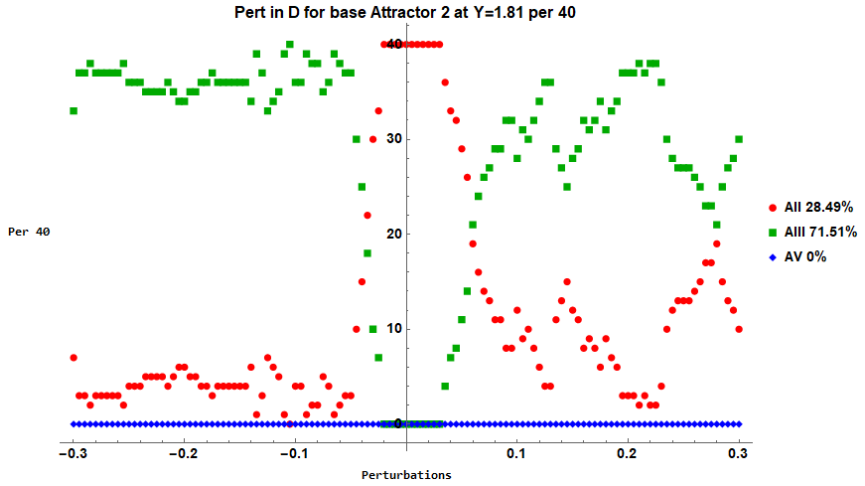
Pert in D for base Attractor 2 at Y=1.81 per 40
Per 40
Perturbations
All 28.49%
AIII 71.51%
AV 0%

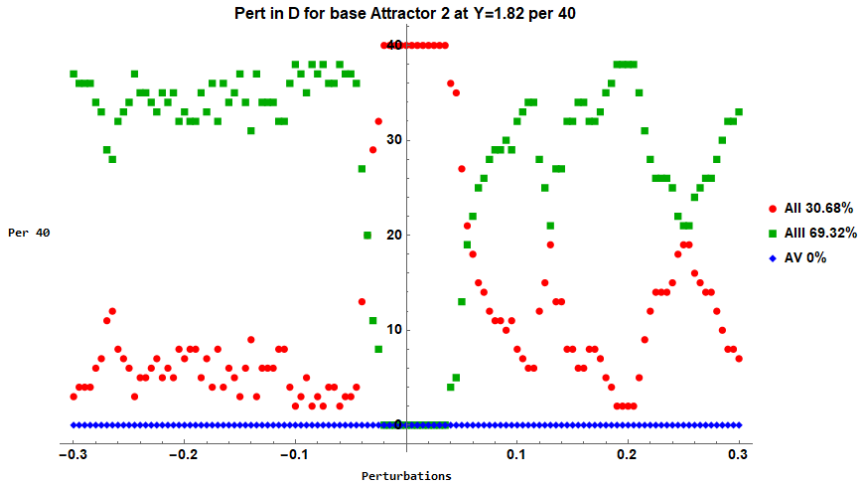
Pert in D for base Attractor 2 at Y=1.82 per 40
Per 40
Perturbations
All 30.68%
AIII 69.32%
AV 0%

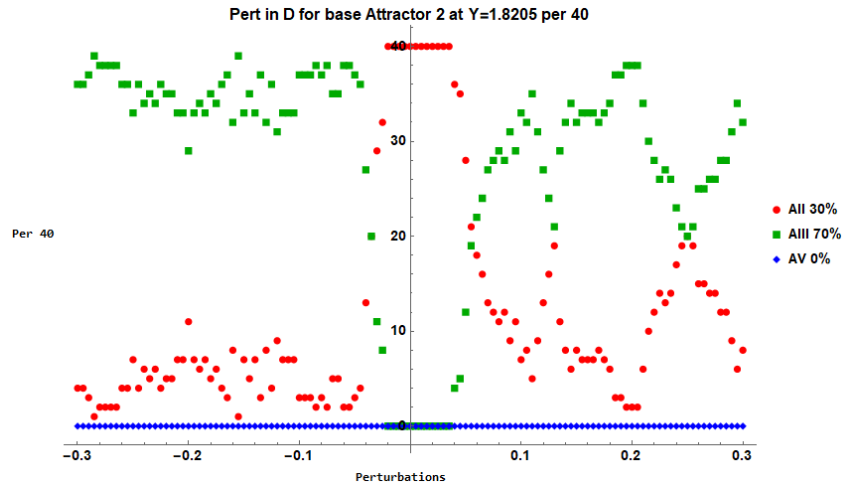
Pert in D for base Attractor 2 at Y=1.8205 per 40
Per 40
Perturbations
AII 30%
AIII 70%
AV 0%

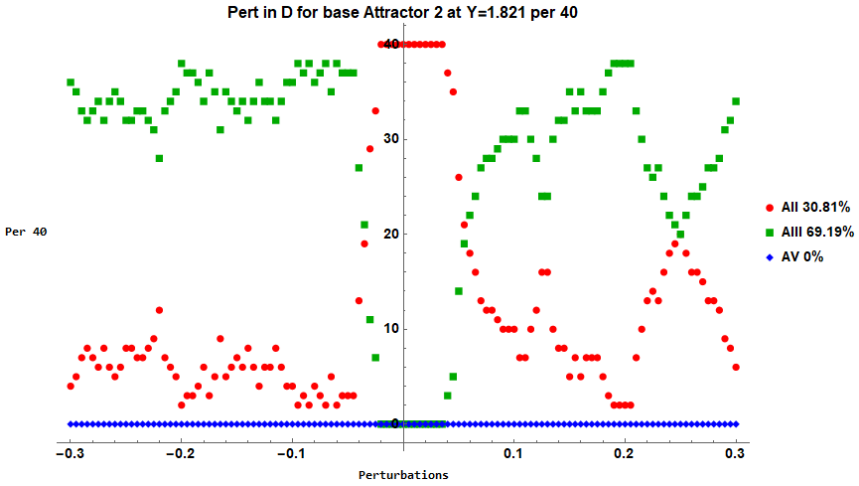
Pert in D for base Attractor 2 at Y=1.821 per 40
Per 40
Perturbations
AII 30.81%
AIII 69.19%
AV 0%

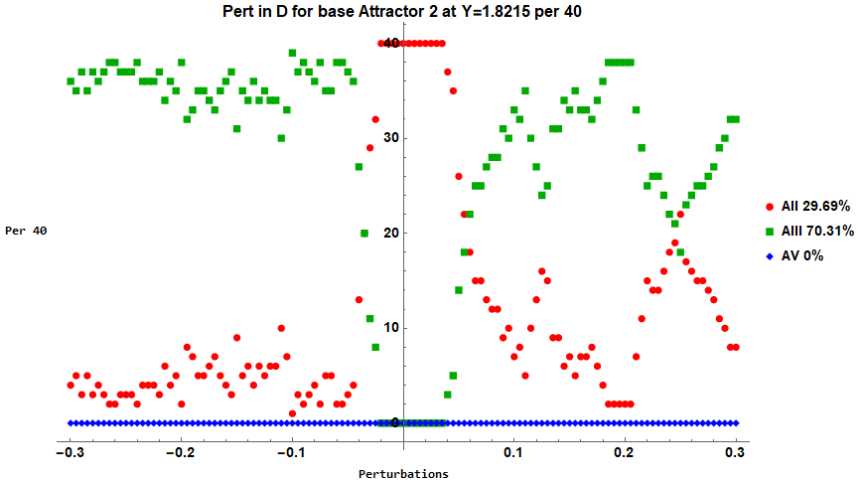
Pert in D for base Attractor 2 at Y=1.8215 per 40
Per 40
Perturbations
AII 29.69%
AIII 70.31%
AV 0%

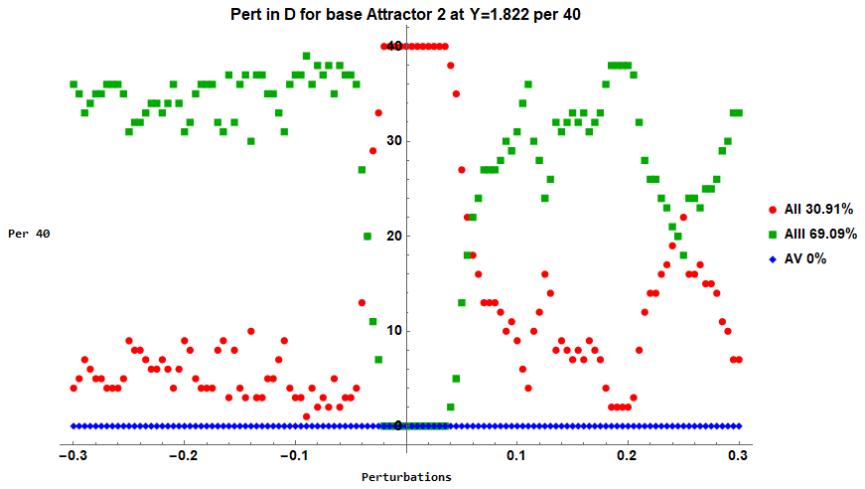
Pert in D for base Attractor 2 at Y=1.822 per 40
Per 40
Perturbations
AII 30.91%
AIII 69.09%
AV 0%

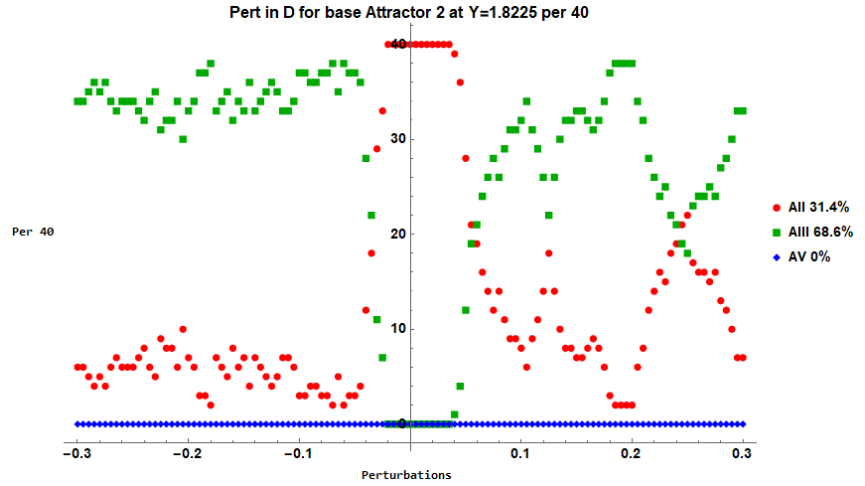
Pert in D for base Attractor 2 at Y=1.8225 per 40
Per 40
Perturbations
AII 31.4%
AIII 68.6%
AV 0%

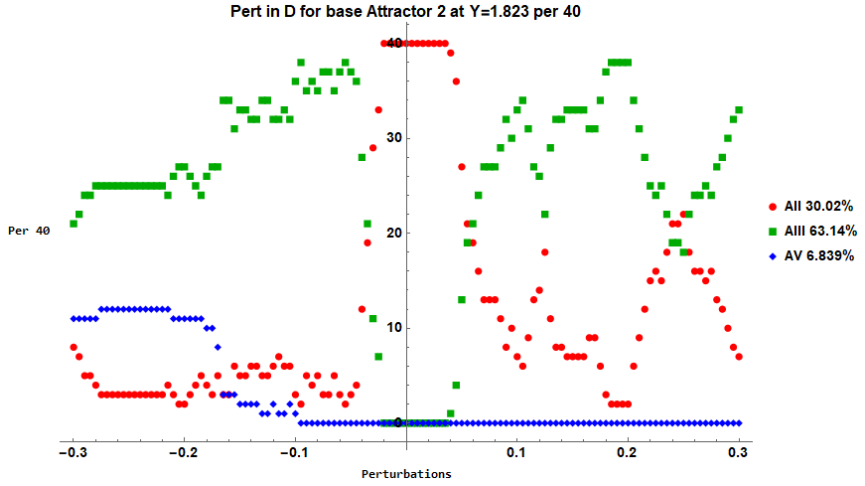
Pert in D for base Attractor 2 at Y=1.823 per 40
Per 40
Perturbations
AII 30.02%
AIII 63.14%
AV 6.839%

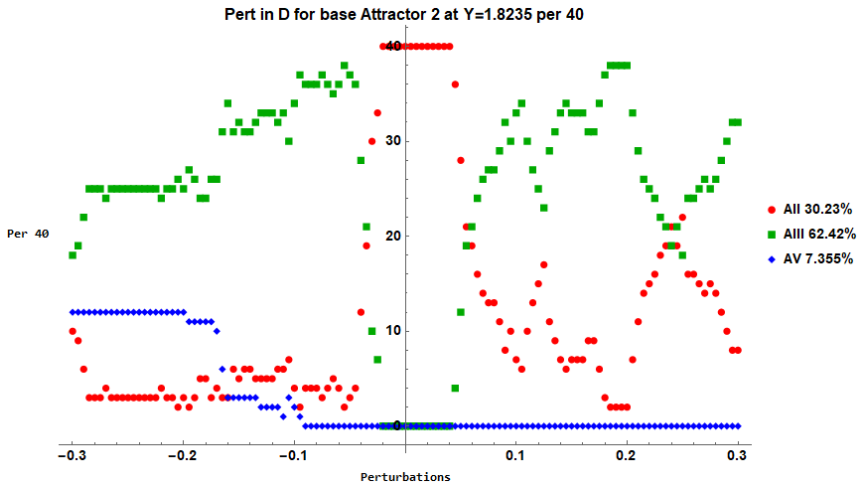
Pert in D for base Attractor 2 at Y=1.8235 per 40
Per 40
Perturbations
All 30.23%
AIII 62.42%
AV 7.355%

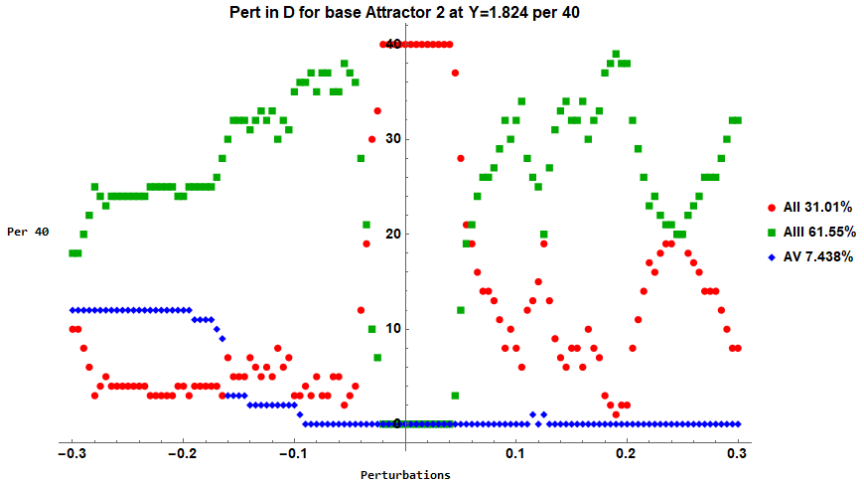
Pert in D for base Attractor 2 at Y=1.824 per 40
Per 40
Perturbations
All 31.01%
AIII 61.55%
AV 7.438%

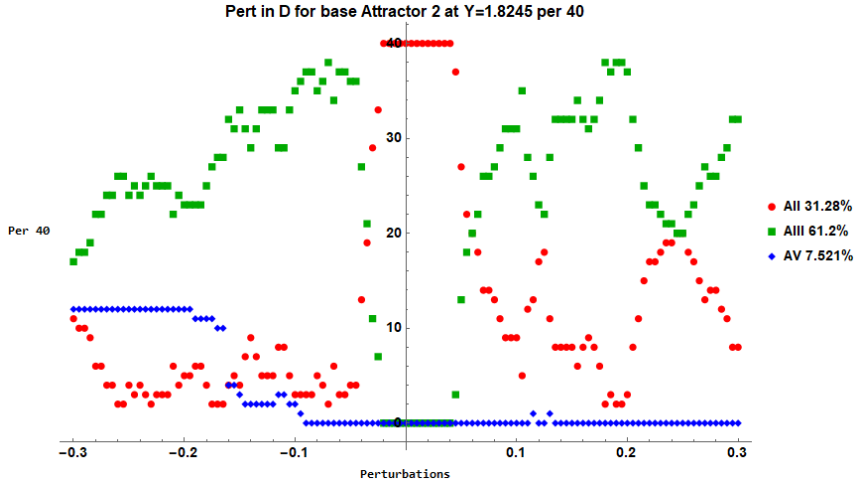
Pert in D for base Attractor 2 at Y=1.8245 per 40
Per 40
Perturbations
All 31.28%
AIII 61.2%
AV 7.521%

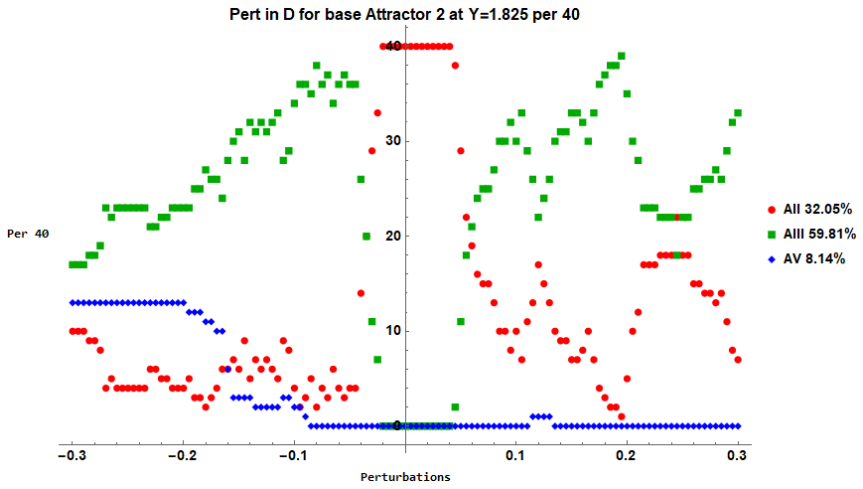
Pert in D for base Attractor 2 at Y=1.825 per 40
Per 40
Perturbations
All 32.05%
AIII 59.81%
AV 8.14%

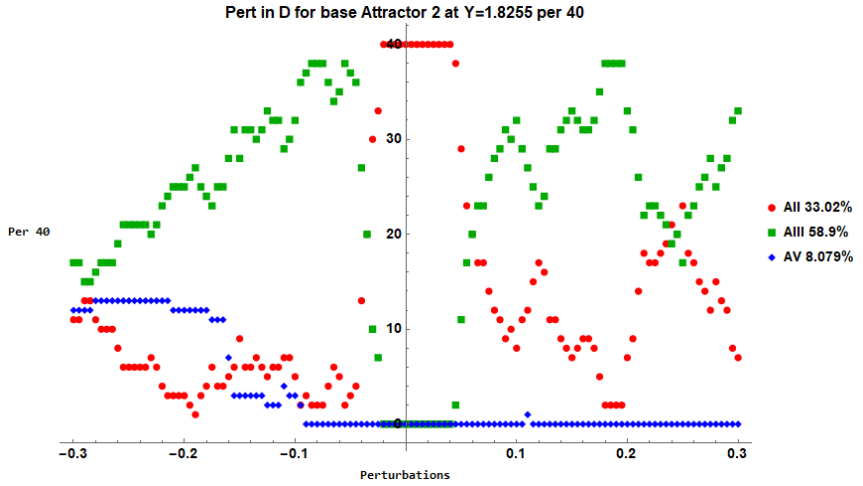
Pert in D for base Attractor 2 at Y=1.8255 per 40
Per 40
Perturbations
All 33.02%
AIII 58.9%
AV 8.079%

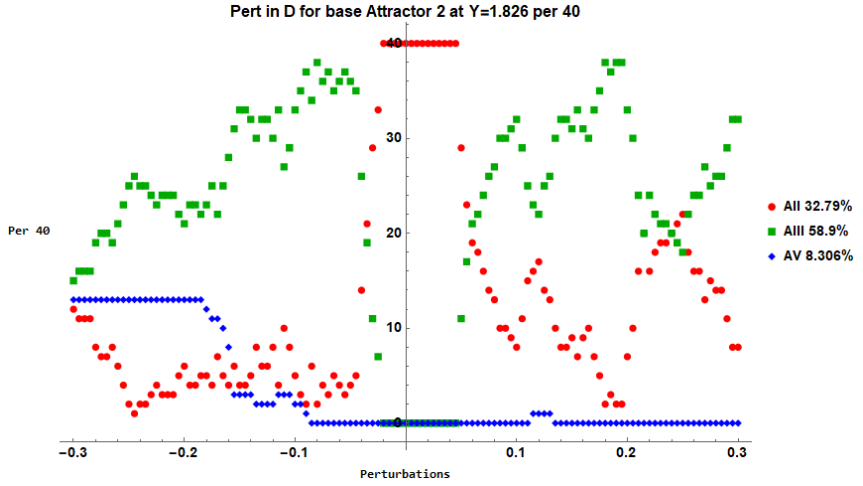
Pert in D for base Attractor 2 at Y=1.826 per 40
Per 40
Perturbations
All 32.79%
AIII 58.9%
AV 8.306%

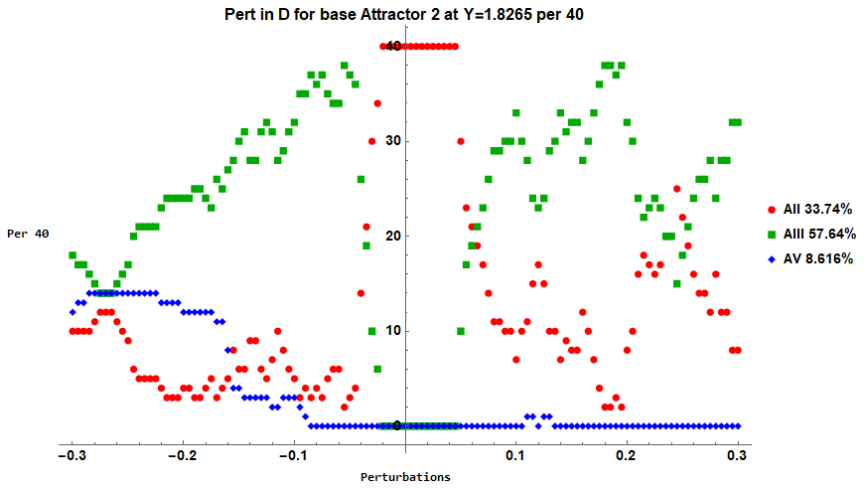
Pert in D for base Attractor 2 at Y=1.8265 per 40
Per 40
Perturbations
All 33.74%
AIII 57.64%
AV 8.616%

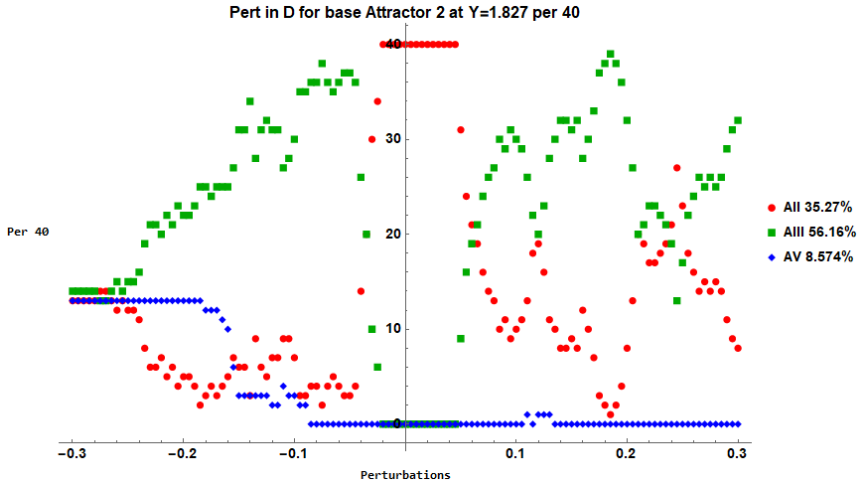
Pert in D for base Attractor 2 at Y=1.827 per 40
Per 40
Perturbations
All 35.27%
AIII 56.16%
AV 8.574%

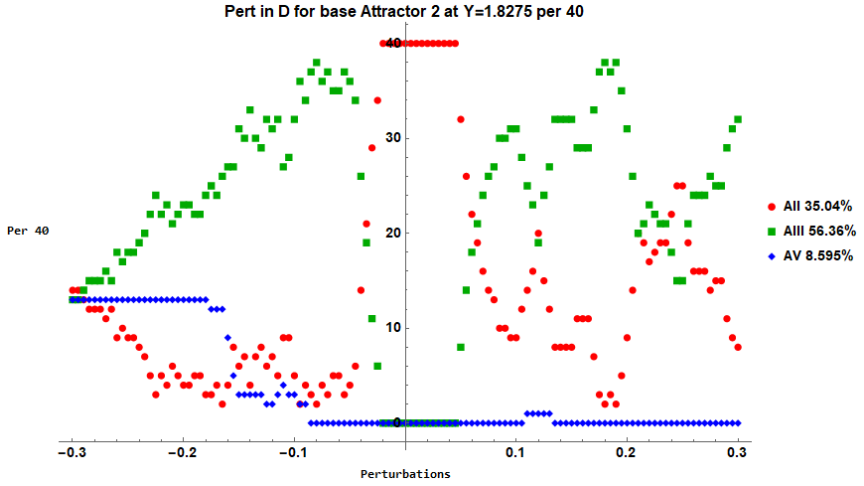
Pert in D for base Attractor 2 at Y=1.8275 per 40
Per 40
Perturbations
All 35.04%
AIII 56.36%
AV 8.595%

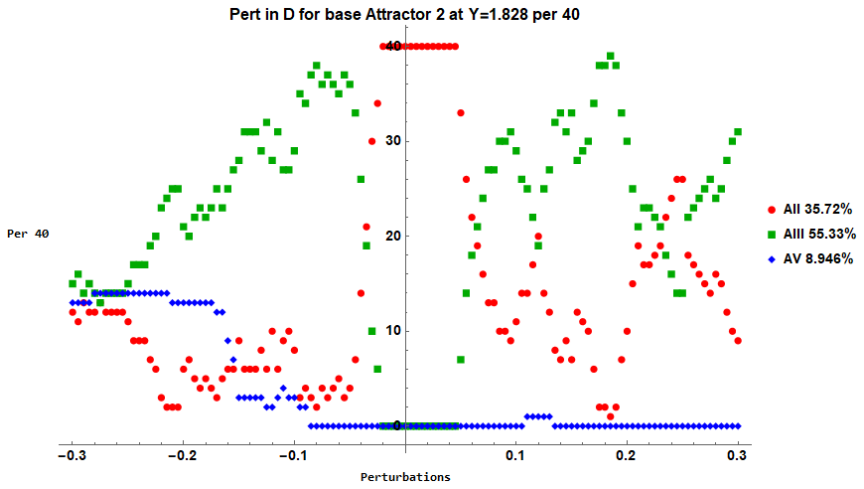
Pert in D for base Attractor 2 at Y=1.828 per 40
Per 40
Perturbations
All 35.72%
AIII 55.33%
AV 8.946%

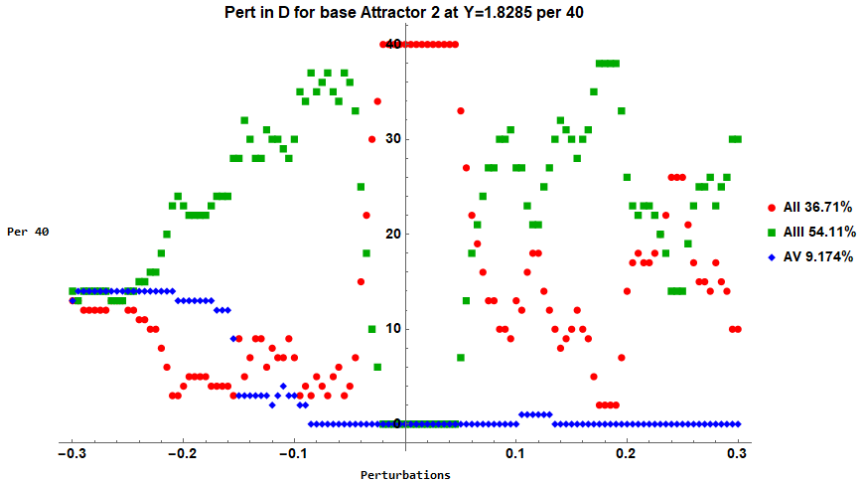
Pert in D for base Attractor 2 at Y=1.8285 per 40
Per 40
Perturbations
All 36.71%
AIII 54.11%
AV 9.174%

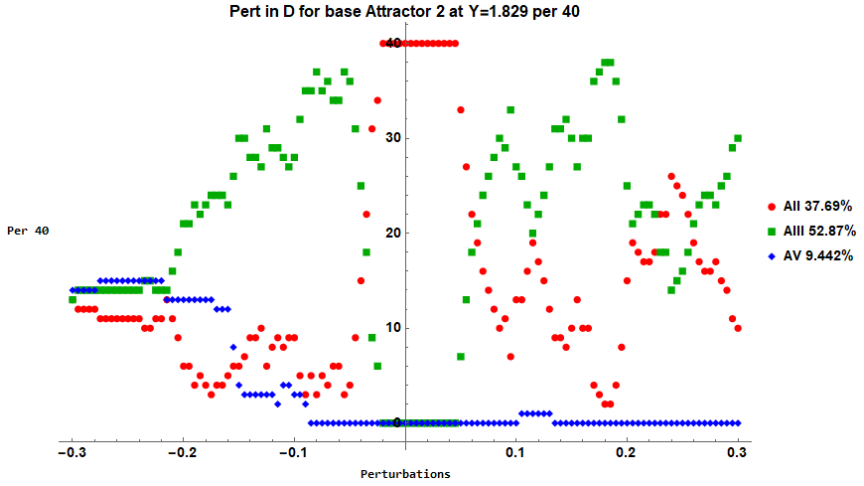
Pert in D for base Attractor 2 at Y=1.829 per 40
Per 40
Perturbations
All 37.69%
AIII 52.87%
AV 9.442%

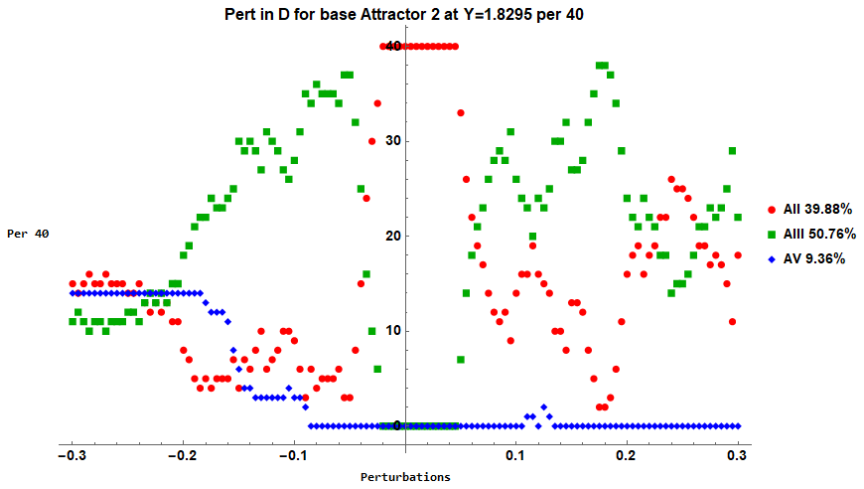
Pert in D for base Attractor 2 at Y=1.8295 per 40
Per 40
Perturbations
All 39.88%
AIII 50.76%
AV 9.36%

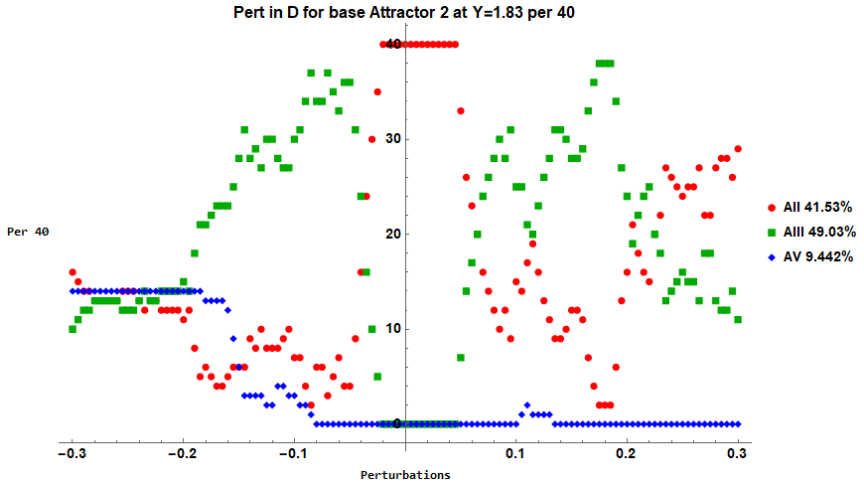
Pert in D for base Attractor 2 at Y=1.83 per 40
Per 40
Perturbations
All 41.53%
AIII 49.03%
AV 9.442%

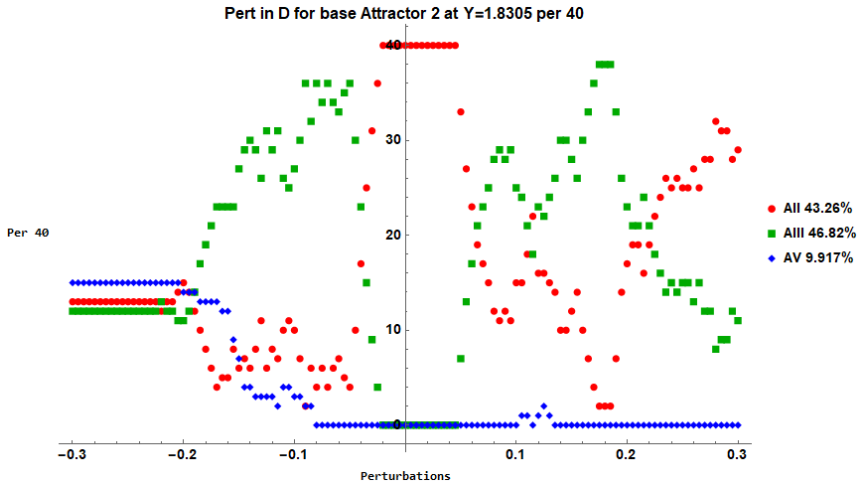
Pert in D for base Attractor 2 at Y=1.8305 per 40
Per 40
Perturbations
All 43.26%
AIII 46.82%
AV 9.917%

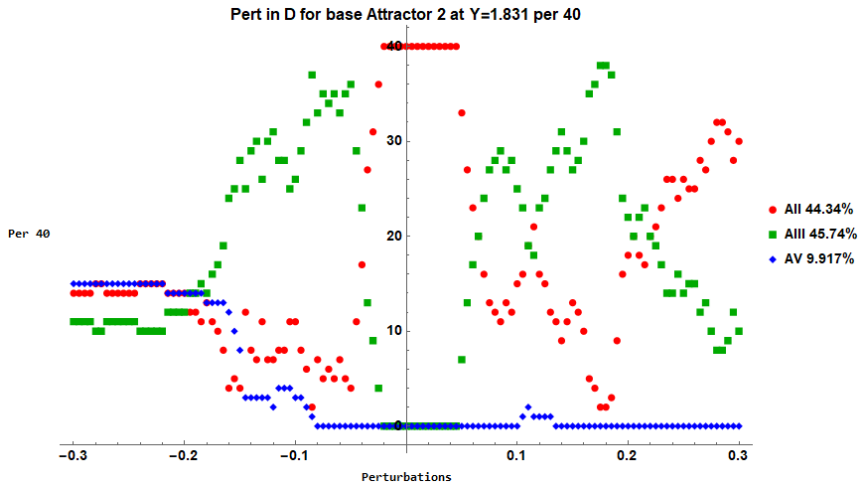
Pert in D for base Attractor 2 at Y=1.831 per 40
Per 40
Perturbations
All 44.34%
AIII 45.74%
AV 9.917%

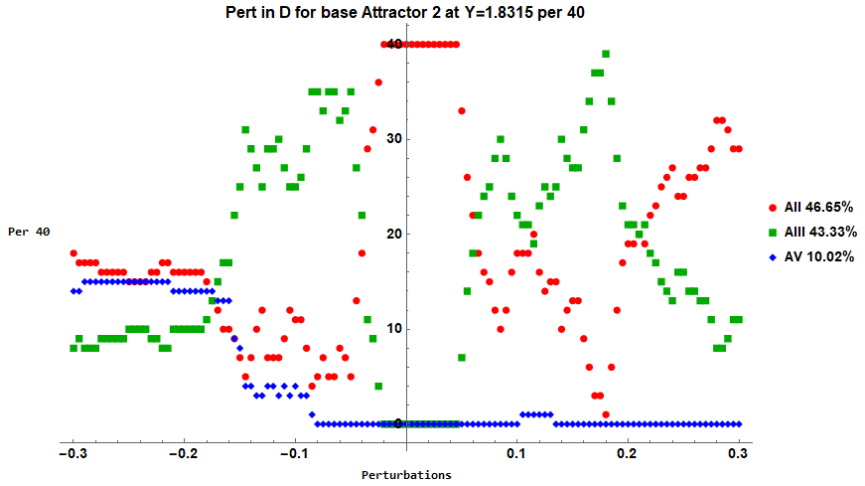
Pert in D for base Attractor 2 at Y=1.8315 per 40
Per 40
Perturbations
All 46.65%
AIII 43.33%
AV 10.02%

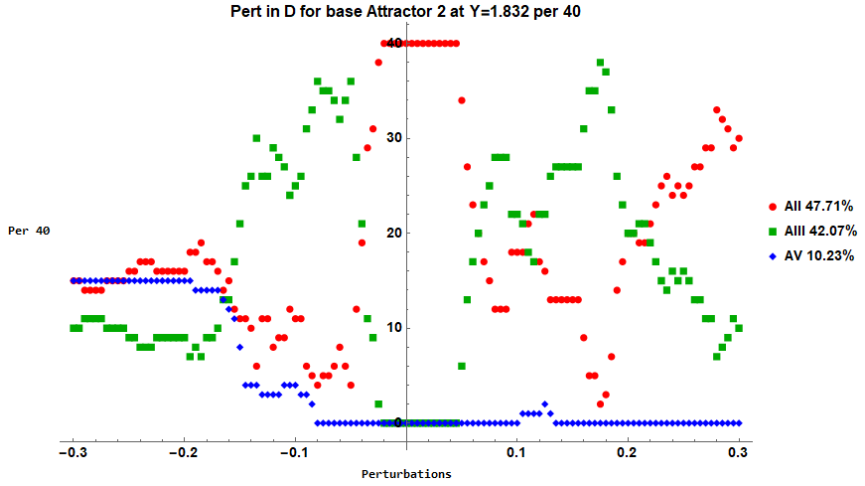
Pert in D for base Attractor 2 at Y=1.832 per 40
Per 40
Perturbations
All 47.71%
AIII 42.07%
AV 10.23%

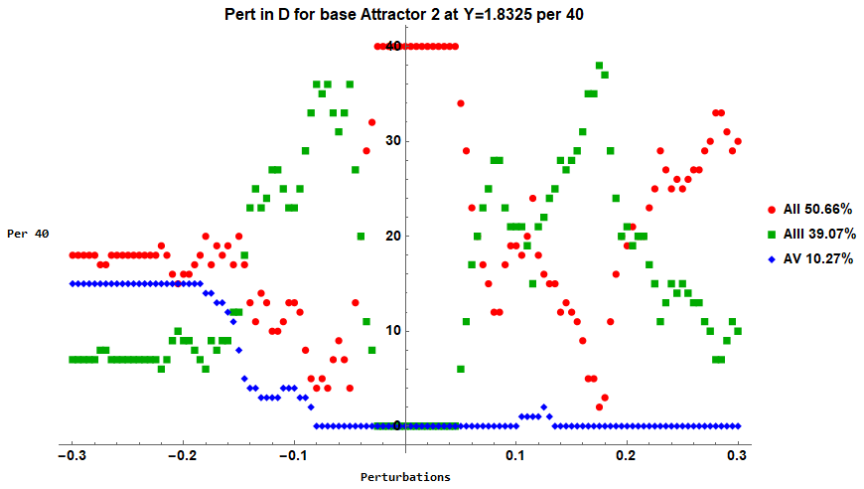
Pert in D for base Attractor 2 at Y=1.8325 per 40
Per 40
Perturbations
All 50.66%
AIII 39.07%
AV 10.27%

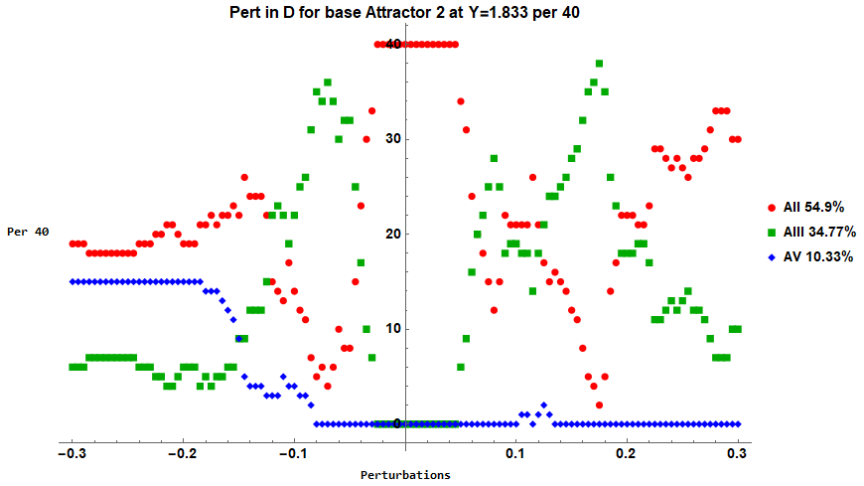
Pert in D for base Attractor 2 at Y=1.833 per 40
Per 40
Perturbations
All 54.9%
AIII 34.77%
AV 10.33%

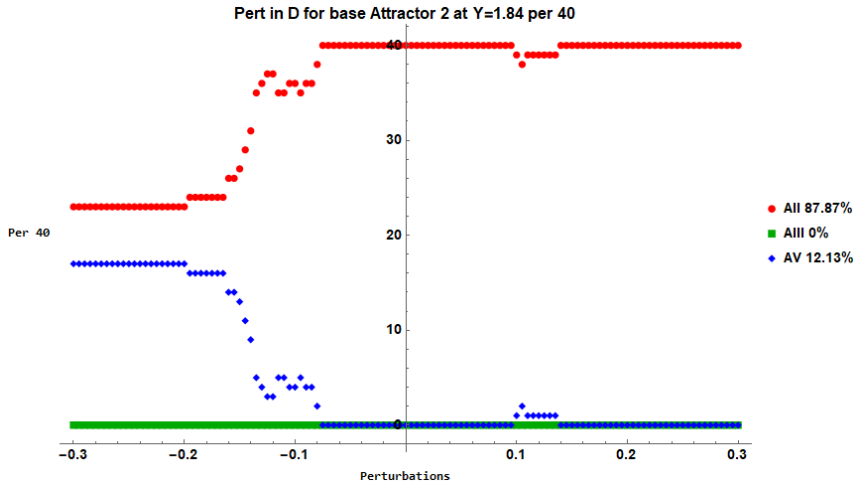
Pert in D for base Attractor 2 at Y=1.84 per 40
Per 40
Perturbations
All 87.87%
AIII 0%
AV 12.13%

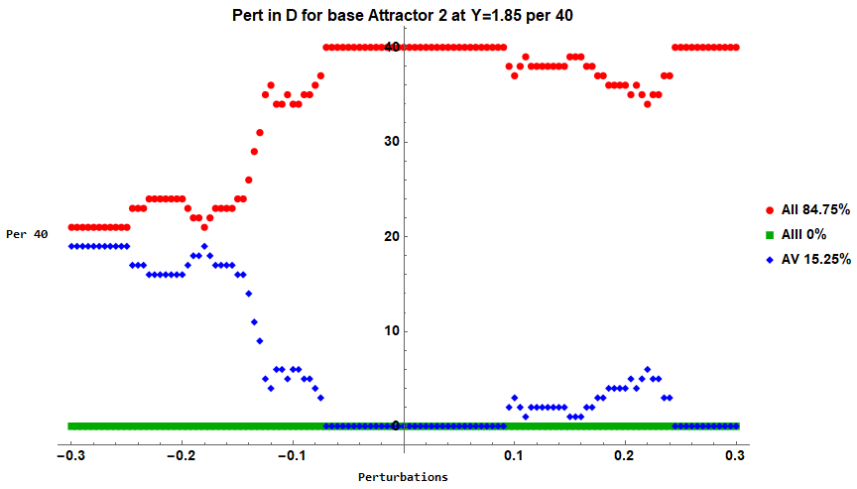
Pert in D for base Attractor 2 at Y=1.85 per 40
Per 40
Perturbations
AII 84.75%
AIII 0%
AV 15.25%

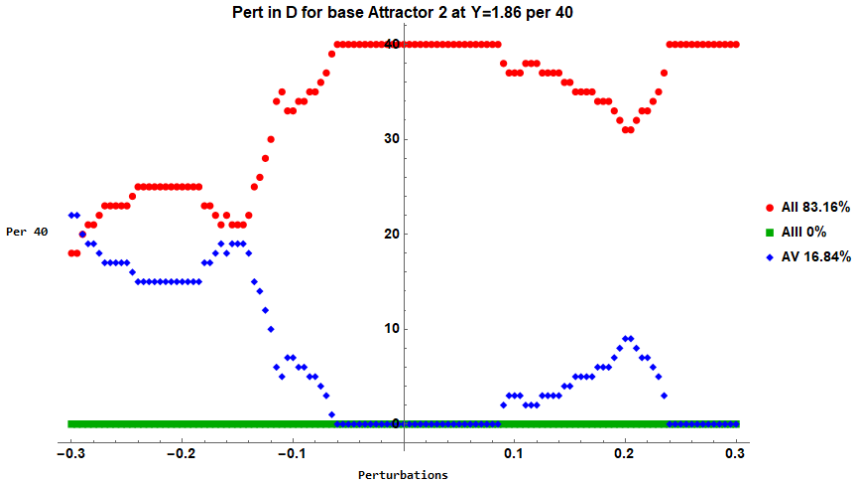
Pert in D for base Attractor 2 at Y=1.86 per 40
Per 40
Perturbations
AII 83.16%
AIII 0%
AV 16.84%

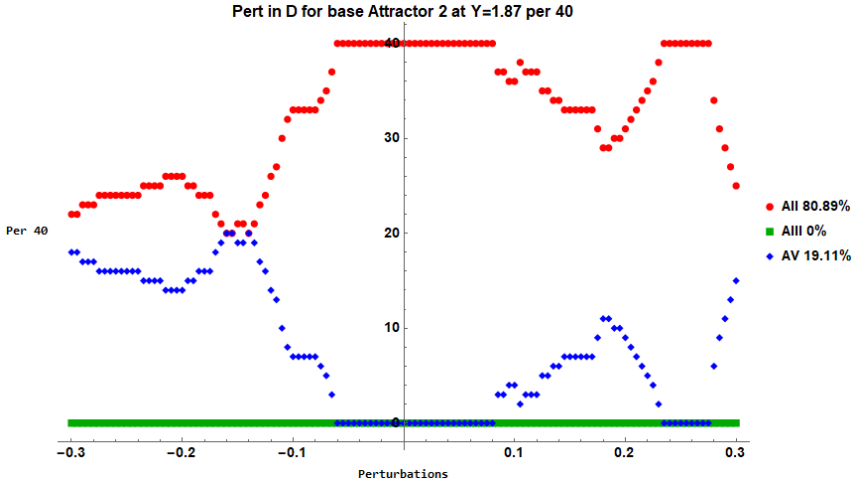
Pert in D for base Attractor 2 at Y=1.87 per 40
Per 40
Perturbations
AII 80.89%
AIII 0%
AV 19.11%

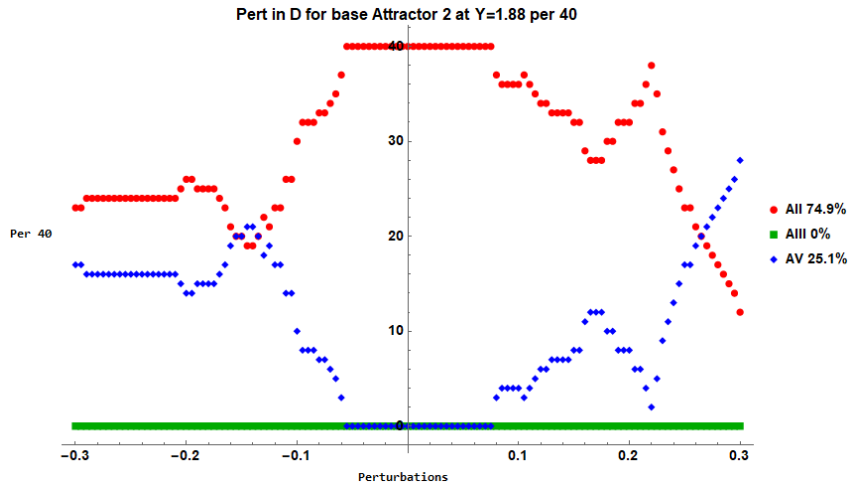
Pert in D for base Attractor 2 at Y=1.88 per 40
Per 40
Perturbations
All 74.9%
AIII 0%
AV 25.1%

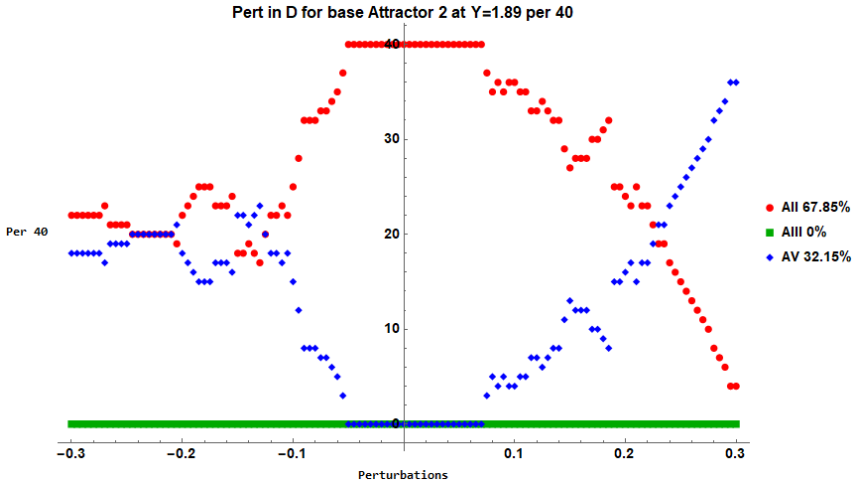
Pert in D for base Attractor 2 at Y=1.89 per 40
Per 40
Perturbations
All 67.85%
AIII 0%
AV 32.15%

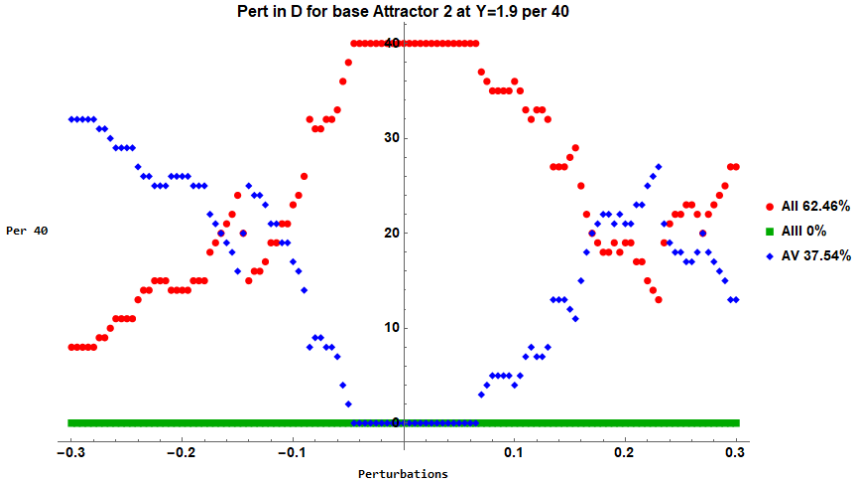
Pert in D for base Attractor 2 at Y=1.9 per 40
Per 40
Perturbations
All 62.46%
AIII 0%
AV 37.54%

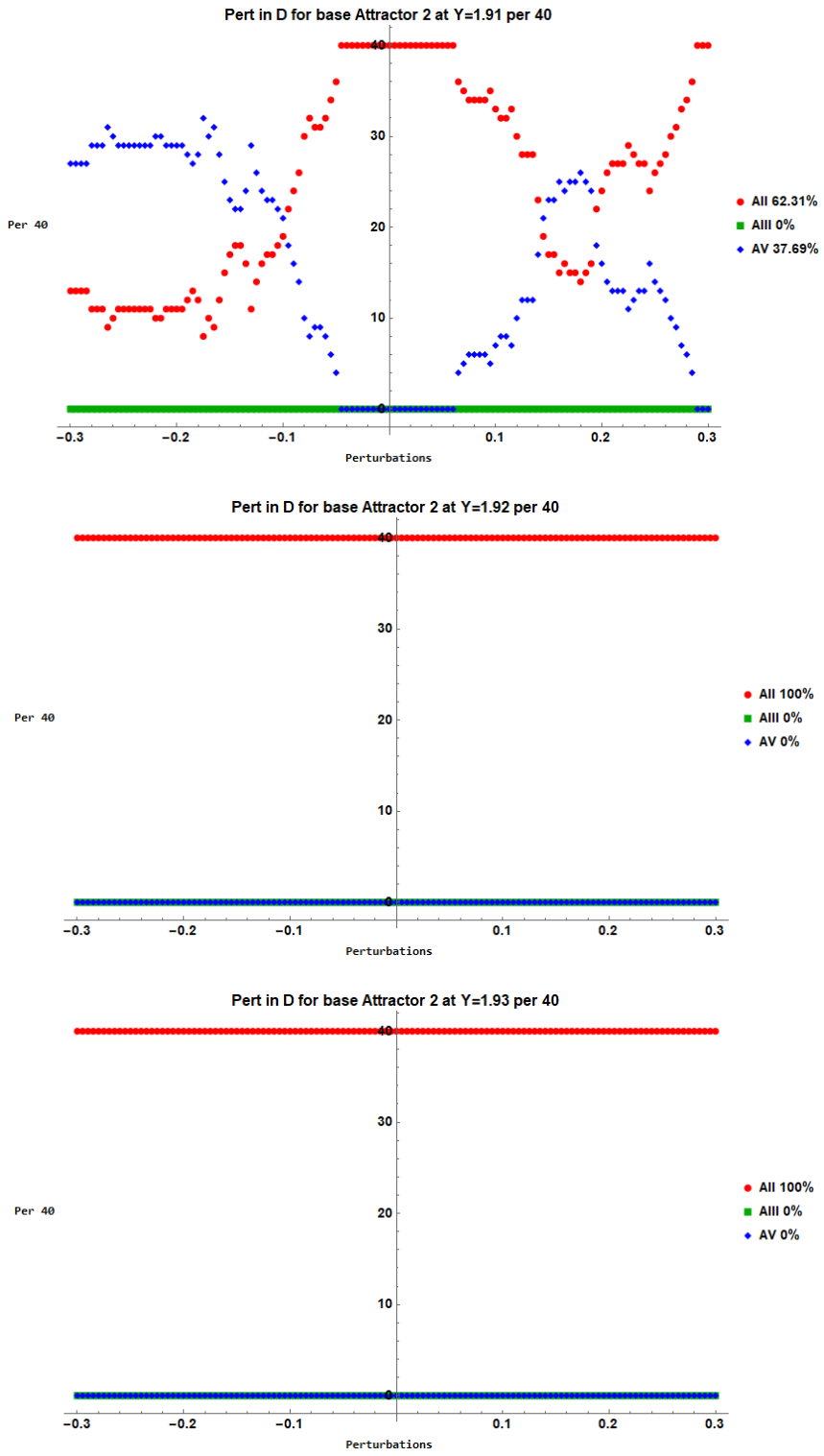

Figure A5. Perturbations of AII for *1.62<Y<1.93*. Each plot has the percentage chance of transitioning attractors for the total range of perturbations displayed.

Appendix 4.2. AIII Perturbations

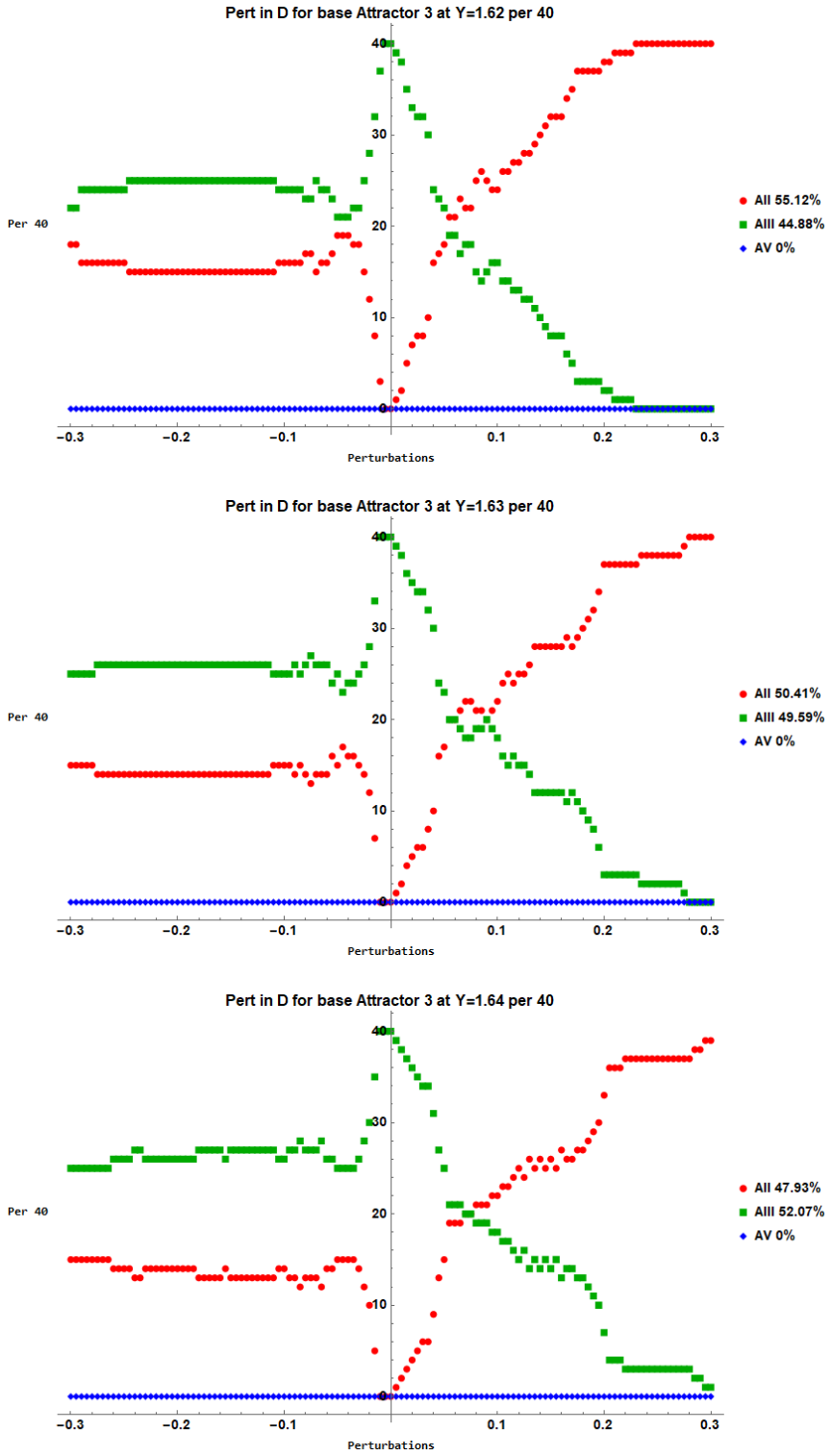

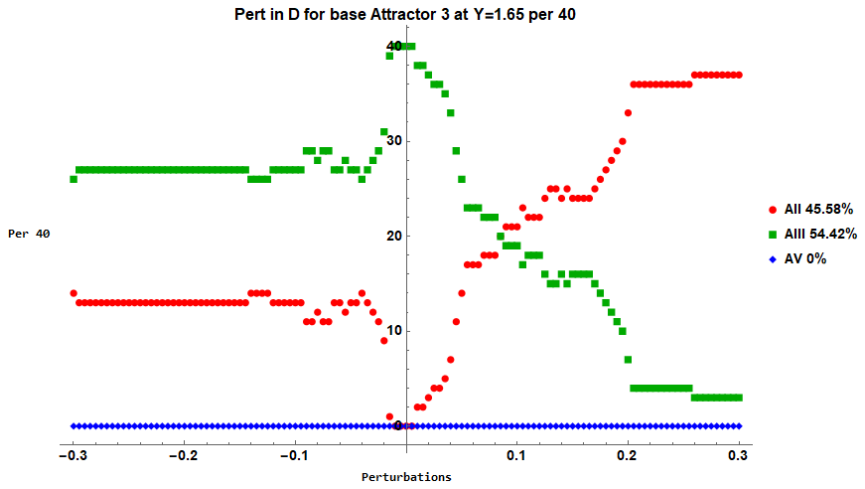
Pert in D for base Attractor 3 at Y=1.65 per 40
Per 40
Perturbations
AII 45.58%
AIII 54.42%
AV 0%

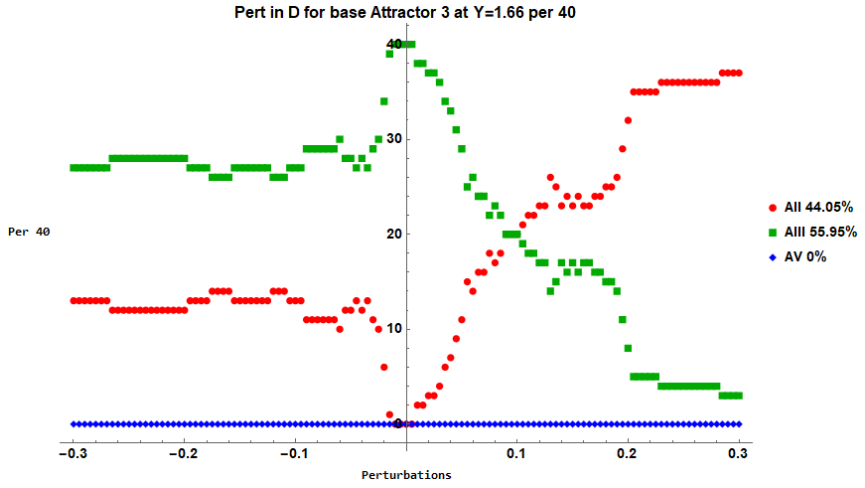
Pert in D for base Attractor 3 at Y=1.66 per 40
Per 40
Perturbations
AII 44.05%
AIII 55.95%
AV 0%

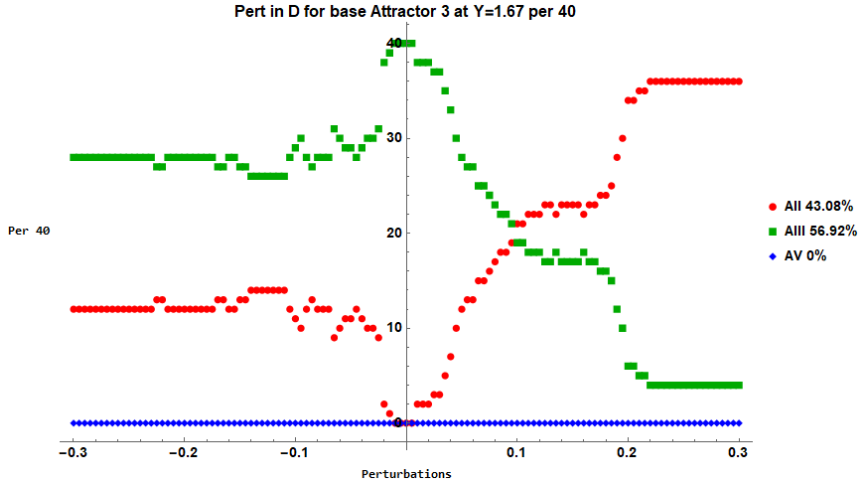
Pert in D for base Attractor 3 at Y=1.67 per 40
Per 40
Perturbations
AII 43.08%
AIII 56.92%
AV 0%

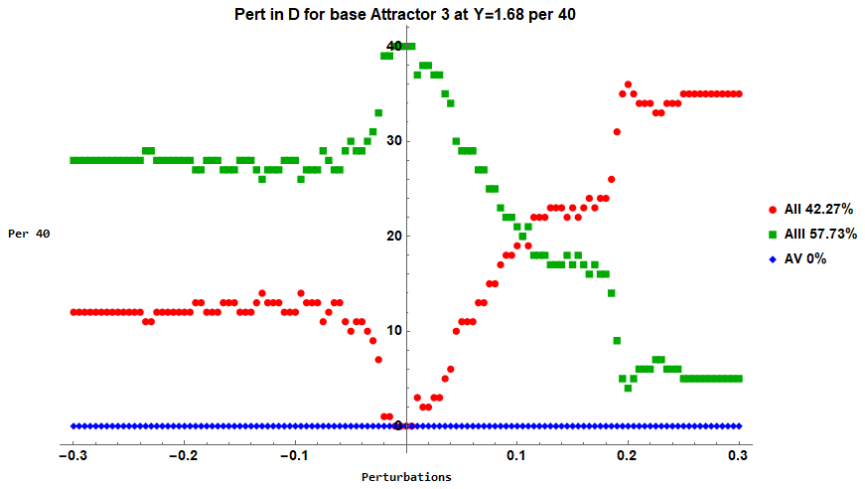
Pert in D for base Attractor 3 at Y=1.68 per 40
Per 40
Perturbations
AII 42.27%
AIII 57.73%
AV 0%

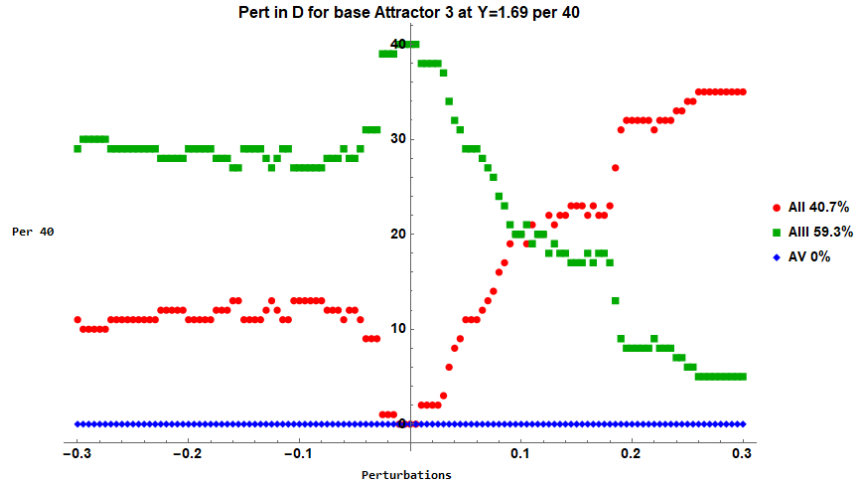
Pert in D for base Attractor 3 at Y=1.69 per 40
Per 40
Perturbations
AII 40.7%
AIII 59.3%
AV 0%

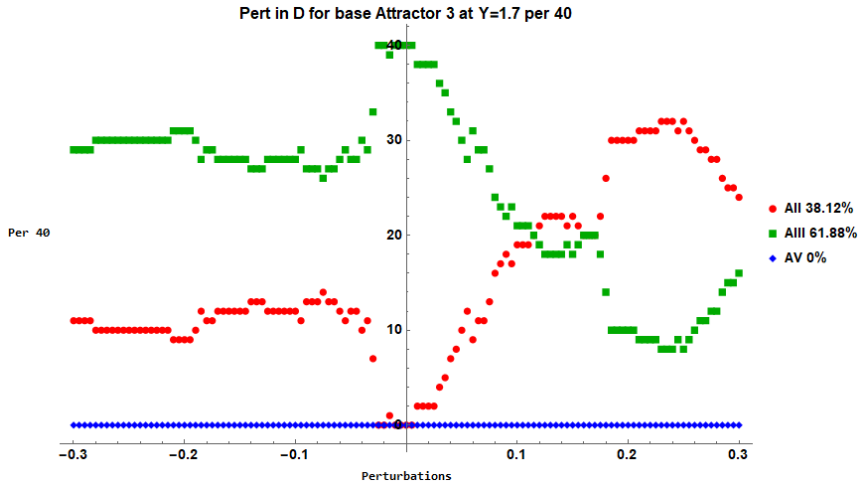
Pert in D for base Attractor 3 at Y=1.7 per 40
Per 40
Perturbations
AII 38.12%
AIII 61.88%
AV 0%

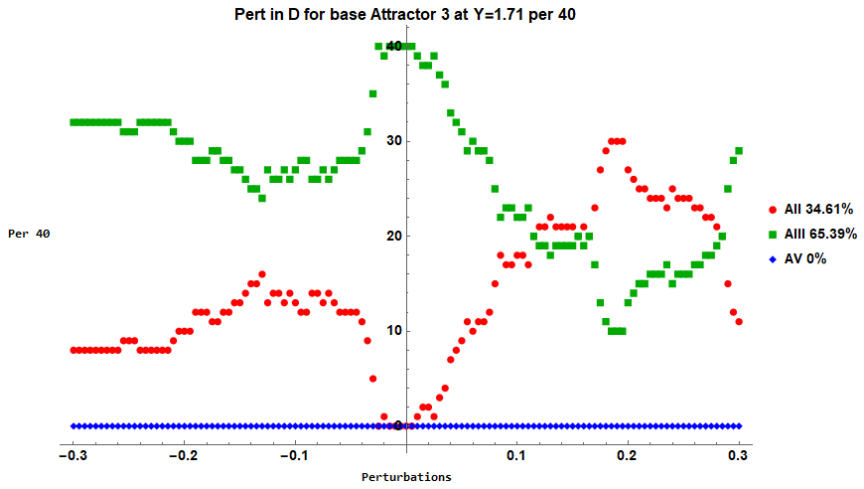
Pert in D for base Attractor 3 at Y=1.71 per 40
Per 40
Perturbations
AII 34.61%
AIII 65.39%
AV 0%

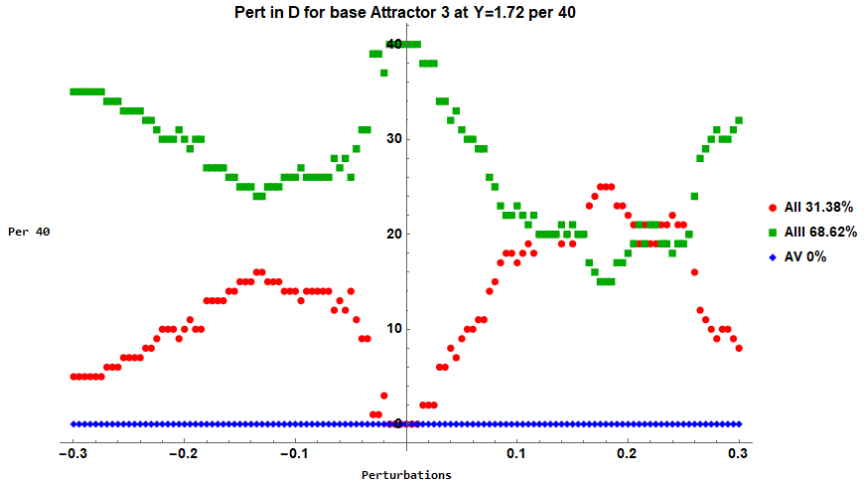
Pert in D for base Attractor 3 at Y=1.72 per 40
Per 40
Perturbations
AII 31.38%
AIII 68.62%
AV 0%

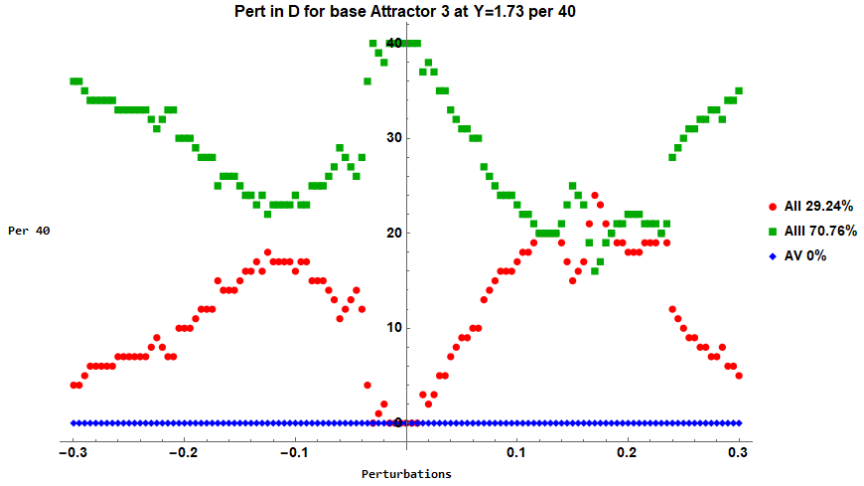
Pert in D for base Attractor 3 at Y=1.73 per 40
Per 40
Perturbations
AII 29.24%
AIII 70.76%
AV 0%

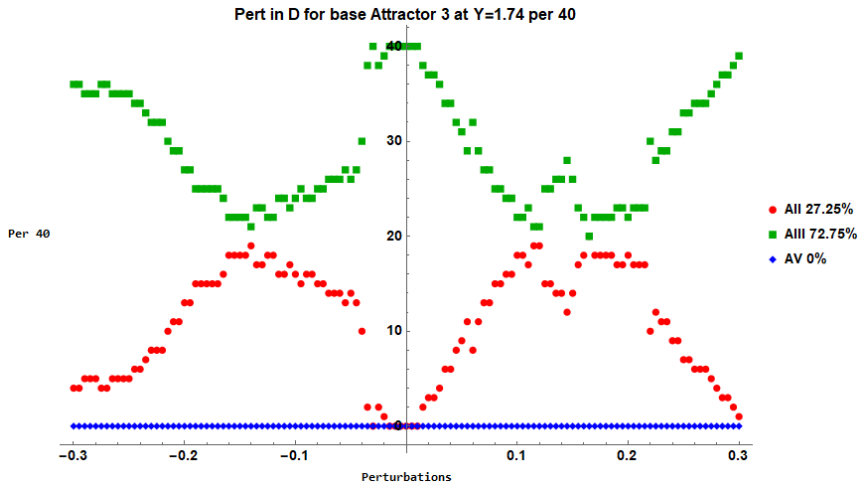
Pert in D for base Attractor 3 at Y=1.74 per 40
Per 40
Perturbations
AII 27.25%
AIII 72.75%
AV 0%

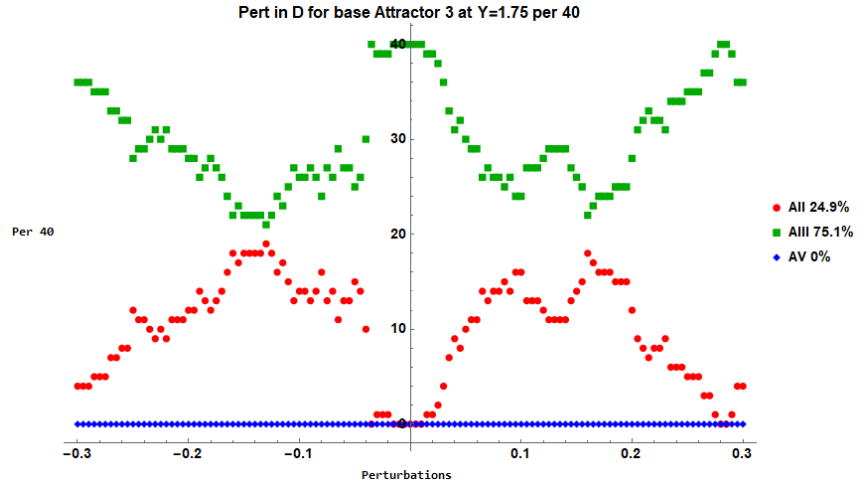
Pert in D for base Attractor 3 at Y=1.75 per 40
Per 40
Perturbations
AII 24.9%
AIII 75.1%
AV 0%

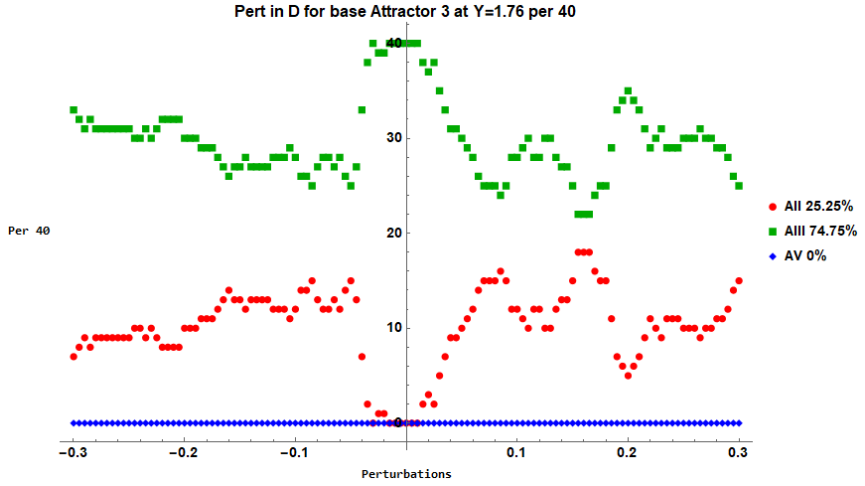
Pert in D for base Attractor 3 at Y=1.76 per 40
Per 40
Perturbations
AII 25.25%
AIII 74.75%
AV 0%

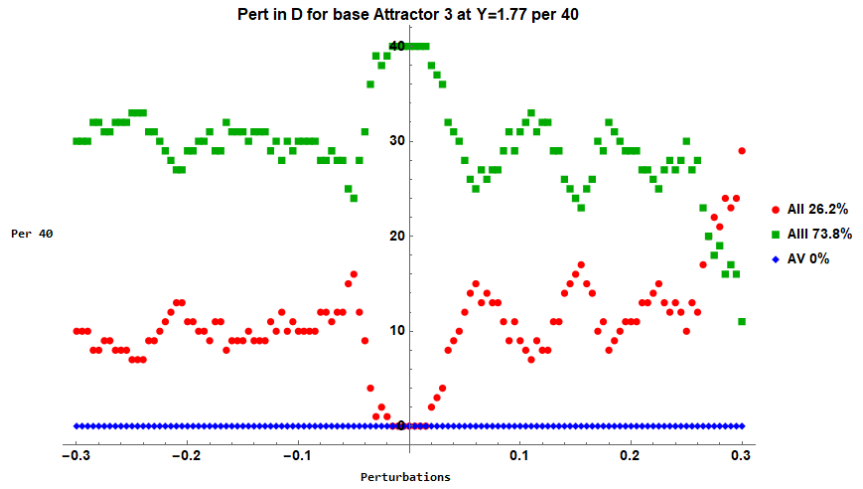
Pert in D for base Attractor 3 at Y=1.77 per 40
Per 40
Perturbations
All 26.2%
AIII 73.8%
AV 0%

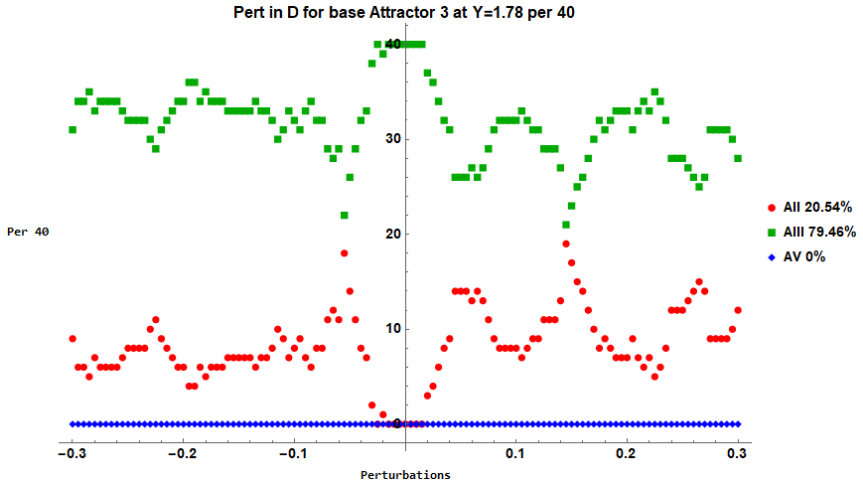
Pert in D for base Attractor 3 at Y=1.78 per 40
Per 40
Perturbations
All 20.54%
AIII 79.46%
AV 0%

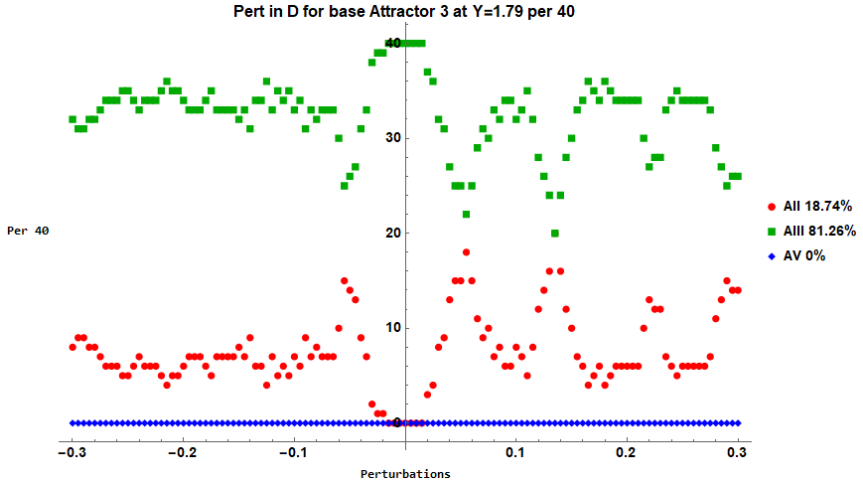
Pert in D for base Attractor 3 at Y=1.79 per 40
Per 40
Perturbations
All 18.74%
AIII 81.26%
AV 0%

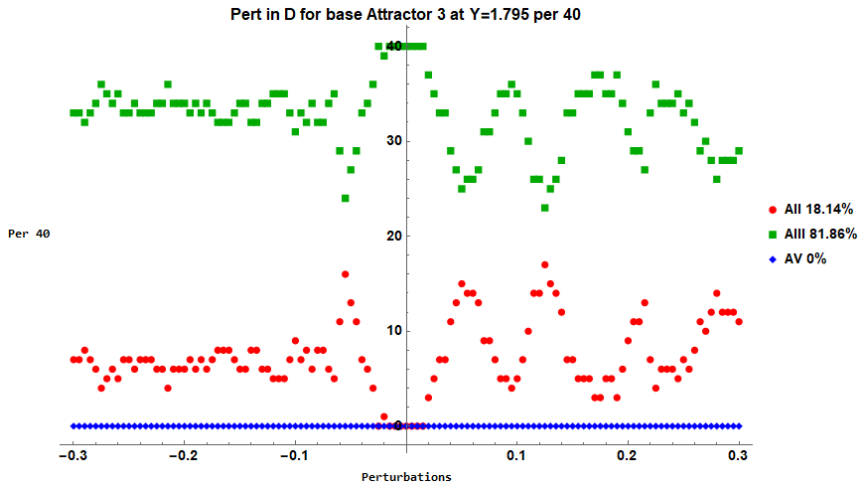
Pert in D for base Attractor 3 at Y=1.795 per 40
Per 40
Perturbations
All 18.14%
AIII 81.86%
AV 0%

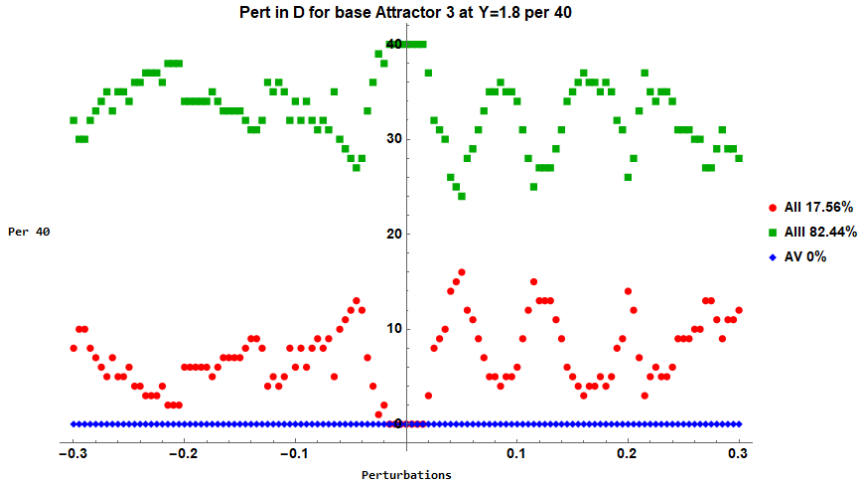
Pert in D for base Attractor 3 at Y=1.8 per 40
Per 40
Perturbations
All 17.56%
AIII 82.44%
AV 0%

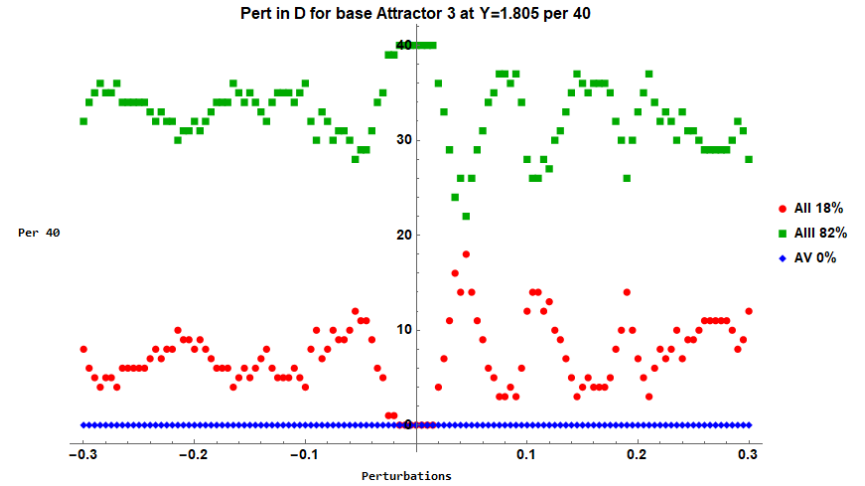
Pert in D for base Attractor 3 at Y=1.805 per 40
Per 40
Perturbations
All 18%
AIII 82%
AV 0%

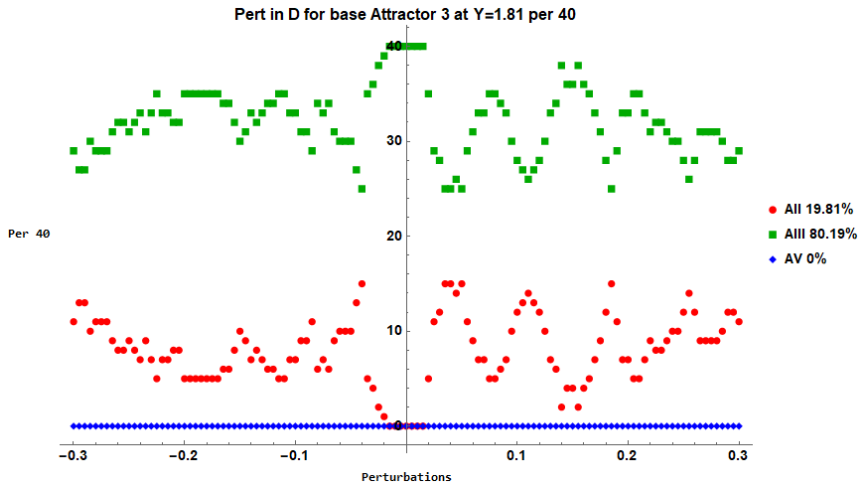
Pert in D for base Attractor 3 at Y=1.81 per 40
Per 40
Perturbations
AII 19.81%
AIII 80.19%
AV 0%

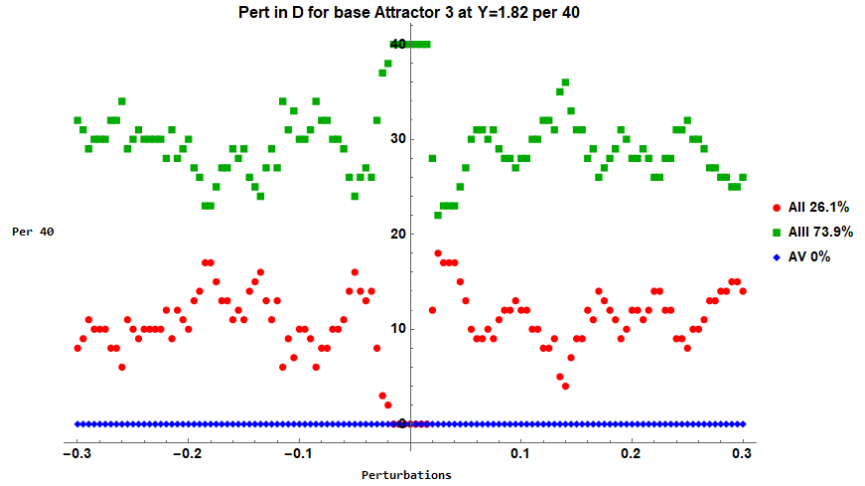
Pert in D for base Attractor 3 at Y=1.82 per 40
Per 40
Perturbations
AII 26.1%
AIII 73.9%
AV 0%

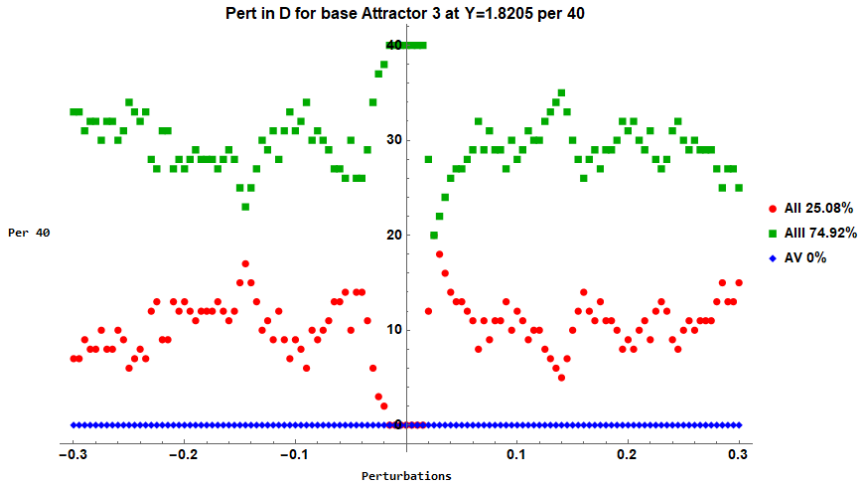
Pert in D for base Attractor 3 at Y=1.8205 per 40
Per 40
Perturbations
AII 25.08%
AIII 74.92%
AV 0%

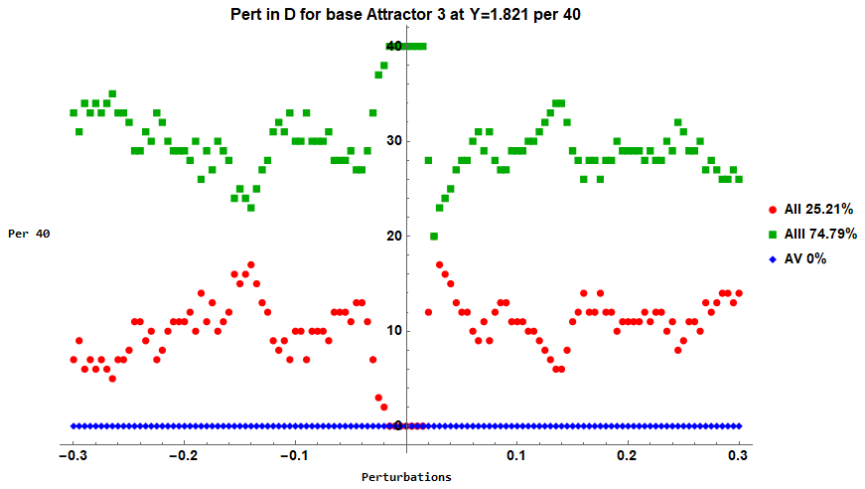
Pert in D for base Attractor 3 at Y=1.821 per 40
Per 40
Perturbations
AII 25.21%
AIII 74.79%
AV 0%

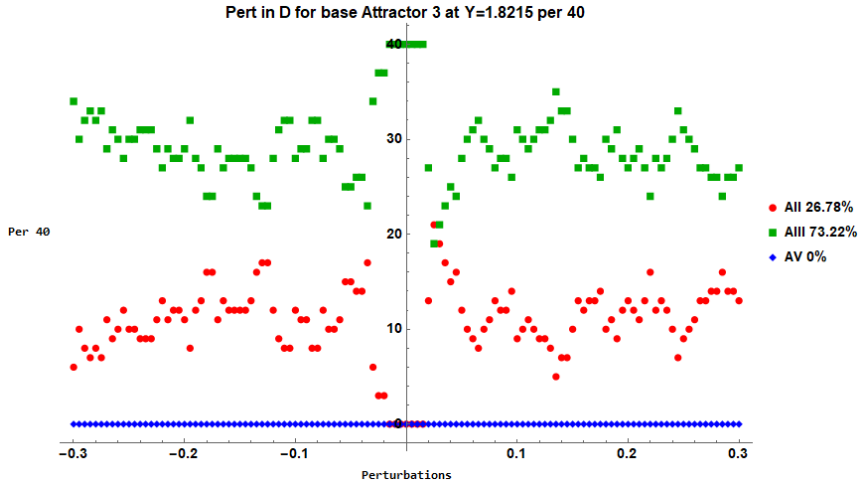
Pert in D for base Attractor 3 at Y=1.8215 per 40
Per 40
Perturbations
AII 26.78%
AIII 73.22%
AV 0%

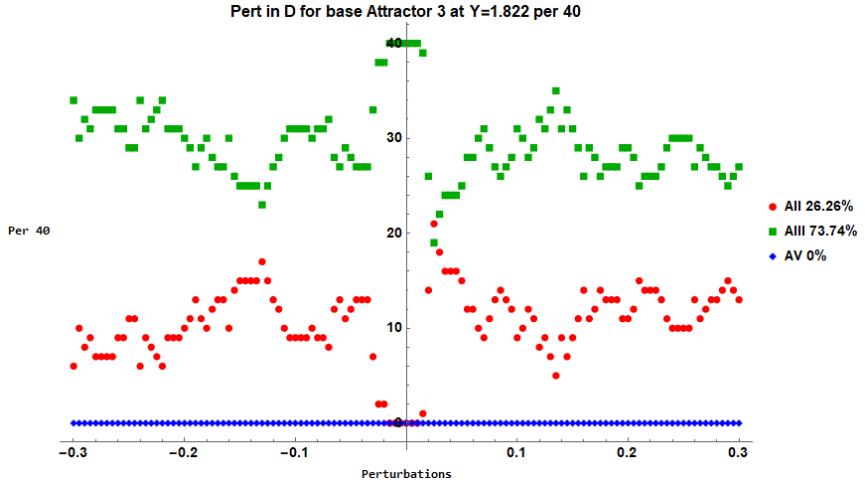
Pert in D for base Attractor 3 at Y=1.822 per 40
Per 40
Perturbations
AII 26.26%
AIII 73.74%
AV 0%

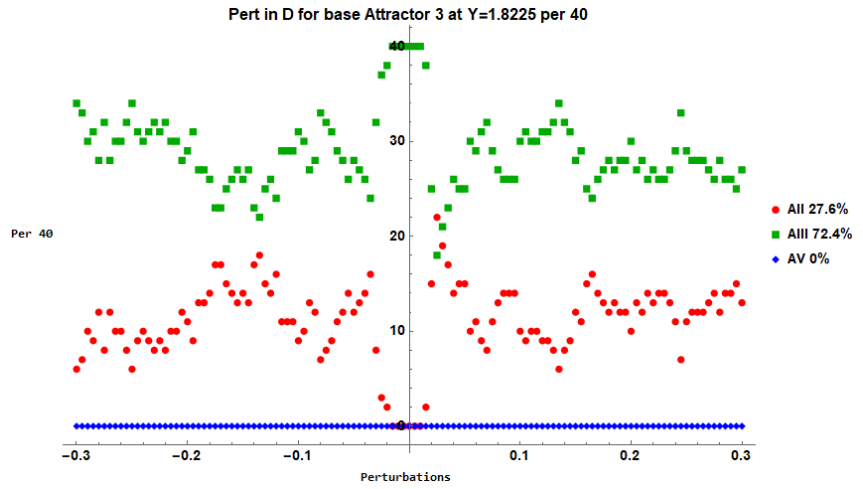
Pert in D for base Attractor 3 at Y=1.8225 per 40
Per 40
Perturbations
AII 27.6%
AIII 72.4%
AV 0%

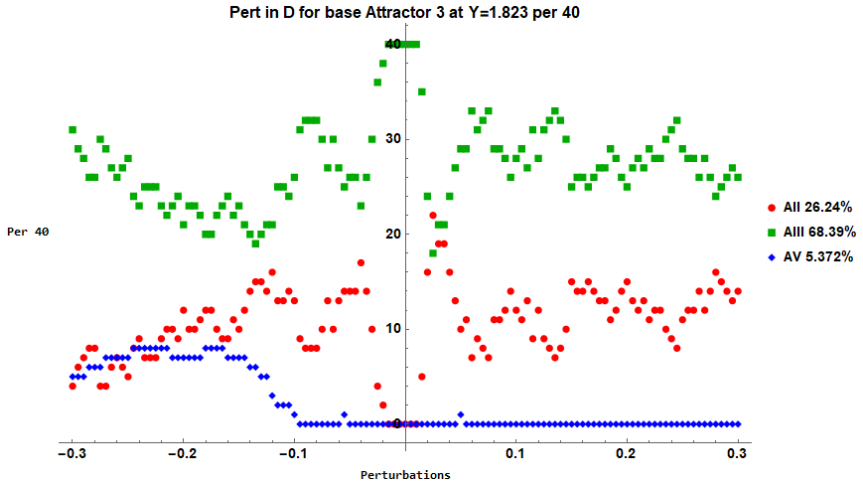
Pert in D for base Attractor 3 at Y=1.823 per 40
Per 40
Perturbations
AII 26.24%
AIII 68.39%
AV 5.372%

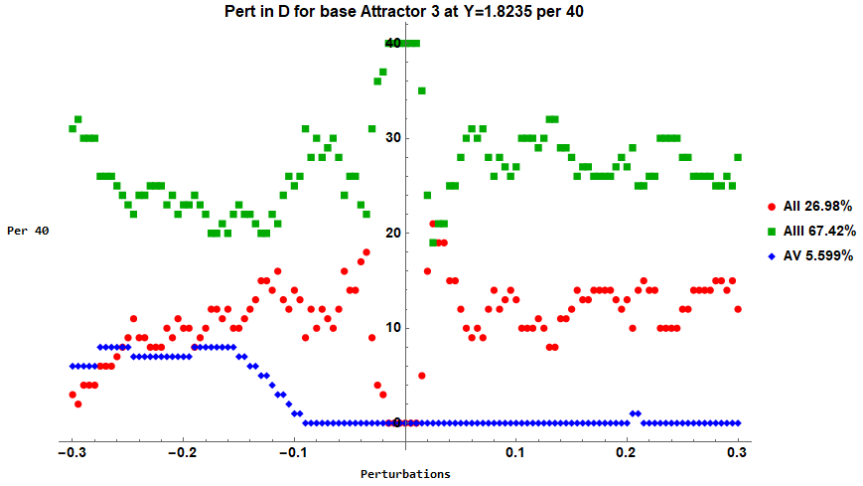
Pert in D for base Attractor 3 at Y=1.8235 per 40
Per 40
Perturbations
AII 26.98%
AIII 67.42%
AV 5.599%

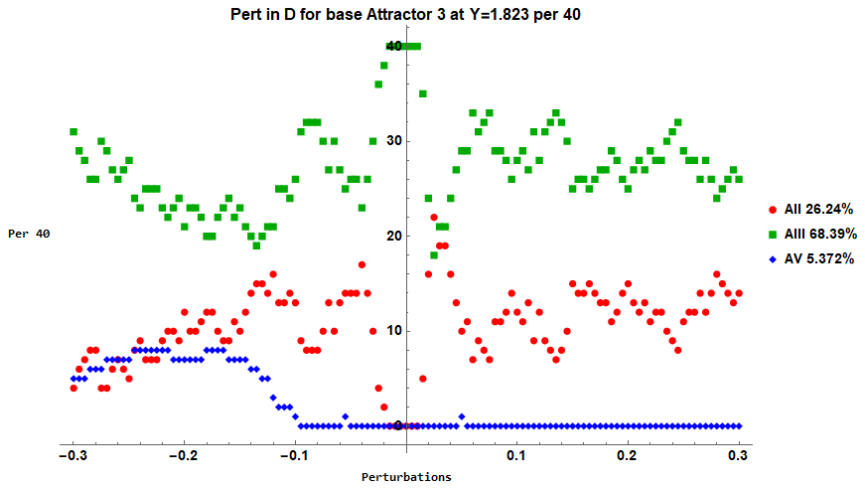
Pert in D for base Attractor 3 at Y=1.823 per 40
Per 40
Perturbations
All 26.24%
AIII 68.39%
AV 5.372%

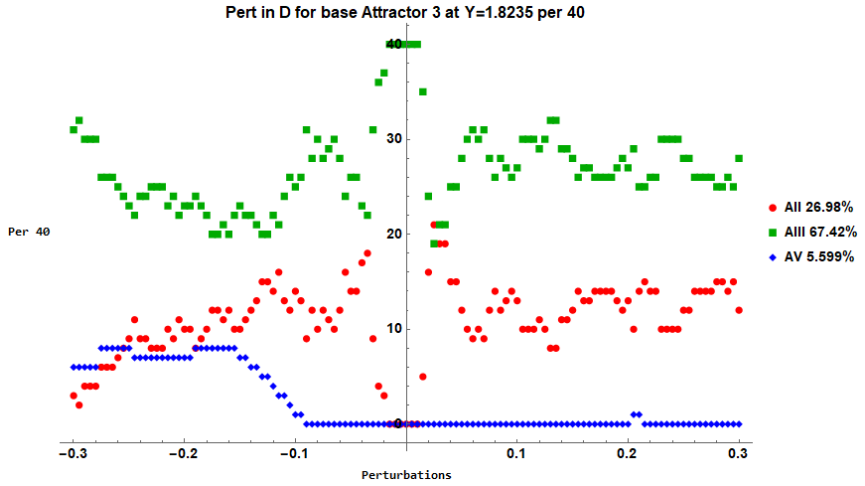
Pert in D for base Attractor 3 at Y=1.8235 per 40
Per 40
Perturbations
All 26.98%
AIII 67.42%
AV 5.599%

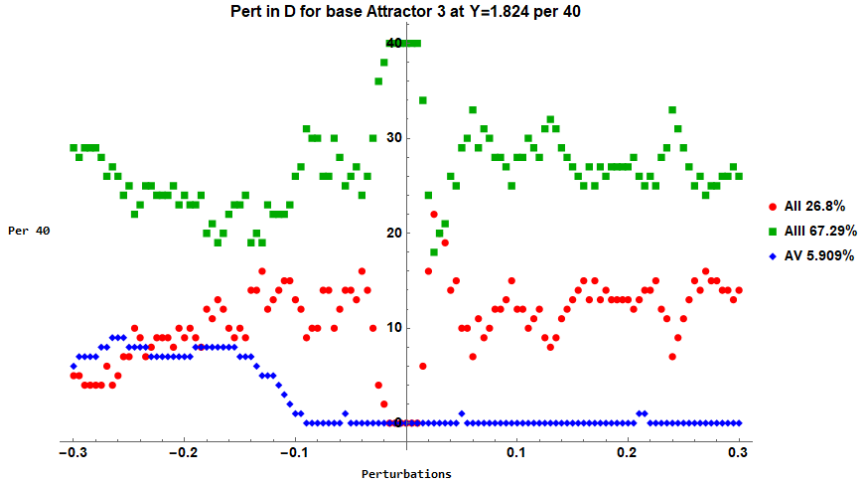
Pert in D for base Attractor 3 at Y=1.824 per 40
Per 40
Perturbations
All 26.8%
AIII 67.29%
AV 5.909%

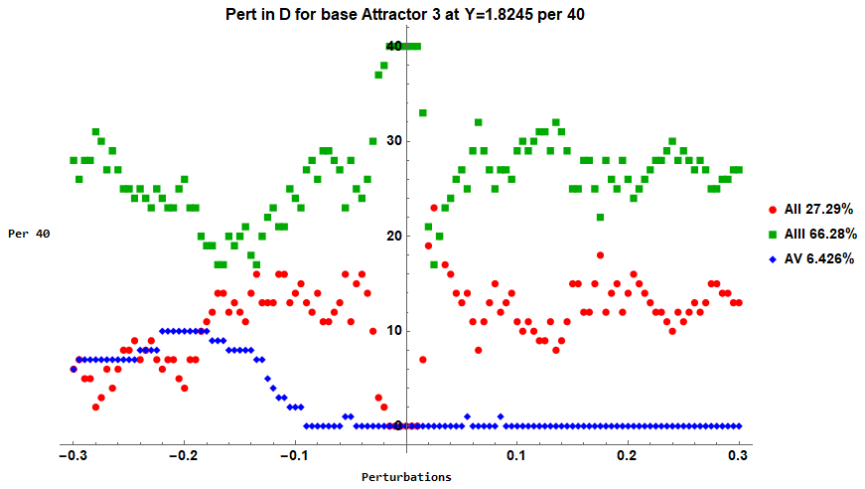
Pert in D for base Attractor 3 at Y=1.8245 per 40
Per 40
Perturbations
AII 27.29%
AIII 66.28%
AV 6.426%

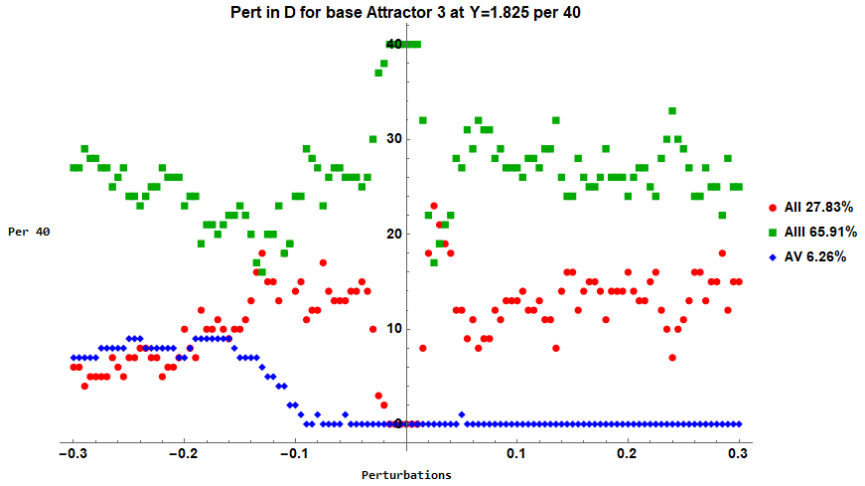
Pert in D for base Attractor 3 at Y=1.825 per 40
Per 40
Perturbations
AII 27.83%
AIII 65.91%
AV 6.26%

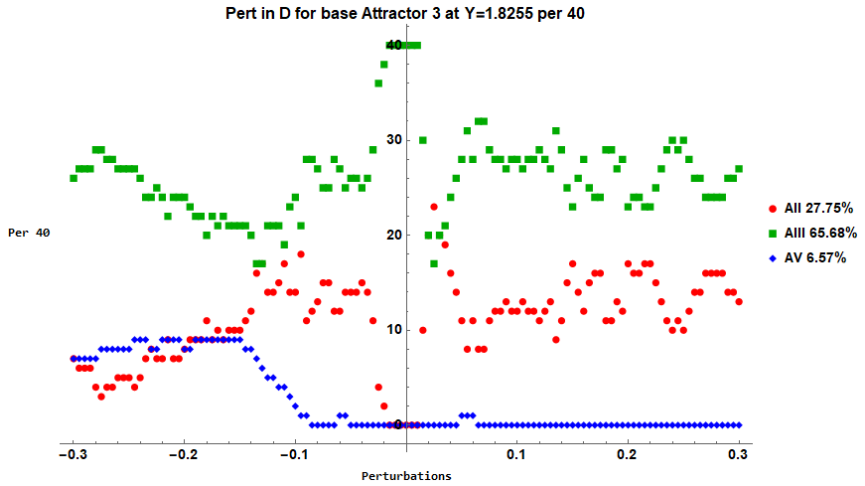
Pert in D for base Attractor 3 at Y=1.8255 per 40
Per 40
Perturbations
AII 27.75%
AIII 65.68%
AV 6.57%

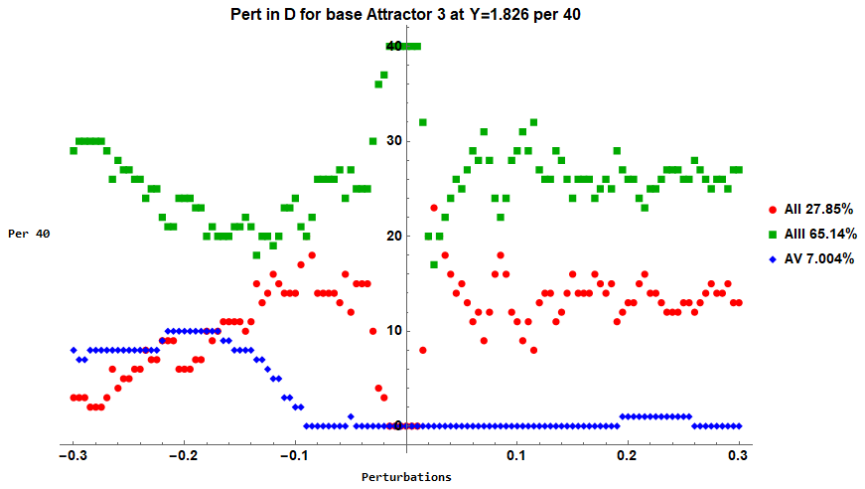
Pert in D for base Attractor 3 at Y=1.826 per 40
Per 40
Perturbations
AII 27.85%
AIII 65.14%
AV 7.004%

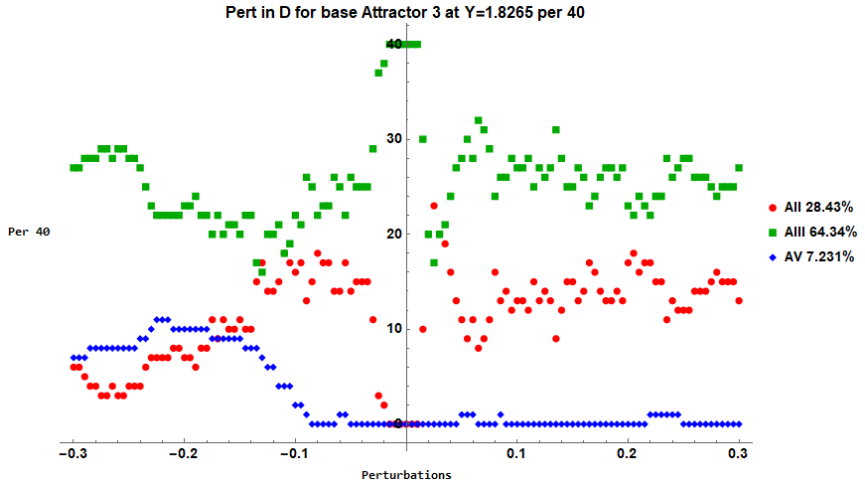
Pert in D for base Attractor 3 at Y=1.8265 per 40
Per 40
Perturbations
AII 28.43%
AIII 64.34%
AV 7.231%

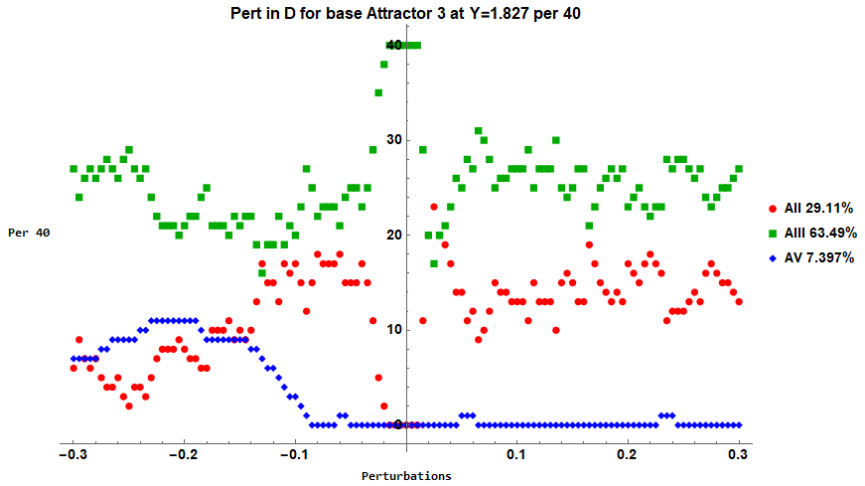
Pert in D for base Attractor 3 at Y=1.827 per 40
Per 40
Perturbations
AII 29.11%
AIII 63.49%
AV 7.397%

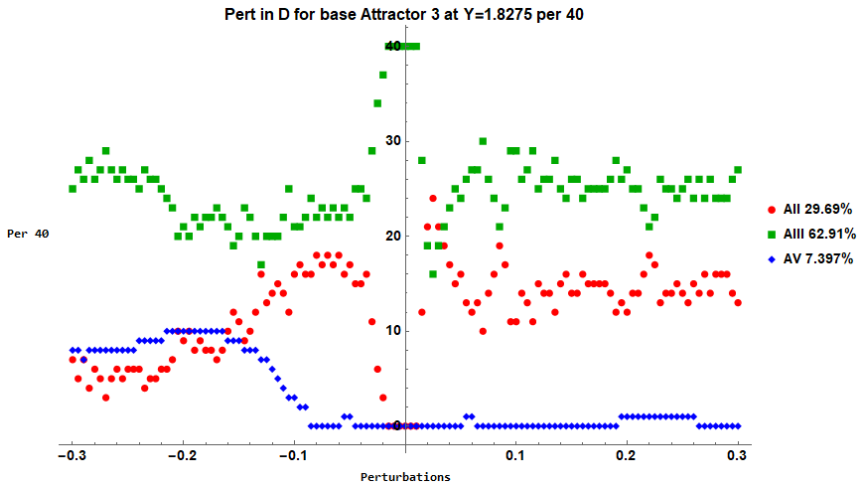
Pert in D for base Attractor 3 at Y=1.8275 per 40
Per 40
Perturbations
All 29.69%
AIII 62.91%
AV 7.397%

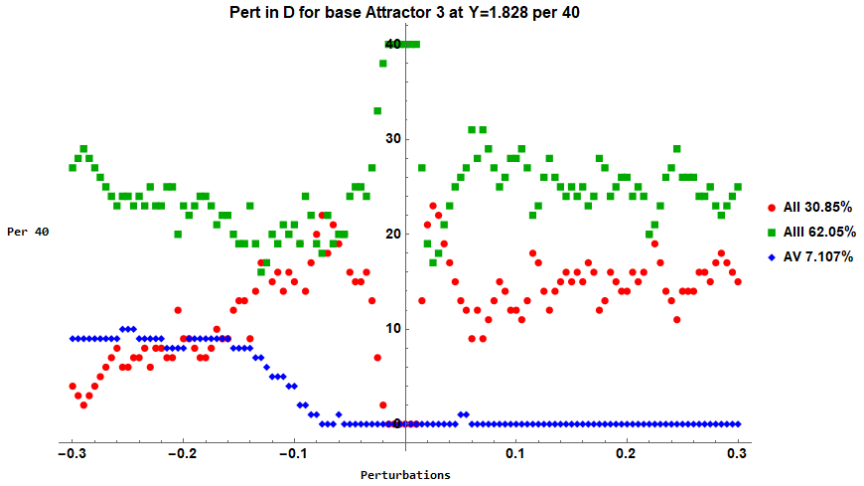
Pert in D for base Attractor 3 at Y=1.828 per 40
Per 40
Perturbations
All 30.85%
AIII 62.05%
AV 7.107%

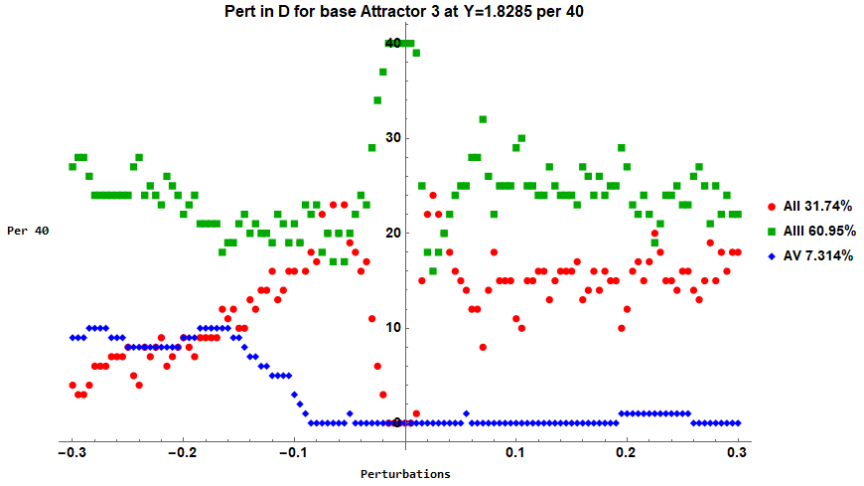
Pert in D for base Attractor 3 at Y=1.8285 per 40
Per 40
Perturbations
All 31.74%
AIII 60.95%
AV 7.314%

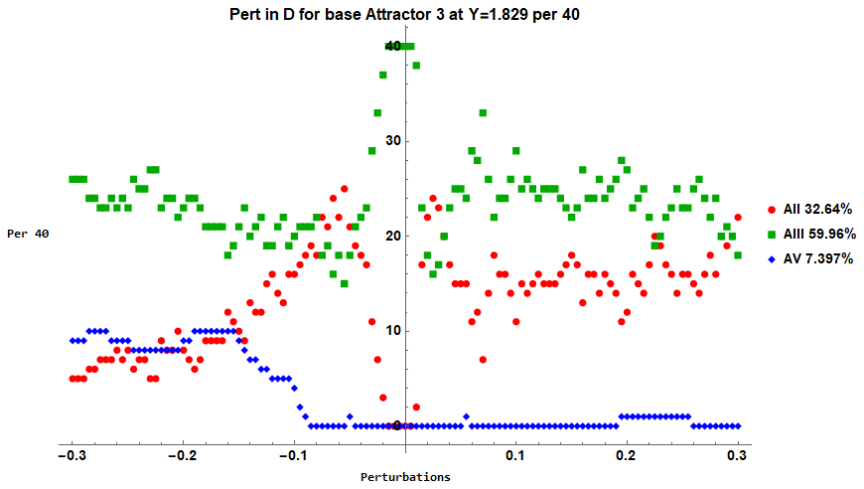
Pert in D for base Attractor 3 at Y=1.829 per 40
Per 40
Perturbations
AII 32.64%
AIII 59.96%
AV 7.397%

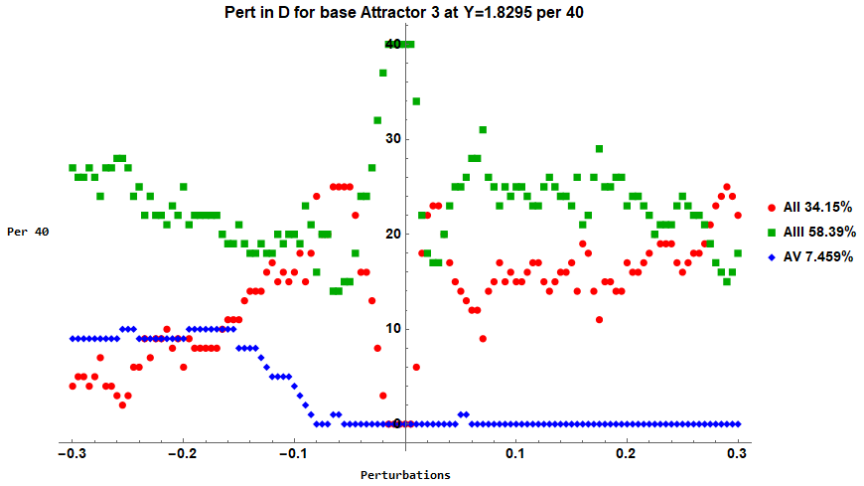
Pert in D for base Attractor 3 at Y=1.8295 per 40
Per 40
Perturbations
AII 34.15%
AIII 58.39%
AV 7.459%

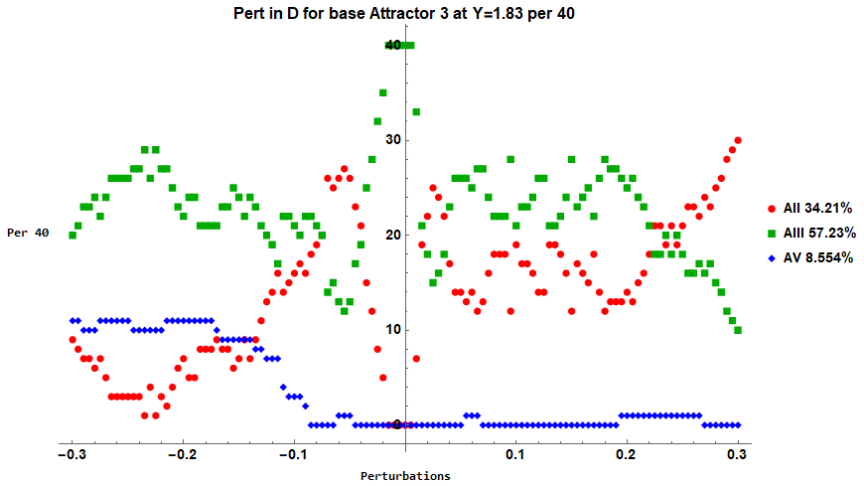
Pert in D for base Attractor 3 at Y=1.83 per 40
Per 40
Perturbations
AII 34.21%
AIII 57.23%
AV 8.554%

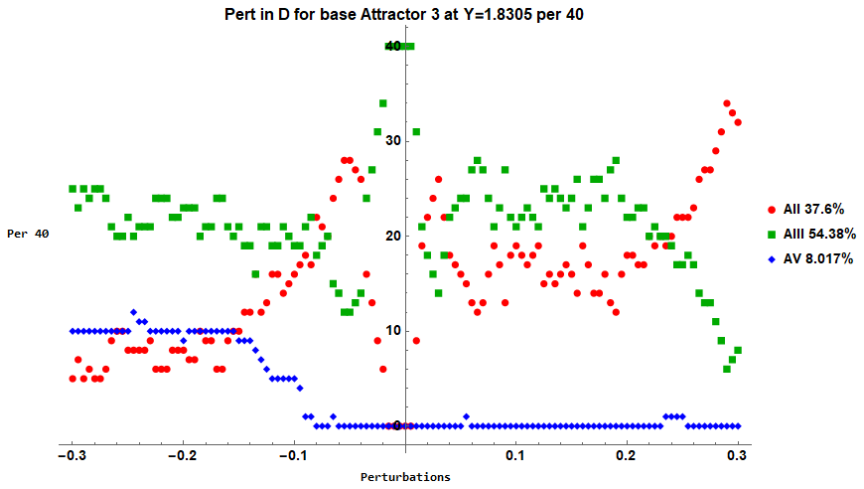
Pert in D for base Attractor 3 at Y=1.8305 per 40
Per 40
Perturbations
AII 37.6%
AIII 54.38%
AV 8.017%

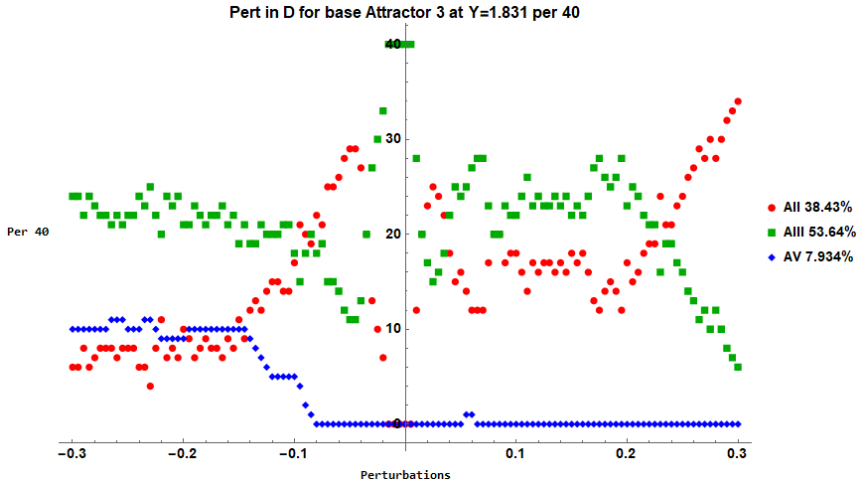
Pert in D for base Attractor 3 at Y=1.831 per 40
Per 40
Perturbations
AII 38.43%
AIII 53.64%
AV 7.934%

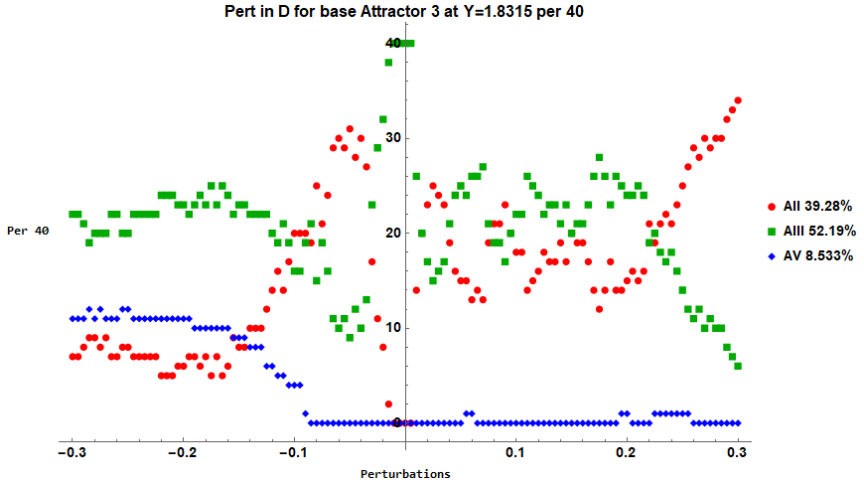
Pert in D for base Attractor 3 at Y=1.8315 per 40
Per 40
Perturbations
AII 39.28%
AIII 52.19%
AV 8.533%

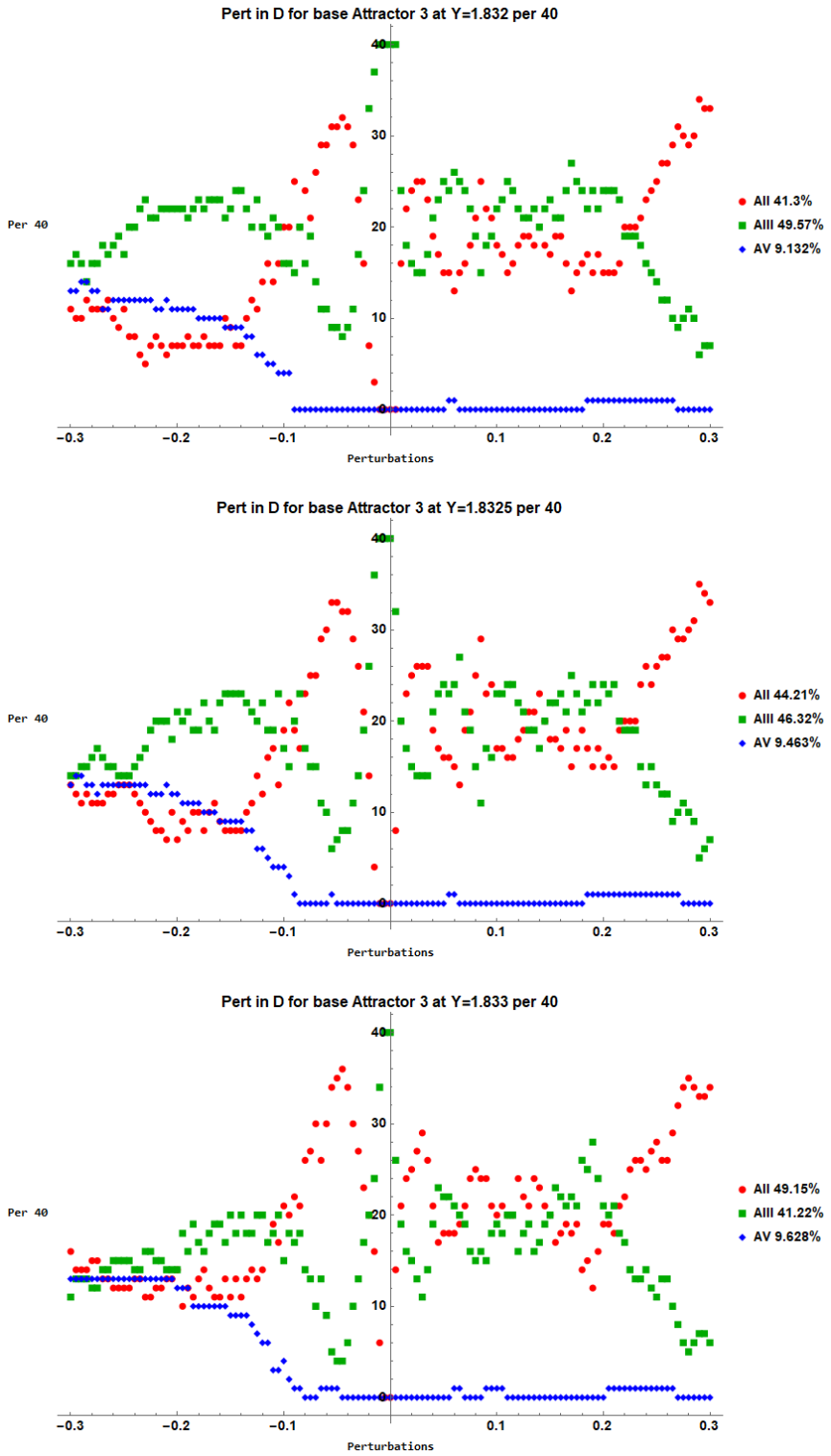

Figure A6. Perturbations of AIII for 1.62<Y<1.83. Each plot has the percentage chance of transitioning attractors for the total range of perturbations displayed.

Appendix 4.3. AV Perturbations

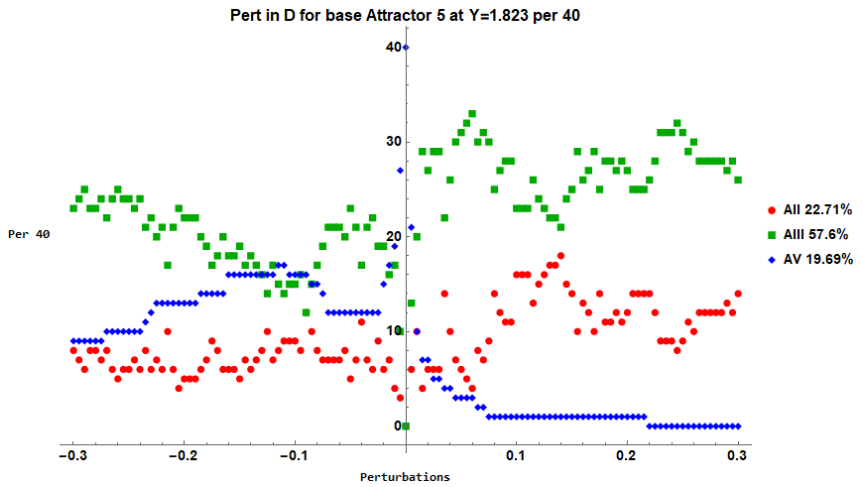
Pert in D for base Attractor 5 at Y=1.823 per 40
Per 40
Perturbations
AII 22.71%
AIII 57.6%
AV 19.69%

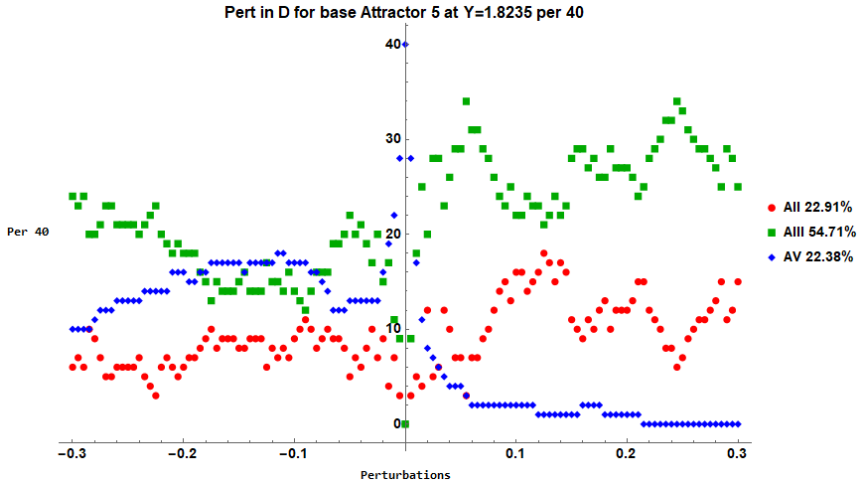
Pert in D for base Attractor 5 at Y=1.8235 per 40
Per 40
Perturbations
AII 22.91%
AIII 54.71%
AV 22.38%

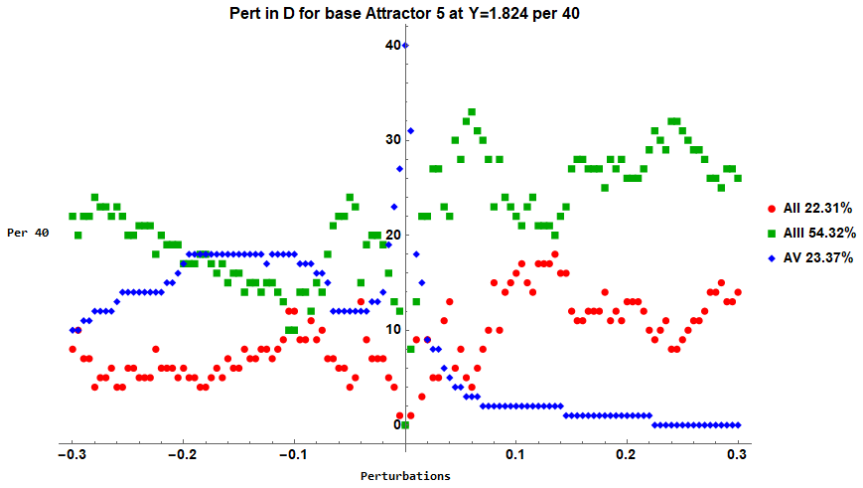
Pert in D for base Attractor 5 at Y=1.824 per 40
Per 40
Perturbations
AII 22.31%
AIII 54.32%
AV 23.37%

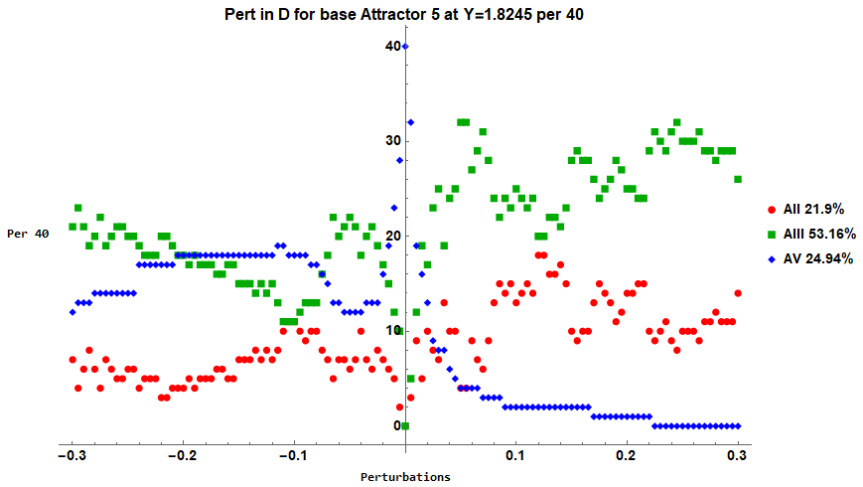
Pert in D for base Attractor 5 at Y=1.8245 per 40
Per 40
Perturbations
All 21.9%
AIII 53.16%
AV 24.94%

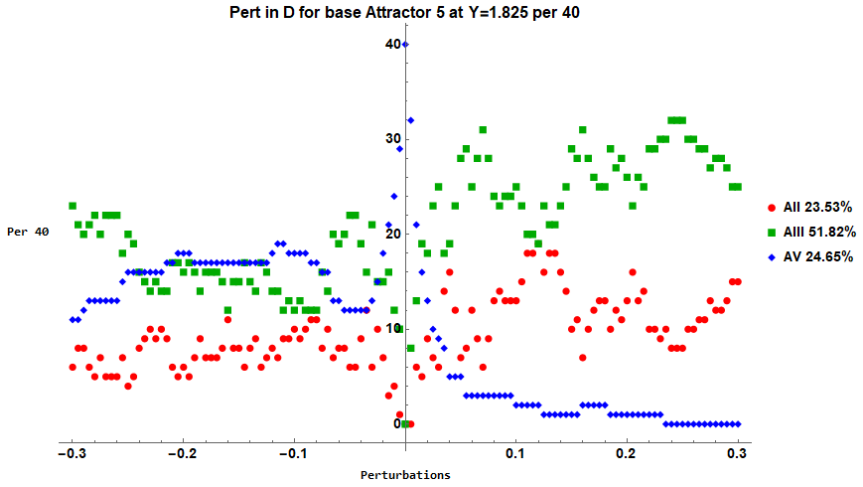
Pert in D for base Attractor 5 at Y=1.825 per 40
Per 40
Perturbations
All 23.53%
AIII 51.82%
AV 24.65%

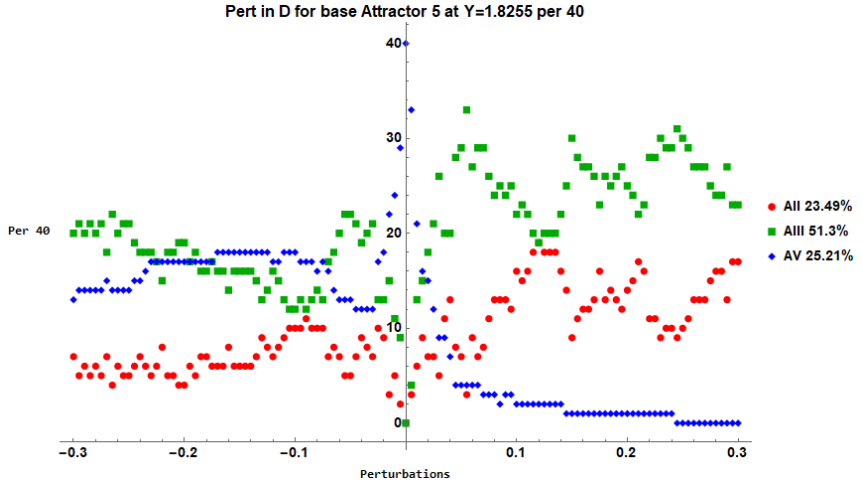
Pert in D for base Attractor 5 at Y=1.8255 per 40
Per 40
Perturbations
All 23.49%
AIII 51.3%
AV 25.21%

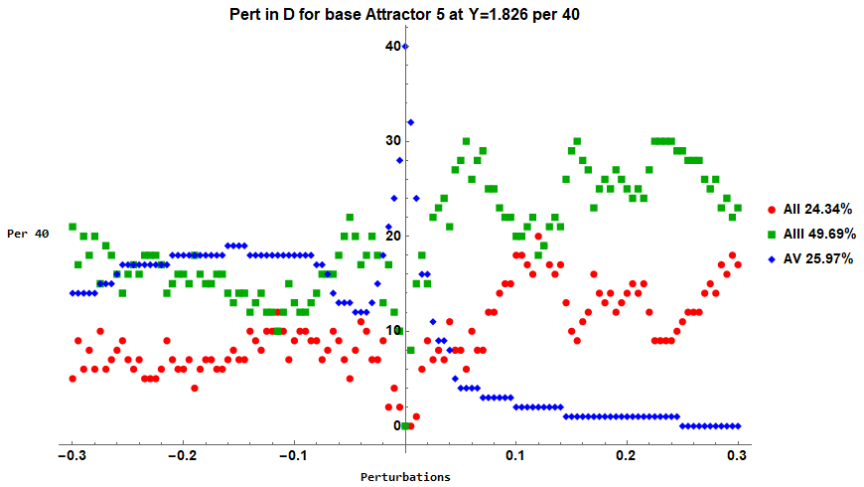
Pert in D for base Attractor 5 at Y=1.826 per 40
Per 40
Perturbations
All 24.34%
AIII 49.69%
AV 25.97%

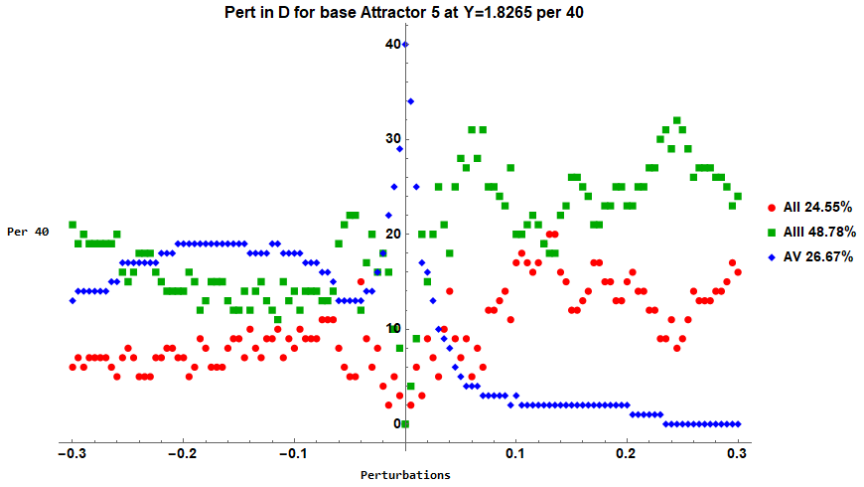
Pert in D for base Attractor 5 at Y=1.8265 per 40
Per 40
Perturbations
All 24.55%
AIII 48.78%
AV 26.67%

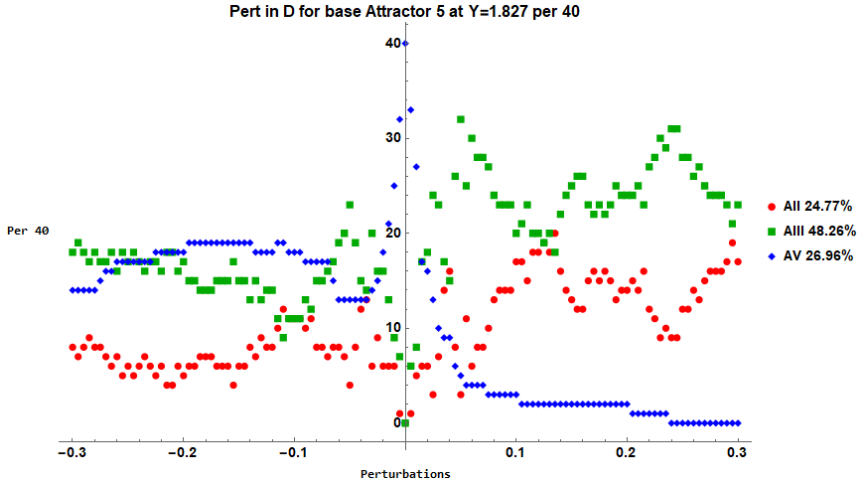
Pert in D for base Attractor 5 at Y=1.827 per 40
Per 40
Perturbations
All 24.77%
AIII 48.26%
AV 26.96%

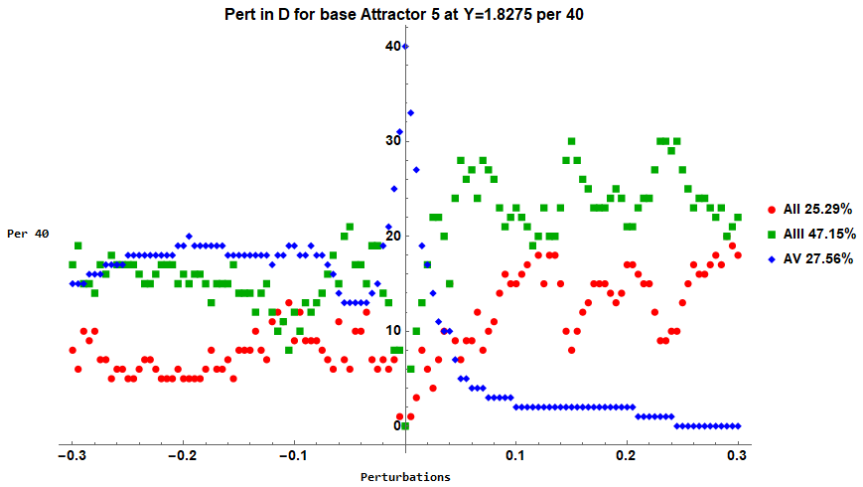
Pert in D for base Attractor 5 at Y=1.8275 per 40
Per 40
Perturbations
All 25.29%
AIII 47.15%
AV 27.56%

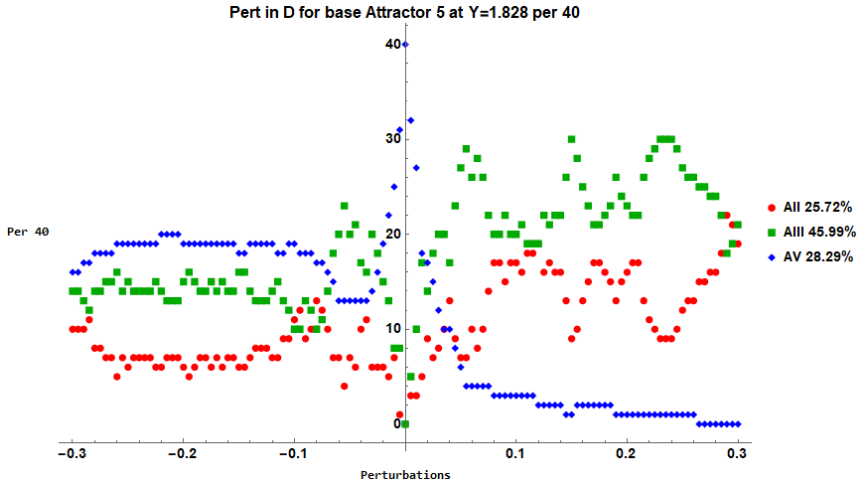
Pert in D for base Attractor 5 at Y=1.828 per 40
Per 40
Perturbations
All 25.72%
AIII 45.99%
AV 28.29%

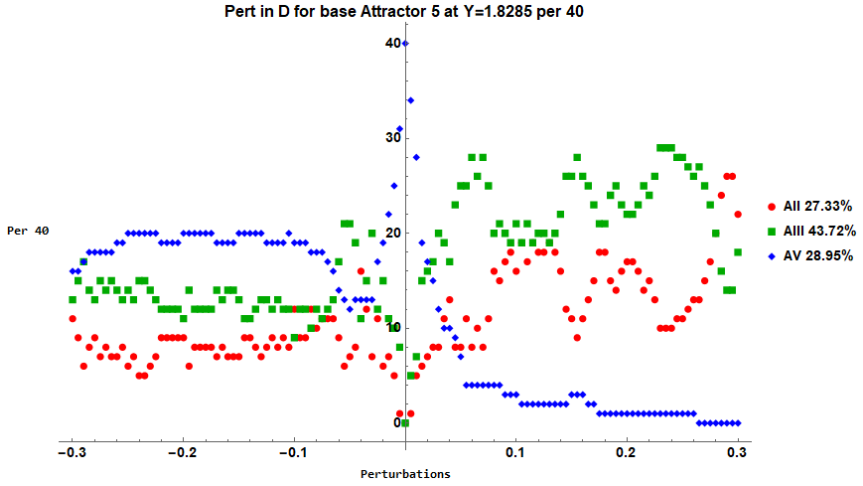
Pert in D for base Attractor 5 at Y=1.8285 per 40
Per 40
Perturbations
All 27.33%
AIII 43.72%
AV 28.95%

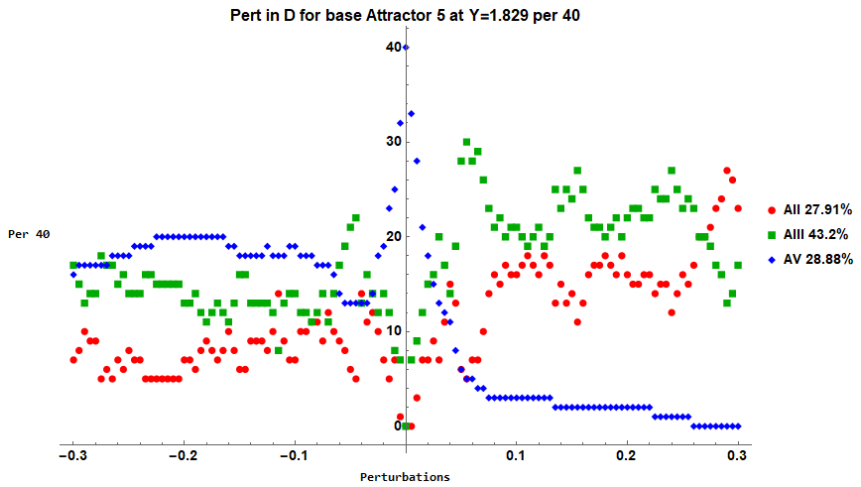
Pert in D for base Attractor 5 at Y=1.829 per 40
Per 40
Perturbations
All 27.91%
AIII 43.2%
AV 28.88%

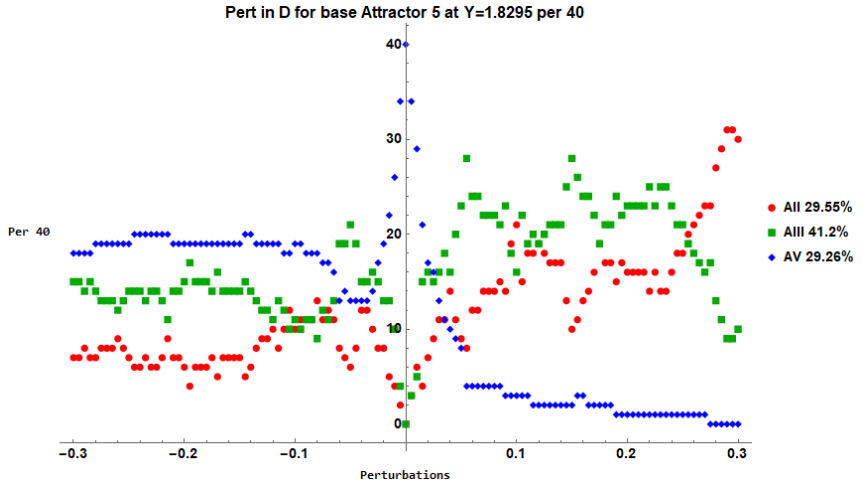
Pert in D for base Attractor 5 at Y=1.8295 per 40
Per 40
Perturbations
All 29.55%
AIII 41.2%
AV 29.26%

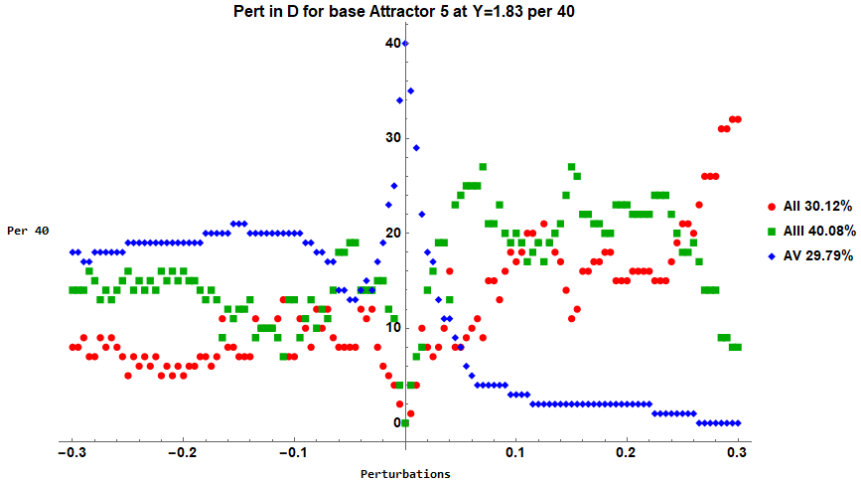
Pert in D for base Attractor 5 at Y=1.83 per 40
Per 40
Perturbations
All 30.12%
AIII 40.08%
AV 29.79%

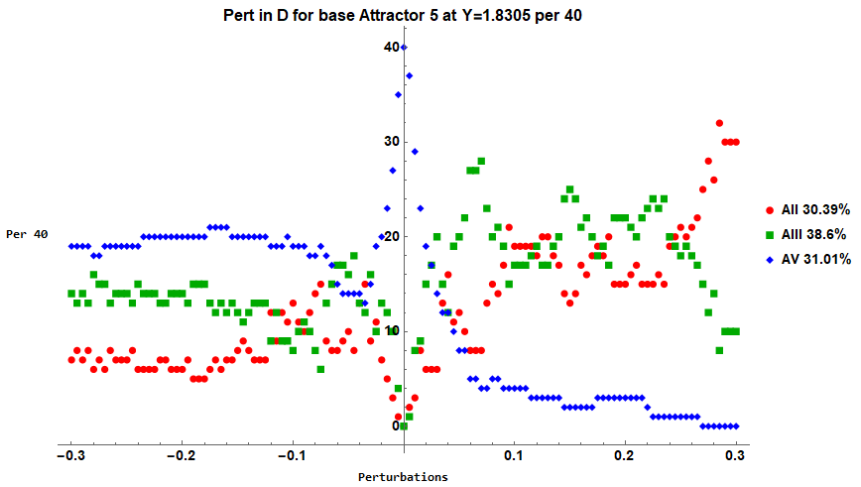
Pert in D for base Attractor 5 at Y=1.8305 per 40
Per 40
Perturbations
All 30.39%
AIII 38.6%
AV 31.01%

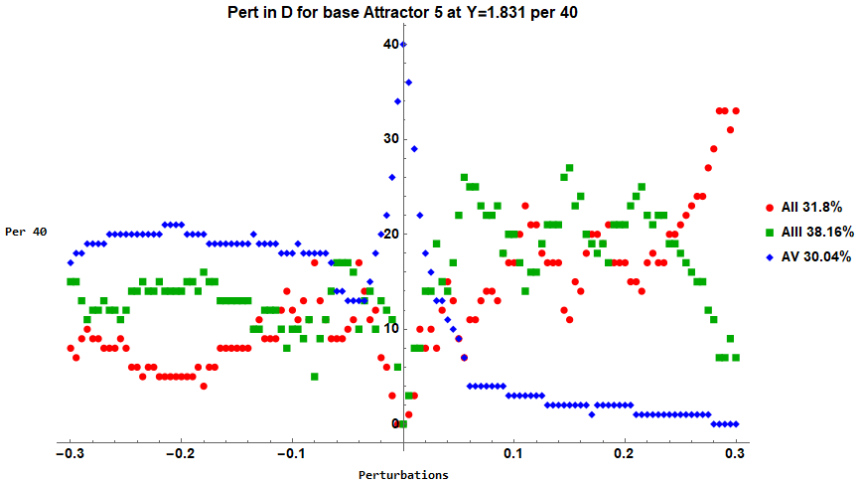
Pert in D for base Attractor 5 at Y=1.831 per 40
Per 40
Perturbations
All 31.8%
AIII 38.16%
AV 30.04%

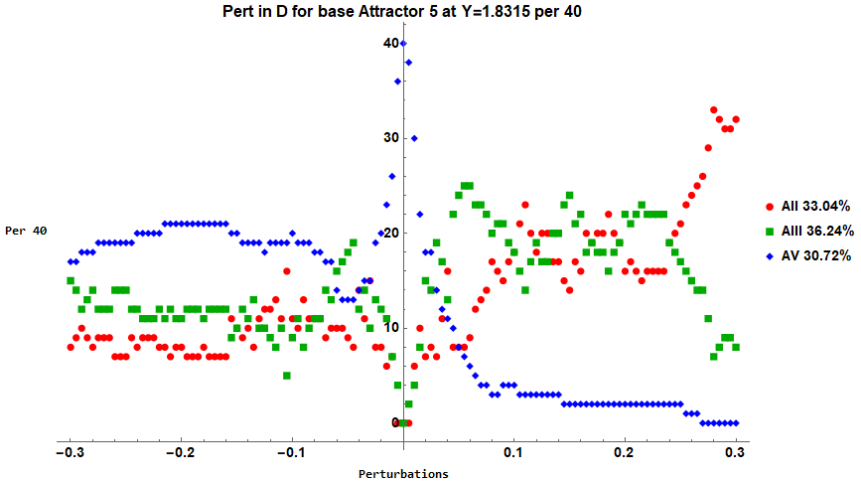
Pert in D for base Attractor 5 at Y=1.8315 per 40
Per 40
Perturbations
All 33.04%
AIII 36.24%
AV 30.72%

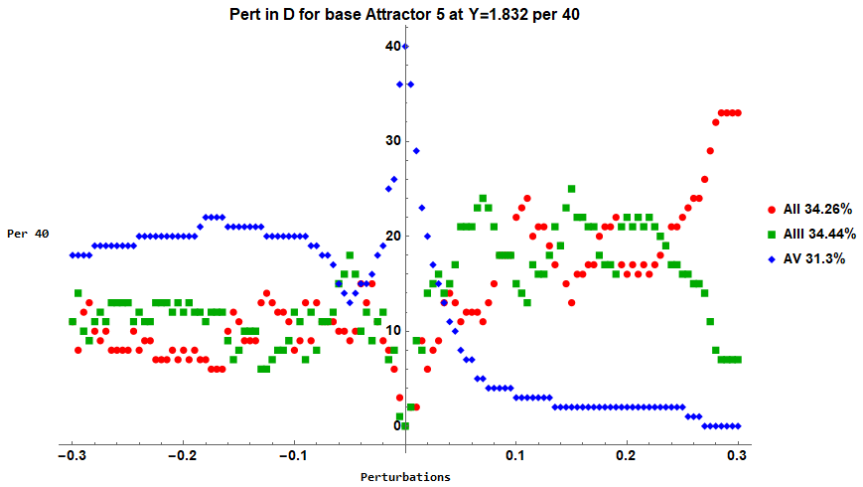
Pert in D for base Attractor 5 at Y=1.832 per 40
Per 40
Perturbations
All 34.26%
AIII 34.44%
AV 31.3%

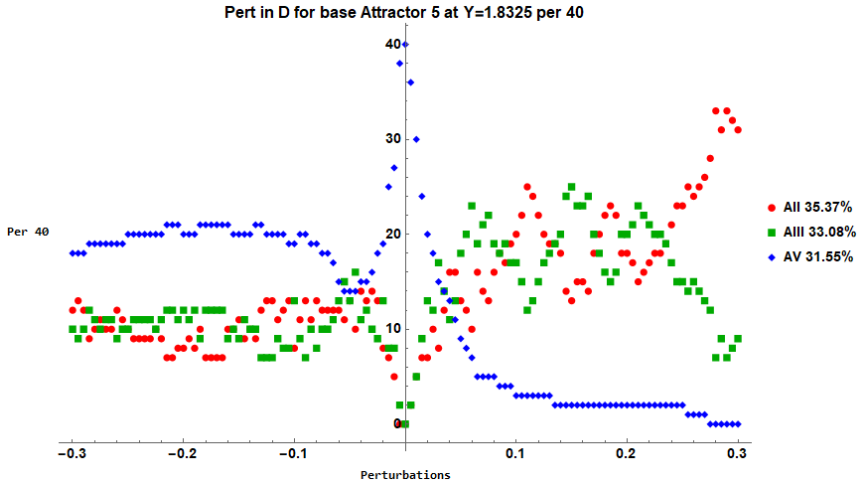
Pert in D for base Attractor 5 at Y=1.8325 per 40
Per 40
Perturbations
All 35.37%
AIII 33.08%
AV 31.55%

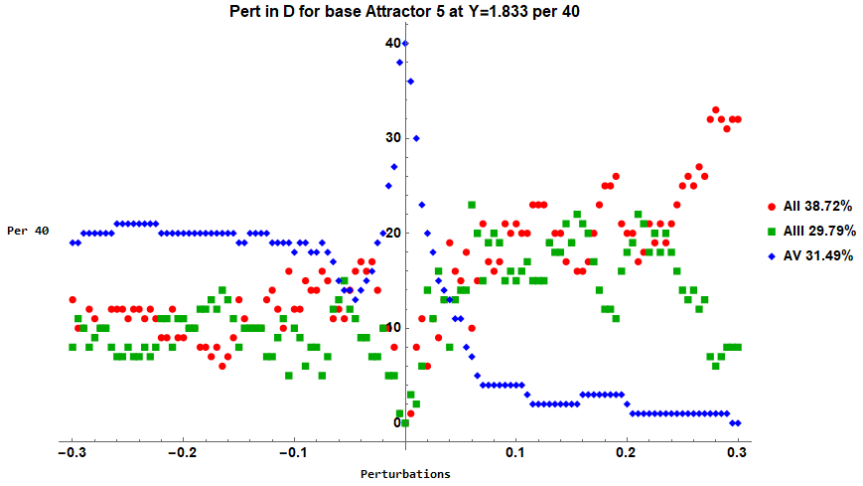
Pert in D for base Attractor 5 at Y=1.833 per 40
Per 40
Perturbations
All 38.72%
AIII 29.79%
AV 31.49%

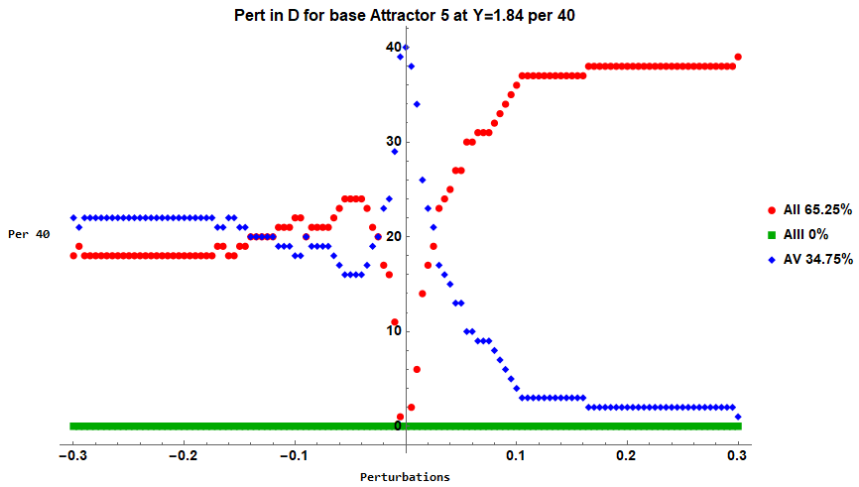
Pert in D for base Attractor 5 at Y=1.84 per 40
Per 40
Perturbations
All 65.25%
AIII 0%
AV 34.75%

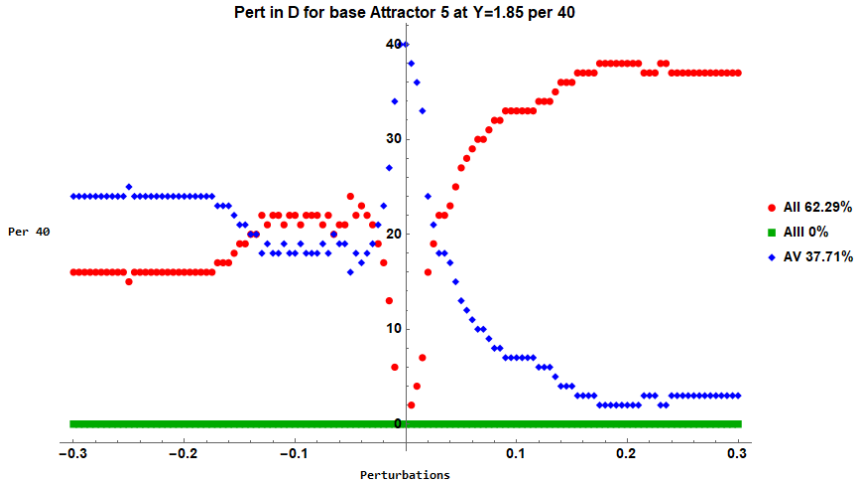
Pert in D for base Attractor 5 at Y=1.85 per 40
Per 40
Perturbations
All 62.29%
AIII 0%
AV 37.71%

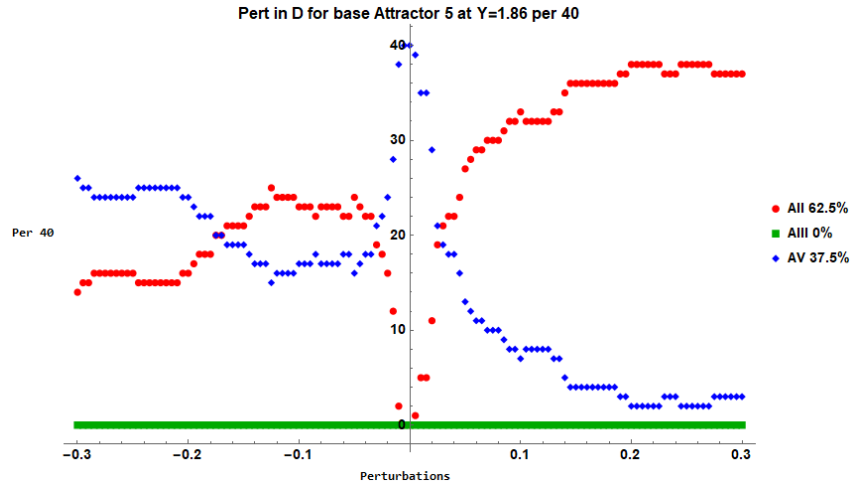
Pert in D for base Attractor 5 at Y=1.86 per 40
Per 40
Perturbations
All 62.5%
AIII 0%
AV 37.5%

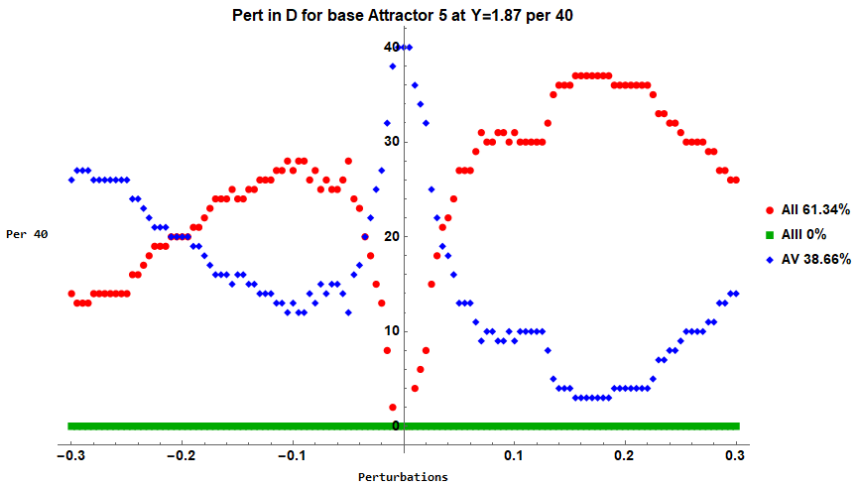
Pert in D for base Attractor 5 at Y=1.87 per 40
Per 40
Perturbations
All 61.34%
AIII 0%
AV 38.66%

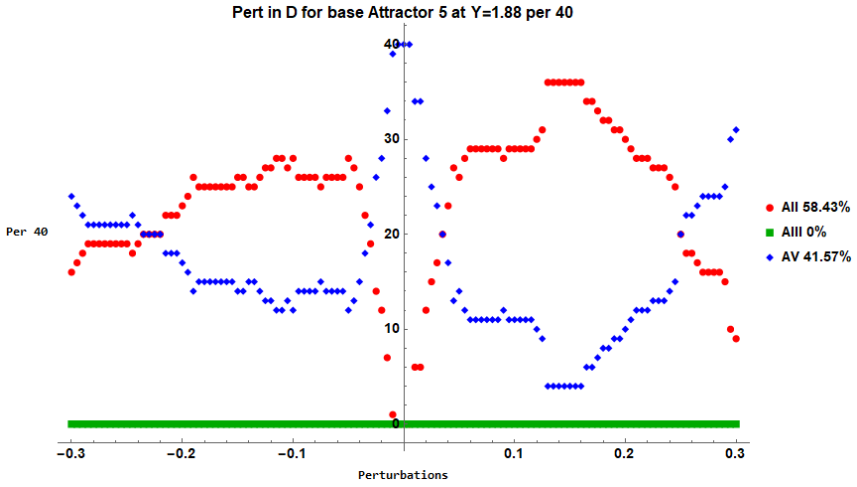
Pert in D for base Attractor 5 at Y=1.88 per 40
Per 40
Perturbations
All 58.43%
AIII 0%
AV 41.57%

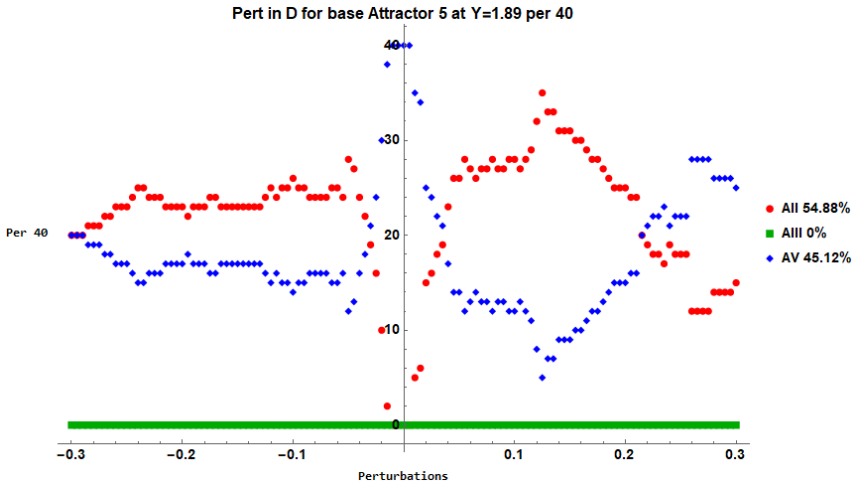
Pert in D for base Attractor 5 at Y=1.89 per 40
Per 40
Perturbations
All 54.88%
AIII 0%
AV 45.12%

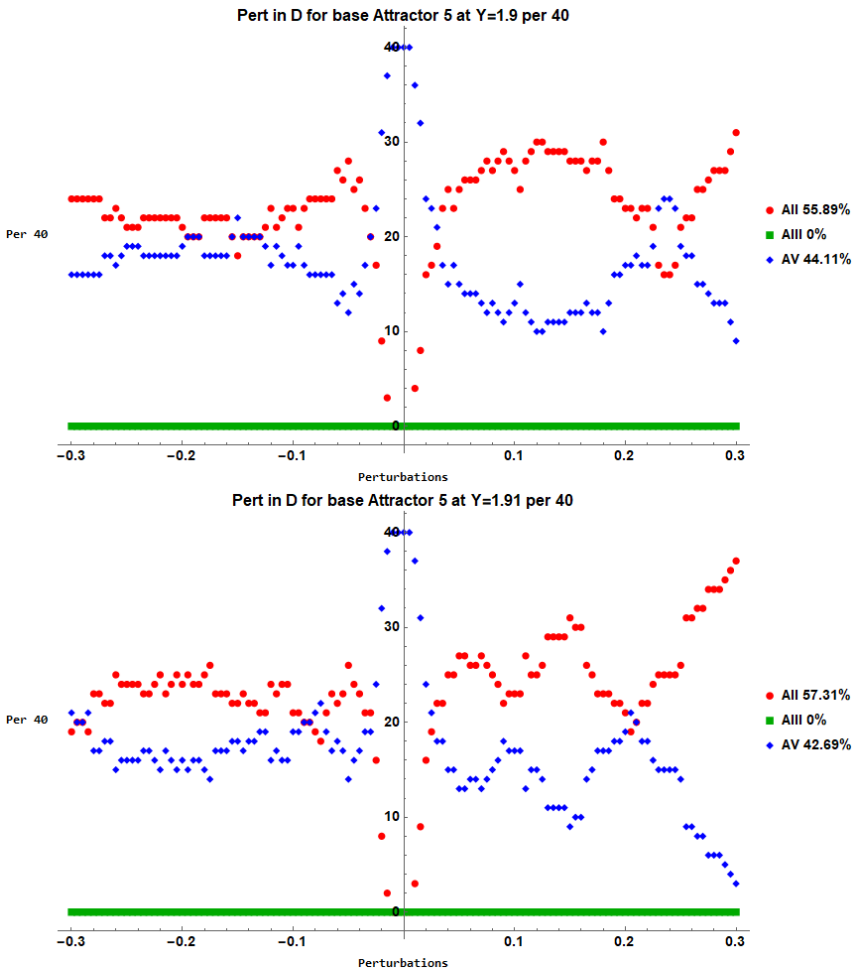
Pert in D for base Attractor 5 at Y=1.9 per 40
Per 40
40
30
20
10
0
−0.3
−0.2
−0.1
0.1
0.2
0.3
Perturbations
All 55.89%
AIII 0%
AV 44.11%
Pert in D for base Attractor 5 at Y=1.91 per 40
Per 40
40
30
20
10
0
−0.3
−0.2
−0.1
0.1
0.2
0.3
Perturbations
All 57.31%
AIII 0%
AV 42.69%

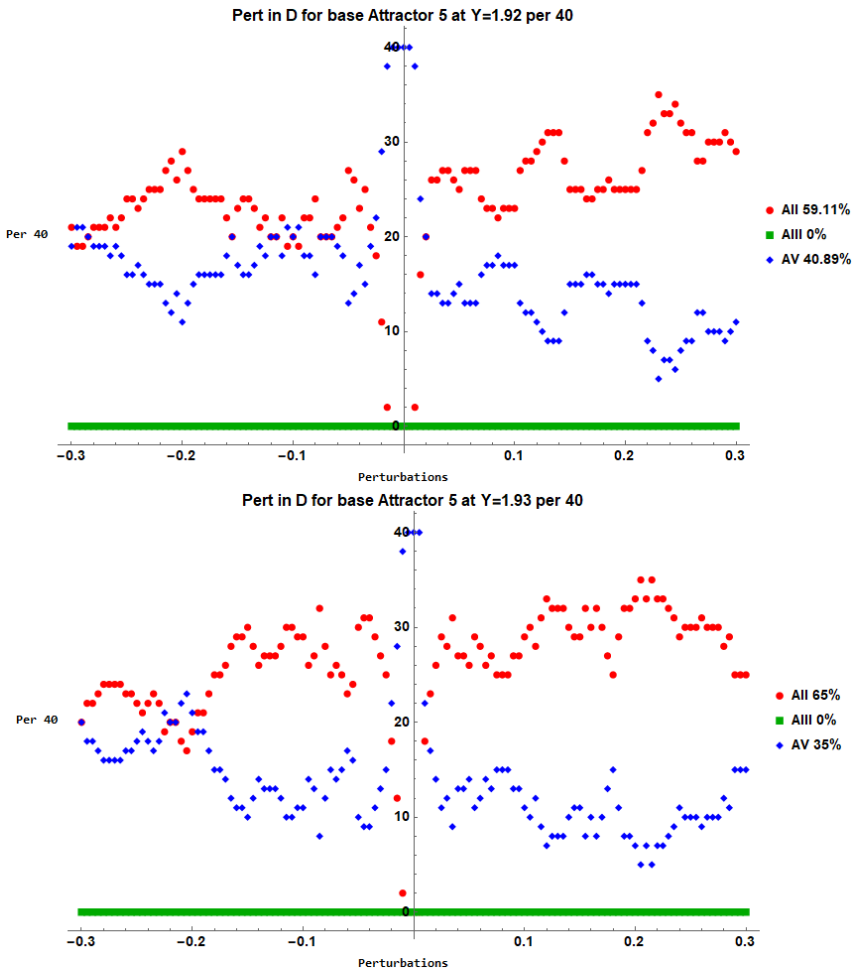

Figure A7. Perturbations of AV for 1.82<Y<1.93. Each plot has the percentage chance of transitioning attractors for the total range of perturbations displayed.

Appendix 5. Mathematica Code

Appendix 5.1. Steady State and Stability Analysis

```
(*Using the Solved determinate of a 5x5 matrix it checks to see where
 the stable region starts and plots the graph on the xy plane with Y vs X*)


Clear["Global`*"]
Case = 2;

If[Case == 2,
  c = 3.0;
  K = 0.1;
  ϕ = -0.5 * K;
  γ = 0.01;
  Δ = 0.5];


stp = 4;
Adj = -0.5;
out = "Lis System\\Case 2\\SteadyStates\\Steady state curve.csv";

SSC = {{"Y", "X", "Stable-1, unstable-0"}};
 m = {};
q = Range[0, stp, 0.05];
y1 = x ((1 - (2 c / (1 + Δ^2 + x^2))) ^2 + (2 c Δ / (1 + Δ^2 + x^2) - (ϕ / K)) ^2) ^ (1 / 2);
t1 = Table[y1, {x, 0, stp, 0.05}];
For[n = 1, n <= Length[t1], n++, m = Append[m, {Extract[t1, n], Extract[q, n]}]];
mn = {Table[{y1, x}, {x, 0, stp, 0.005}]};
bool = True;
yd = D[y1, x];

x = 0; While[x ≤ 5.0,
 c0 = 1;
 c1 = 2 + γ + 2 K;
 c2 = 1 + 2 γ + Abs[x]^2 γ + Δ^2 + 4 K + 2 γ K + K^2 + ϕ^2 - 4 c K / (1 + Δ^2 + Abs[x]^2) - 4 c Δ^2 K / (1 + Δ^2 + Abs[x]^2);
 c3 = γ + Abs[x]^2 γ + γ Δ^2 + 2 K + 4 γ K + 2 Abs[x]^2 γ K + 2 Δ^2 K + 2 K^2 +
    γ K^2 + 2 ϕ^2 + γ ϕ^2 - 4 c K / (1 + Δ^2 + Abs[x]^2) - 4 c γ K / (1 + Δ^2 + Abs[x]^2) - 2 c Abs[x]^2 γ K / (1 + Δ^2 + Abs[x]^2) -
    4 c Δ^2 K / (1 + Δ^2 + Abs[x]^2) - 4 c γ Δ^2 K / (1 + Δ^2 + Abs[x]^2) - 4 c K^2 / (1 + Δ^2 + Abs[x]^2) - 4 c Δ^2 K^2 / (1 + Δ^2 + Abs[x]^2);
```

$$c4 = 2\gamma K + 2\,\text{Abs}[x]^2\gamma K + 2\gamma\Delta^2 K + K^2 + 2\gamma K^2 + \text{Abs}[x]^2\gamma K^2 + \Delta^2 K^2 + \phi^2 + 2\gamma\phi^2 + \text{Abs}[x]^2\gamma\phi^2 + \Delta^2\phi^2 + \frac{4c^2K^2}{\left(1+\Delta^2+\text{Abs}[x]^2\right)^2} + \frac{8c^2\Delta^2K^2}{\left(1+\Delta^2+\text{Abs}[x]^2\right)^2} + \frac{4c^2\Delta^4K^2}{\left(1+\Delta^2+\text{Abs}[x]^2\right)^2} - \frac{4c\gamma K}{1+\Delta^2+\text{Abs}[x]^2} - \frac{4c\gamma\Delta^2K}{1+\Delta^2+\text{Abs}[x]^2} - \frac{4cK^2}{1+\Delta^2+\text{Abs}[x]^2} - \frac{4c\gamma K^2}{1+\Delta^2+\text{Abs}[x]^2} + \frac{2c\,\text{Abs}[x]^2\gamma K^2}{1+\Delta^2+\text{Abs}[x]^2} - \frac{4c\Delta^2K^2}{1+\Delta^2+\text{Abs}[x]^2} - \frac{4c\,\gamma\Delta^2K^2}{1+\Delta^2+\text{Abs}[x]^2} - \frac{4c\Delta K\phi}{1+\Delta^2+\text{Abs}[x]^2} - \frac{2c\,\text{Abs}[x]^2\gamma\Delta K\phi}{1+\Delta^2+\text{Abs}[x]^2} - \frac{4c\Delta^3K\phi}{1+\Delta^2+\text{Abs}[x]^2};$$

$$c5 = \gamma K^2 + \text{Abs}[x]^2\gamma K^2 + \gamma\Delta^2K^2 + \gamma\phi^2 + \text{Abs}[x]^2\gamma\phi^2 + \gamma\Delta^2\phi^2 + \frac{4c^2\gamma K^2}{\left(1+\Delta^2+\text{Abs}[x]^2\right)^2} - \frac{4c^2\,\text{Abs}[x]^2\gamma K^2}{\left(1+\Delta^2+\text{Abs}[x]^2\right)^2} + \frac{8c^2\gamma\Delta^2K^2}{\left(1+\Delta^2+\text{Abs}[x]^2\right)^2} - \frac{4c^2\,\text{Abs}[x]^2\gamma\Delta^2K^2}{\left(1+\Delta^2+\text{Abs}[x]^2\right)^2} + \frac{4c^2\gamma\Delta^4K^2}{\left(1+\Delta^2+\text{Abs}[x]^2\right)^2} - \frac{4c\gamma K^2}{1+\Delta^2+\text{Abs}[x]^2} - \frac{4c\gamma\Delta^2K^2}{1+\Delta^2+\text{Abs}[x]^2} - \frac{4c\gamma\Delta K\phi}{1+\Delta^2+\text{Abs}[x]^2} - \frac{4c\gamma\Delta^3K\phi}{1+\Delta^2+\text{Abs}[x]^2};$$

```
h1 = c1;
h2 = c1 c2 - c0 c3;
h3 = c1 (c2 c3 - c1 c4) - c0 (c3^2 - c1 c5);
h4 = c1 (-c5 (c2^2 - c0 c4) + c4 (c2 c3 - c1 c4)) - c0 (-c5 (c2 c3 - c0 c5) + c4 (c3^2 - c1 c5));
h5 = c5 h4;

If[c1 < 0, bool = False , bool = True ];
If[bool, True, Goto[end]];
If[c2 < 0, bool = False, bool = True ];
If[bool, True, Goto[end]];
If[c3 < 0,  bool = False, bool = True ];
If[bool, True, Goto[end]];
If[c4 < 0, bool = False, bool = True ];
If[bool, True, Goto[end]];
If[c5 < 0, bool = False, bool = True ];
If[bool, True, Goto[end]];
If[h1 < 0,  bool = False, bool = True ];
If[bool, True, Goto[end]];
If[h2 < 0, bool = False, bool = True ];
If[bool, True, Goto[end]];
If[h3 < 0, bool = False , bool = True];
If[bool, True, Goto[end]];
If[h4 < 0, bool = False , bool = True ];
If[bool, True, Goto[end]];
```

```
If[h5 < 0, bool = False, bool = True];
If[bool, True, Goto[end]];
Label[end];
x1 = x;
```

Appendix 5.2. Lyapunov Exponents

```
Clear["Global`*"];
LLEs = False;
MSKIP = 10000;
Case = 2;
Attractor = 5;
m = 1;
MMAX = 40000;
pLE = 4;
Δt = 0.02;
t_min = 0;
t_max = 20000;
Y1 = 1.88;
Y = Y1;
YLoad = 1.88;
YMax = 1.91;
YMin = 1.88;
YStep = 0.0001;
tLag = 10000;
If[Case == 1,
  c = 20.0;
  K = 0.5;
  ϕ = -1.0;
  γ = 0.05;
  Δ = 1.0];
If[Case == 2,
  c = 3.0;
  K = 0.1;
  ϕ = -0.5 * K;
  γ = 0.01;
  Δ = 0.5];
If[Case == 3,
  c = 3.0;
  K = 0.1;
```

```
  ϕ = -0.5 * K;
  γ = 4.0 * 10^-4;
  Δ = 0.5];
If[Case == 4,
  c = 3.0;
  K = 5.24;
  ϕ = -1.0;
  γ = 1.0 * 10^-4;
  Δ = 1.0];
If[Case == 5,
  c = 3;
  K = 1.0/3.0;
  ϕ = -3.0/2.0;
  γ = 0.0006;
  Δ = 0.5];
If[Case == 2.2,
  c = 3.2;
  K = 0.1;
  ϕ = -0.5 * K;
  γ = 0.01;
  Δ = 0.5];
Upload = True;

LLETotal = -K - K - 1 - 1 - γ;

If[Upload == True,
  file = ToExpression[Import["Lis System\\Case " <> ToString[Case] <> "\\Attractor " <>
      ToString[Attractor] <> "\\SteadyState Y=" <> ToString[YLoad] <> ".txt"]];

  A₀ = file[[1]];
  B₀ = file[[2]];
  R₀ = file[[3]];
  S₀ = file[[4]];
  d₀ = file[[5]];
  Print[{A₀, B₀, R₀, S₀, d₀}];
  ,
  {A₀, B₀, R₀, S₀, d₀}];


Zss = file;
If[Upload == False,
  Zss = {0.9999, 0.1, 0, 0, 0.1}];
```

```
Fun[q10_, b10_, r10_, s10_, e10_, q20_, b20_, r20_, s20_,
    e20_, q30_, b30_, r30_, s30_, e30_, q40_, b40_, r40_, s40_, e40_] :=
  Fun[q10, b10, r10, s10, e10, q20, b20, r20, s20, e20, q30, b30, r30, s30, e30,
    q40, b40, r40, s40, e40] = With[{q1 = q10, b1 = b10, r1 = r10, s1 = s10,
      e1 = e10, q2 = q20, b2 = b20, r2 = r20, s2 = s20, e2 = e20, q3 = q30, b3 = b30,
      r3 = r30, s3 = s30, e3 = e30, q4 = q40, b4 = b40, r4 = r40, s4 = s40, e4 = e40},
    If[t > tLag, V1 = {q1, b1, r1, s1, e1};
      V2 = {q2, b2, r2, s2, e2};


V3 = {q3, b3, r3, s3, e3};
V4 = {q4, b4, r4, s4, e4};


a1 = N[V1, 64];
α1 = N[Norm[a1], 64];
W1 = N[(a1/α1), 64];
El1 = N[Log[α1], 64];

a2 = N[(V2 - (V2.W1) W1), 64];
α2 = N[Norm[a2], 64];
W2 = N[(a2/α2), 64];
El2 = N[Log[α2], 64];

a3 = N[(V3 - (V3.W2) W2 - (V3.W1) W1), 64];
α3 = N[Norm[a3], 64];
W3 = N[(a3/α3), 64];
El3 = N[Log[α3], 64];

a4 = N[(V4 - (V4.W3) W3 - (V4.W2) W2 - (V4.W1) W1), 64];
α4 = N[Norm[a4], 64];
W4 = N[(a4/α4), 64];
El4 = N[Log[α4], 64];


El5 = LLETotal - El4 - El3 - El2 - El1;

For[j = 1, j ≤ 4, j++, Vj = Wj;
 qj = SetAccuracy[Wj[[1]], 64];
 bj = SetAccuracy[Wj[[2]], 64];
 rj = SetAccuracy[Wj[[3]], 64];
 sj = SetAccuracy[Wj[[4]], 64];
 ej = SetAccuracy[Wj[[5]], 64];];
If[LLEs == True, If[Mod[m, NSKIP] == 0,
  AppendTo[letest, {lepoint, Elm1, Elm2, Elm3, Elm4, Elm5, q0, b0, r0, s0, e0}];
  lepoint++;, False], False];
```

```
Eone += N[El_1, 64];
Etwo += N[El_2, 64];
Ethree += N[El_3, 64];
Efour += N[El_4, 64];
Efive += N[El_5, 64];
```

```
If[Mod[m, MSKIP] == 0,
 Print["Y, c"];
 Print[Y];
 CC = SetPrecision[c, 4];
 Print[CC];
 Print[" "];
 Print[m];
 E1 = SetPrecision[Eone / m, 4];
 Print[E1];
 E2 = SetPrecision[Etwo / m, 4];
 Print[E2];
 E3 = SetPrecision[Ethree / m, 4];
 Print[E3];
 E4 = SetPrecision[Efour / m, 4];
 Print[E4];
 E5 = SetPrecision[Efive / m, 4];
 Print[E5];
 Print[" "], False];

If[MMAX ≤ m,
 Print[" "];
 Print["Y, c"];
 Print[Y];
 CC = SetPrecision[c, 4];
 Print[CC];
 Print["FINAL FIVE Lyp Exps"];
 Print[m];
 E1 = Eone / m;
 Print[E1];
 E2 = Etwo / m;
 Print[E2];
 E3 = Ethree / m;
 Print[E3];
 E4 = Efour / m;
 Print[E4];
 E5 = Efive / m;
 Print[E5];
 Print[E1 + E2 + E3 + E4 + E5];
 Print[" "], False];
m++;];];
```

```
j = 1; While[j ≤ pLE,
 qⱼ = If[j == 1, 1, 0];
 bⱼ = If[j == 2, 1, 0];
 rⱼ = If[j == 3, 1, 0];
 sⱼ = If[j == 4, 1, 0];
 eⱼ = If[j == 5, 1, 0];

 j++];
CreateDirectory["Lis System\\Case " <> ToString[Case] <>

    "\\Attractor " <> ToString[Attractor] <> "\\Excel Data"];
 (*While[ΔMin≤ Δ≤ΔMax,*)
 tempytable = {{"Y", "E1", "E2", "E3", "E4", "E5"}};
 Y = Y1;
 q₀ = SetAccuracy[Z_ss[[1]], 64];
 b₀ = SetAccuracy[Z_ss[[2]], 64];
 r₀ = SetAccuracy[Z_ss[[3]], 64];
 s₀ = SetAccuracy[Z_ss[[4]], 64];
 e₀ = SetAccuracy[Z_ss[[5]], 64];

 While[YMin ≤ Y ≤ YMax,

   solution0 = NDSolve[{
      q0'[t] == -K * (q0[t] + (b0[t] * ϕ/K) - Y + (2.0 * c * r0[t])),
      b0'[t] == -K * (b0[t] - (q0[t] * ϕ/K) + (2.0 * c * s0[t])),
      r0'[t] == -(r0[t] - (Δ * s0[t])) + (q0[t] * e0[t]),
      s0'[t] == -((Δ * r0[t]) + s0[t]) + (b0[t] * e0[t]),
      e0'[t] == -γ * ((q0[t] * r0[t]) + (b0[t] * s0[t]) + e0[t] + 1.0),
      q0[0] == q₀,
      b0[0] == b₀,
      r0[0] == r₀,
      s0[0] == s₀,
      e0[0] == e₀
     }, {q0, b0, r0, s0, e0}, {t, t_max, t_max}, PrecisionGoal → ∞,
     MaxSteps → ∞, MaxStepSize → Δt, Method → "StiffnessSwitching"];
   (*these will be put into the NDSolve for Jaco*)
   AA[t_] := q0[t] /. solution0;
   BB[t_] := b0[t] /. solution0;
   RR[t_] := r0[t] /. solution0;
   SS[t_] := s0[t] /. solution0;
   dd[t_] := e0[t] /. solution0;
   Z_ss = SetAccuracy[Flatten[
      Table[{q0[t], b0[t], r0[t], s0[t], e0[t]}, {t, t_max, t_max, 1}] /. solution0], 64];
   X = Sqrt[Z_ss[[1]] * Z_ss[[1]] + Z_ss[[2]] * Z_ss[[2]]];
   P = Sqrt[Z_ss[[3]] * Z_ss[[3]] + Z_ss[[4]] * Z_ss[[4]]];
```

```
  If[Mod[m, NSKIP] == 0,
   tb5 = Append[tb5, {Z_ss[[1]], Z_ss[[2]], Z_ss[[5]]}];
   tb6 = Append[tb6, {Z_ss[[3]], Z_ss[[4]], Z_ss[[5]]}];
   tb7 = Append[tb7, {X, P, Z_ss[[5]]}], False];
  Clear[solution0];
  q_0 = SetAccuracy[Z_ss[[1]], 64];
  b_0 = SetAccuracy[Z_ss[[2]], 64];
  r_0 = SetAccuracy[Z_ss[[3]], 64];
  s_0 = SetAccuracy[Z_ss[[4]], 64];
  e_0 = SetAccuracy[Z_ss[[5]], 64];

  (*Put above M loop*)

Eone = 0;
Etwo = 0;
Ethree = 0;
Efour = 0;
Efive = 0;
(*M loop*)
m = 1;
```

```
solution1 = NDSolve[{
   q0'[t] == -K * (q0[t] + (b0[t] * ϕ/K) - Y + (2.0 * c * r0[t])),
   b0'[t] == -K * (b0[t] - (q0[t] * ϕ/K) + (2.0 * c * s0[t])),
   r0'[t] == -(r0[t] - (Δ * s0[t])) + (q0[t] * e0[t]),
   s0'[t] == -((Δ * r0[t]) + s0[t]) + (b0[t] * e0[t]),
   e0'[t] == -γ * ((q0[t] * r0[t]) + (b0[t] * s0[t]) + e0[t] + 1.0),
   q0[0] == q_0,
   b0[0] == b_0,
   r0[0] == r_0,
   s0[0] == s_0,
   e0[0] == e_0,
   q1'[t] == -K * q1[t] - b1[t] * ϕ - (2.0 * c * K * r1[t]),
   b1'[t] == q1[t] * ϕ + -K * b1[t] - (2.0 * c * K * s1[t]),
   r1'[t] == q1[t] * e0[t] - r1[t] + Δ * s1[t] + q0[t] * e1[t],
   s1'[t] == b1[t] * e0[t] - Δ * r1[t] - s1[t] + b0[t] * e1[t],
   e1'[t] == -γ * q1[t] * r0[t] - γ * b1[t] * s0[t] - γ * q0[t] * r1[t] - γ * b0[t] * s1[t] -
     γ * e1[t], q2'[t] == -K * q2[t] - b2[t] * ϕ - (2.0 * c * K * r2[t]),
   b2'[t] == q2[t] * ϕ + -K * b2[t] - (2.0 * c * K * s2[t]),
   r2'[t] == q2[t] * e0[t] - r2[t] + Δ * s2[t] + q0[t] * e2[t],
   s2'[t] == b2[t] * e0[t] - Δ * r2[t] - s2[t] + b0[t] * e2[t],
```

```
  e2'[t] == -γ * q2[t] * r0[t] - γ * b2[t] * s0[t] - γ * q0[t] * r2[t] - γ * b0[t] * s2[t] -
    γ * e2[t], q3'[t] == -K * q3[t] - b3[t] * ϕ - (2.0 * c * K * r3[t]),
  b3'[t] == q3[t] * ϕ + -K * b3[t] - (2.0 * c * K * s3[t]),
  r3'[t] == q3[t] * e0[t] - r3[t] + Δ * s3[t] + q0[t] * e3[t],
  s3'[t] == b3[t] * e0[t] - Δ * r3[t] - s3[t] + b0[t] * e3[t],
  e3'[t] ==
   -γ * q3[t] * r0[t] - γ * b3[t] * s0[t] - γ * q0[t] * r3[t] - γ * b0[t] * s3[t] - γ * e3[t],
  q4'[t] == -K * q4[t] - b4[t] * ϕ - (2.0 * c * K * r4[t]),
  b4'[t] == q4[t] * ϕ + -K * b4[t] - (2.0 * c * K * s4[t]),
  r4'[t] == q4[t] * e0[t] - r4[t] + Δ * s4[t] + q0[t] * e4[t],
  s4'[t] == b4[t] * e0[t] - Δ * r4[t] - s4[t] + b0[t] * e4[t],
  e4'[t] ==
   -γ * q4[t] * r0[t] - γ * b4[t] * s0[t] - γ * q0[t] * r4[t] - γ * b0[t] * s4[t] - γ * e4[t],
  q1[0] == q1,
  b1[0] == b1,


   r1[0] == r1,
   s1[0] == s1,
   e1[0] == e1,
   q2[0] == q2,
   b2[0] == b2,
   r2[0] == r2,
   s2[0] == s2,
   e2[0] == e2,
   q3[0] == q3,
   b3[0] == b3,
   r3[0] == r3,
   s3[0] == s3,
   e3[0] == e3,
   q4[0] == q4,
   b4[0] == b4,
   r4[0] == r4,
   s4[0] == s4,
   e4[0] == e4, WhenEvent[Mod[t, 1] == 0,
    {Fun[q1[t], b1[t], r1[t], s1[t], e1[t], q2[t], b2[t], r2[t], s2[t], e2[t], q3[t],
      b3[t], r3[t], s3[t], e3[t], q4[t], b4[t], r4[t], s4[t], e4[t]], q1[t] → q1,
     b1[t] → b1, r1[t] → r1, s1[t] → s1, e1[t] → e1, q2[t] → q2, b2[t] → b2,
     r2[t] → r2, s2[t] → s2, e2[t] → e2, q3[t] -> q3, b3[t] -> b3, r3[t] -> r3, s3[t] -> s3,
     e3[t] -> e3, q4[t] -> q4, b4[t] -> b4, r4[t] -> r4, s4[t] -> s4, e4[t] -> e4}]
  }, {q1, b1, r1, s1, e1, q2, b2, r2, s2, e2, q3, b3, r3, s3, e3, q4, b4, r4, s4,
   e4, q0, b0, r0, s0, e0}, {t, MMAX + tLag, MMAX + tLag}, PrecisionGoal → ∞,
  MaxSteps → ∞, MaxStepSize → Δt, Method → "StiffnessSwitching"];
q0 = q0[MMAX + tLag] /. solution1[[1]];
b0 = b0[MMAX + tLag] /. solution1[[1]];
r0 = r0[MMAX + tLag] /. solution1[[1]];
s0 = s0[MMAX + tLag] /. solution1[[1]];
e0 = e0[MMAX + tLag] /. solution1[[1]];

If[FileExistsQ[
  "Lis System\\Case " <> ToString[Case] <> "\\Attractor " <> ToString[Attractor] <>
   "\\Excel Data\\LE Y range of " <> ToString[YMin] <> " to " <> ToString[YMax] <> ".csv"],
```

```
   tempytable = Import["Lis System\\Case " <> ToString[Case] <> "\\Attractor " <>
        ToString[Attractor] <> "\\Excel Data\\LE Y range of " <>
        ToString[YMin] <> " to " <> ToString[YMax] <> ".csv"];,
   CreateDirectory["Lis System\\Case " <> ToString[Case] <> "\\Attractor " <>
     ToString[Attractor] <> "\\Excel Data\\"]];
  tempytable = Append[tempytable, {Y, E1, E2, E3, E4, E5}];
  Export["Lis System\\Case " <> ToString[Case] <>
    "\\Attractor " <> ToString[Attractor] <> "\\Excel Data\\LE Y range of " <>
    ToString[YMin] <> " to " <> ToString[YMax] <> ".csv", tempytable];

  Export["Lis System\\Case " <> ToString[Case] <> "\\Attractor " <> ToString[Attractor] <>
    "\\SteadyState Y=" <> ToString[Y] <> ".txt", {{q₀, b₀, r₀, s₀, e₀}}];
  Y += YStep;];

(*Δ+=Δstep;];*)
```

Appendix 5.3. Perturbation Program

```
Clear["Global`*"]
Case = 2;
Attractor = 2;
YLoad = 1.8;
YInitial = 1.8;

bool = False;
int = 1;
δδv = 0.005;
endv = 0.3;
endint = 40;

thr = 0.1;

YMax = 1.80;
YMin = 1.79;
YStep = 0.005;
thres = 0.5;
Y = YInitial;
Upload = True;

δv = 0.01;
A0 = δv;
B0 = δv;
R0 = δv;
S0 = δv;
d0 = δv;
tab2 = {{"Y", "Ω Zero"}};
Δt = 0.02;
tLimit = 30000;
tmax = 30000.6;


If[Case == 2,
  c = 3.0;
  k = 0.1;
  ϕ = -0.5 * k;
  γ = 0.01;
  Δ = 0.5];

A5peaks[yv_] := -263.55 yv^2 + 982.43 yv - 912.61;
A3peaks[yv_] := -5414.9 yv^4 + 37358 yv^3 - 96674 yv^2 + 111207 yv - 47975;

While[YMin ≤ Y ≤ YMax,
  ik = 1;
  int = 1;
  If[DirectoryQ["Lis System\\PCase " <> ToString[Case] <>
     "\\Attractor " <> ToString[Attractor] <> "\\Y=" <> ToString[Y]],
   While[DirectoryQ["Lis System\\PCase " <> ToString[Case] <> "\\Attractor " <>
      ToString[Attractor] <> "\\Y=" <> ToString[Y] <> "\\Run " <>
```

```
    ToString[ik] <> " per " <> ToString[endint]], ++ik;]
 ,];
CreateDirectory[
 "Lis System\\PCase " <> ToString[Case] <> "\\Attractor " <> ToString[Attractor] <>
  "\\Y=" <> ToString[Y] <> "\\Run " <> ToString[ik] <> " per " <> ToString[endint]];

attrat = {{"Pert", "Att 2", "Att 3", "Att 5"}};
If[Upload,
 file = ToExpression[Import["Lis System\\Case " <> ToString[Case] <> "\\Attractor " <>
     ToString[Attractor] <> "\\SteadyState Y=" <> ToString[Y] <> ".txt"]];

 A₀ = file[[1]];
 B₀ = file[[2]];
 R₀ = file[[3]];
 S₀ = file[[4]];
 d₀ = file[[5]];
 ,
 {A₀, B₀, R₀, S₀, d₀}];

solution = NDSolve[{
   A'[t] == -k * (A[t] + (B[t] * ϕ/k) - Y + (2 * c * R[t])),
   B'[t] == -k * (B[t] - (A[t] * ϕ/k) + (2 * c * S[t])),
   R'[t] == -(R[t] - (Δ * S[t])) + (A[t] * d[t]),
   S'[t] == -((Δ * R[t]) + S[t]) + (B[t] * d[t]),
   d'[t] == -γ * ((A[t] * R[t]) + (B[t] * S[t]) + d[t] + 1),
   A[0] == A₀,
   B[0] == B₀,
   R[0] == R₀,
   S[0] == S₀,
   d[0] == d₀
  }, {A, B, S, R, d}, {t, 0, tmax}, PrecisionGoal → ∞, MaxSteps → ∞, MaxStepSize → Δt];
AA1[t_] := A[t] /. solution[[1]];
BB1[t_] := B[t] /. solution[[1]];
RR1[t_] := R[t] /. solution[[1]];
SS1[t_] := S[t] /. solution[[1]];
dd1[t_] := d[t] /. solution[[1]];

atrad[t_] := {AA1[t], BB1[t], RR1[t], SS1[t], dd1[t]} /. solution[[1]];
tempx[t_] := Sqrt[AA1[t]^2 + BB1[t]^2] /. solution[[1]];
(*Fourier for *)
perdy = {};
t2 = tmax;
t1 = t2/2;
xtabtemp = Table[tempx[t], {t, t1, t2}];
FX = Flatten[Abs[Fourier[xtabtemp]]];
FX =
 Drop[Table[{N[(n - 1.5)/(t2 - t1)] * 2 Pi, Extract[FX, {n}]}, {n, 0, Length[FX] - 1}], 2];
fouriertab = {};
```

```
top = Max[Table[FX[[it, 2]], {it, 1, Length[FX]}]] * 1.1;
temp1 = 0;
temp2 = 0;
temp3 = 0;
thres = 1;
ofx = {Y};
n = 2; While[n ≤ Length[FX] - 1,
 temp1 = Extract[FX, {n, 2}];
 temp2 = Extract[FX, {n + 1, 2}];
 temp3 = Extract[FX, {n - 1, 2}];
 If[temp1 > temp2 && temp3 < temp1,
  ptn = ListPlot[{Tooltip[Extract[FX, n]]},
    PlotStyle → {PointSize[0.009], RGBColor[.847, 0.347, 0]}];
  If[temp1 > thres, AppendTo[perdy, Extract[FX, n]];
   fouriertab = Append[fouriertab, ptn];
   If[temp1 > temp2 && temp3 < temp1,
    AppendTo[ofx, Extract[FX, {n, 1}]], False], False], False];

 n++];

Print[(2 Pi) / perdy[[1, 1]]];
prd = (2 Pi) / perdy[[1, 1]];
thp = prd / endint;

coordy = Table[{AA1[t], BB1[t], RR1[t], SS1[t], dd1[t]}, {t, tmax - prd, tmax, thp}];
SetSharedVariable [coordy];

Export["Lis System\\PCase " <> ToString[Case] <> "\\Attractor " <>
  ToString[Attractor] <> "\\Y=" <> ToString[Y] <> "\\Run " <> ToString[ik] <>
  " per " <> ToString[endint] <> "\\Coordinates.csv", coordy];

ParallelDo[
 δv = endv;
 pertnum = Table[{ii, 0, 0, 0}, {ii, -endv, endv, δδv}];
 A0 = coordy[[int, 1]];
 B0 = coordy[[int, 2]];
 R0 = coordy[[int, 3]];
 S0 = coordy[[int, 4]];
 d0 = coordy[[int, 5]];

 While[-endv <= δv <= endv,
  tempatt = {δv};
  placmnt = Position[Round[pertnum, 0.001], Round[δv, 0.001]];
  If[Round[δv, 0.001] == 0.,
   placmnt = placmnt[[Position[placmnt, 1][[-1, 1]], 1]], placmnt = placmnt[[1, 1]]];

  solution = NDSolve[{
     A'[t] == -k * (A[t] + (B[t] * ϕ/k) - Y + (2 * c * R[t])),
     B'[t] == -k * (B[t] - (A[t] * ϕ/k) + (2 * c * S[t])),
```

```
    R'[t] == -(R[t] - (Δ * S[t])) + (A[t] * d[t]),
    S'[t] == -((Δ * R[t]) + S[t]) + (B[t] * d[t]),
    d'[t] == -γ * ((A[t] * R[t]) + (B[t] * S[t]) + d[t] + 1),
    A[0] == A0,
    B[0] == B0,
    R[0] == R0,
    S[0] == S0,
    d[0] == d0 + δv
   }, {A, B, S, R, d}, {t, 0, tLimit},
   PrecisionGoal → ∞, MaxSteps → ∞, MaxStepSize → Δt];

 AA[t_] := A[t] /. solution[[1]];
 BB[t_] := B[t] /. solution[[1]];
 RR[t_] := R[t] /. solution[[1]];
 SS[t_] := S[t] /. solution[[1]];
 dd[t_] := d[t] /. solution[[1]];

 X[t_] := √(AA[t]^2 + BB[t]^2) /. solution;
 P[t_] := Sqrt[RR[t]^2 + SS[t]^2] /. solution;
 cd = Table[{AA[t], BB[t], RR[t], SS[t], dd[t]}, {t, tLimit - (5 prd), tLimit}];

 AEpeaks = {};
 temporalX =
  Table[{t, If[X[t][[1]] > X[t - Δt][[1]] && X[t][[1]] > X[t + Δt][[1]], X[t][[1]];
     AppendTo[AEpeaks, Round[X[t][[1]], 0.0001]], X[t][[1]]]},
   {t, tLimit - 5 prd, tLimit, Δt}];
 AEpeaks = DeleteDuplicates[AEpeaks];
 AtPeakDiff = Sort[Max[AEpeaks] - AEpeaks];

 atout = 0;
 If[Max[AtPeakDiff] ≥ A3peaks[Y] * (1 - thr) &&
   Max[AtPeakDiff] ≤ A3peaks[Y] * (1 + thr), pertnum[[placmnt, 3]]++;
  atout = 3;,
  If[Max[AtPeakDiff] ≥ A5peaks[Y] * (1 - thr) &&
     Max[AtPeakDiff] ≤ A5peaks[Y] * (1 + thr), pertnum[[placmnt, 4]]++;
    atout = 5;,
    pertnum[[placmnt, 2]]++; atout = 2;];];

 δv -= δδv;
];
Export["Lis System\\PCase " <> ToString[Case] <>
  "\\Attractor " <> ToString[Attractor] <> "\\Y=" <> ToString[Y] <> "\\Run " <>
  ToString[ik] <> " per " <> ToString[endint] <> "\\" <> ToString[int] <>
  " perturbation run for base att " <> ToString[Attractor] <> ".csv", pertnum];

, {int, 1, endint}];
int = 1;

pertnumf = Table[{ii, 0, 0, 0}, {ii, -endv, endv, δδv}];
While[int ≤ endint,
```

```
 tempport = Import["Lis System\\PCase " <> ToString[Case] <> "\\Attractor " <>
    ToString[Attractor] <> "\\Y=" <> ToString[Y] <> "\\Run " <> ToString[ik] <>
    " per " <> ToString[endint] <> "\\" <> ToString[int] <>
    " perturbation run for base att " <> ToString[Attractor] <> ".csv"];
 tek = 1;
 While[tek <= Length[tempport], pertnumf[[tek, 2]] += tempport[[tek, 2]];
  pertnumf[[tek, 3]] += tempport[[tek, 3]];
  pertnumf[[tek, 4]] += tempport[[tek, 4]]; tek++;];
 int++;];
Export["Lis System\\PCase " <> ToString[Case] <> "\\Attractor " <>
  ToString[Attractor] <> "\\Y=" <> ToString[Y] <> "\\Run " <> ToString[ik] <>
  " per " <> ToString[endint] <> "\\0 combined perturbation run for base att " <>
  ToString[Attractor] <> ".csv", pertnumf];

Y += YStep;];
```

VITA

Joshua Ray Hall

Candidate for the Degree of

Doctor of Philosophy

Dissertation: ANALYSIS OF ATTRACTOR PATTERNS AND BEHAVIOR FOR THE LASER WITH INJECTED SIGNAL

Major Field: Physics

Biographical:

Education:

Completed the requirements for the Doctor of Philosophy in Physics at Oklahoma State University, Stillwater, Oklahoma in July, 2022.

Completed the requirements for the Bachelor of Science in Physics at Oklahoma State University, Stillwater, Oklahoma in May 2016.

Completed the requirements for the Bachelor of Science in Chemistry at Oklahoma State University, Stillwater, Oklahoma in May 2016.

Experience:

Four publications on the analysis of nonlinear optics in Physics

One publication on 2-D molecular water in Chemistry

Preformed research under Dr. Bandy from June 2013-July 2022

Teaching assistant from 2016-2022

Professional Memberships:

OPTICA